Colorectal cancer patient-derived xenograft (PDX) models as platform for drug screening, molecular and response analysis

vorgelegt von
Diplom-Ingenieurin
Maria Rivera
geb. in Nowosibirsk

von der Fakultät III – Prozesswissenschaften
der Technischen Universität Berlin
zur Erlangung des akademischen Grades
Doktorin der Ingenieurwissenschaften
- Dr.-Ing. -
genehmigte Dissertation

Promotionsausschuss:

Vorsitzender:	Prof. Dr. Peter Neubauer
Gutachter:	Prof. Dr. Roland Lauster
Gutachter:	Prof. Wolfgang Walther
Gutachter:	Prof. Jens Kurreck

Tag der wissenschaftlichen Aussprache: 13. April 2016

Berlin 2016

Zusammenfassung

Präklinische *in vivo* Modelle spielen eine immer größere Rolle auf dem Gebiet der Krebsforschung. Im Hinblick auf die neuesten Entwicklungen in der Onkologie, wie z.B, der personalisierten Medizin und der Entwicklung zielgerichteter Therapeutika, sind vor allem Patienten-abgeleitete Xenograft Modelle (PDX; patient-derived xenograft) verschiedener Tumorentitäten in den Fokus gerückt. Sie stellen eine geeignete Plattform zur Identifizierung und Charakterisierung von neuen Zielmolekülen (Targets) und Biomarkern dar. Dies kann dazu dienen, Patienten besser zu stratifizieren, was wesentlich zur Therapieoptimierung beiträgt. Darüber hinaus können molekularbiologische, korrelative Analysen mittels PDX Modellen wesentlich zur Aufklärung von Resistenzmechanismen beitragen. Diese Arbeit befasste sich daher mit der Etablierung und detaillierten Charakterisierung von PDX Modellen des kolorektalen Karzinoms (CRC), die Tumorentität mit der dritthöchsten Inzidenz weltweit.

Für die vorliegenden Untersuchungen wurden 87 chirurgisch resizierte Tumorproben von CRC Patienten subkutan auf immundefiziente Mäuse transplantiert. Für 49 Tumorproben konnte ein Engraftment und Retransplantation erreicht werden, woraus sich eine Angangsrate von 56% ergibt. Das etablierte PDX Panel setzt sich aus Tumorproben des Kolons und Rektums, sowie Primärtumoren und Lungen- und Lebermetastasen zusammen. Von fünf Patienten wurden Tumorproben verschiedener Lokalisation sowie Zeitpunkten entnommen und als PDX etabliert.

Zur Identitätsprüfung von Primarius und dem daraus abgeleiteten PDX wurden folgende Untersuchungen durchgeführt, die den Erhalt der histopathologischen und molekularen Eigenschaften in den PDX bestätigen:

- Anfärbung des Gewebes mit human-Zellkern spezifischen Antikörpern (Human nuclei staining) zur Identifizierung der humanen Anteile des PDX
- Histopathologischer Vergleich von Primarius und abgeleiteten PDX aus verschiedenen Passagen
- Expressionsanalyse der Marker EpCAM, p53 und EGFR im PDX Gewebe
- Vergleich des Mutationsprofils von ausgewählten PDX Modellen mit dem korrespondierenden primären Patientenmaterial

Nach Identitätsprüfung wurde die Wachstumskinetik und die Tumorverdopplungszeit (TDT; tumor doubling time) der PDX Modelle bestimmt. Der Ursprung der Tumorprobe (Lokalisation, Primärtumor, Metastase) korrelierte nicht mit dem Wachstumsverhalten. Jedoch konnte ein Zusammenhang zwischen PIK3CA Mutationen und einem schnelleren Wachstum nachgewiesen werden. Die Mutationsanalyse der PDX ergab, dass die PDX Modelle verschiedene, individuelle Mutationsprofile aufwiesen, die jedoch in ihrer Varianz mit klinisch erhobenen Mutationsraten im CRC übereinstimmen. Die Mutationsprofile von verschiedenen Proben desselben Patienten hingegen zeigten eine hohe Ähnlichkeit untereinander.

Die etablierten PDX-Modelle wurden bezüglich ihrer Sensitivität gegen Standardchemotherapeutika und zielgerichteter Therapien charakterisiert. In diesen Untersuchungen wurden Ansprechraten zwischen 37% und 46% für Bevacizumab, 5-FU und Oxalipatin in den PDX-Modellen bestimmt. Die gegen den epidermalen Wachstumsrezeptor (EGFR) gerichteten Therapeutika Erlotinib und Cetuximab erreichten Ansprechraten von 63% bzw. 67%. Die höchste Sensitivität konnte jedoch bei der Behandlung mit Irinotecan gezeigt werden (92%).

Bei der molekularbiologischen Analyse der 49 etablierten PDX Modelle konnte eine Korrelation des Expressionslevels der untersuchten EGFR Liganden untereinander nachgewiesen werden, was auch auf die vier Rezeptoren der EGFR Familie zutraf. Die Expressionsniveaus der Liganden korrelierten signifikant zu denen ihrer Rezeptoren. Das kann als Hinweis auf das Vorhandensein eines autokrinen Loops in diesem Signalweg betrachtet werden. Darüber hinaus wurden signifikante Korrelationen zwischen der Expression der EGFR Liganden und der Sensitivität gegenüber Cetuximab, jedoch nicht gegenüber Erlotinib, nachgewiesen, was die unterschiedlichen Wirkmechanismen dieser zwei Therapeutika wiederspiegelt. Die Analyse der Gen-Kopienzahl (GCN; gene copy number) von BRAF, EGFR, KRAS, NRAS und c-MET ergab, dass sie ebenfalls signifikant, positiv mit der Sensitivität gegenüber beiden EGFR Inhibitoren korrelieren. Daraus lässt sich schließen, dass PDX Modelle, die für ihr Wachstum von einem bestimmten Signalweg abhängig sind, auf dessen selektive Blockade sensitiv reagieren. Der Mutationsstatus der Signalwegmoleküle downstream von EGFR bestätigen die Korrelation, die in klinischen Studien ebenfalls beobachtet wurde. Aktivierende Mutationen in KRAS und BRAF korrelierten mit der Resistenz zu Cetuximab in den PDX. Unter diesem Aspekt zeigten PDX Modelle mit dem Wildtyp KRAS, BRAF und PIK3CA

höhere Sensitivität gegenüber den zwei EGFR Signalweg-Inhibitoren im Vergleich zu PDX Modellen mit Mutationen in einem oder mehreren dieser drei Gene.

Für weiterführende, detaillierte Studien zur Untersuchung der Mechanismen der Cetuximab-Resistenz konnten zwei Cetuximab-resistente PDX-Modelle erstmals *in vivo* generiert werden. In diesen beiden Modellen konnte eine erhöhte Expression der EGFR Liganden BTC und TGFα nachgewiesen werden. Es wurde außerdem eine erhöhte Expression von HER2 und HER3 detektiert, gekoppelt mit einer verminderten Expression des EGFR. Diese Ergebnisse zeigen, dass PDX Modelle gezielt genutzt werden können, um Resistenzmechanismen unter anderem gegen Cetuximab *in vivo* zu untersuchen und mögliche Überwindungsstrategien zu entwickeln.

Zusammenfassend zeigt die vorliegende Arbeit, dass die 49 etablieren PDX Modelle adäquat die Heterogenität der CRC in der Klinik wiederspiegeln und eine hohe Übereinstimmung zum Tumormaterial des Patienten aufweisen. Die Chemosensitivitätstestungen sowie die Resistenzmechanismen gegen die Inhibition des EGFR wurden von dem PDX Panel gut abgebildet. Somit zeigt diese Studie, dass PDX Modelle eine geeignete *in vivo* Plattform darstellen, um die Krebstherapie mittels Korrelationsanalysen zwischen Biomarkern und Therapieansprechen, der Identifikation neuer Biomarker sowie von molekularer Signaturen von Response oder Resistenz zu optimieren.

Summary

Appropriate preclinical *in vivo* models are of increasing importance and represent an essential tool in recent cancer research. Regarding the current developments in oncology, and particularly in personalized medicine and due to the emergence of targeted therapies, PDX models represent the essential platform for identifying novel targets, to define new biomarkers and to evaluate therapy response. In fact, this is needed for prediction and better stratification of patients for improved therapy response. Furthermore, PDX models can also be used to elucidate resistance mechanisms to therapeutics at the molecular level. Therefore, this study was aimed at establishment and thorough characterization of PDX models derived from specimens of colorectal carcinoma (CRC), the third most frequently diagnosed cancer worldwide.

In this study 87 surgical tumor samples from CRC patients were subcutaneously transplanted into immunodeficient mice. The resulting PDX were serially transplanted and 49 stably passageable PDX models were obtained, representing a take rate of 56%. In this PDX panel, tumor entities were evenly distributed between colon and rectum, primary tumor and metastasis; lung and liver metastases. For five patients, paired PDX models, derived from different sites or time points, could be established. To validate the identity between patient tumor tissue and its corresponding PDX, the following assays were performed and confirmed the preservation of histopathological and molecular characteristics in the PDX:

- Human nuclei staining of PDX tissue to identify human content within the PDX
- Histopathological comparison of patient and PDX tissue from several passages,
- Expression analyses of EpCAM, p53 and EGFR in the PDX tissue, and
- Comparison of the genetic profile of selected PDX models and corresponding primary patient tumor tissue.

The growth characteristics and tumor doubling time (TDT) of the PDX models was assessed. The origin of the tissue (site of origin, primary vs. metastasis) did not correlate to the growth rate of the PDX models. However, mutation in PIK3CA was a determinant of faster growth. The mutational analyses revealed that every PDX model showed a different and individual mutational profile. The encountered mutations reflected the clinical incidence in CRC patients. Moreover, the mutational profiles of PDX pairs obtained from the same patients were mainly identical.

The characterization of the PDX regarding their sensitivity towards conventional cytotoxic and targeted drugs, revealed that when a statistically significant ($p \leq 0.05$) tumor growth inhibition of ≤ 50% was set as cut off, response rates between 37% and 46% were obtained for bevacizumab, 5-FU and oxaliplatin. For the EGFR-targeting drug treatments with erlotinib and cetuximab 63% and 67% response rates were obtained respectively. The best response rate was obtained with irinotecan treatment (92%).

Molecular characterization of the established 49 PDX showed that the expression levels of the EGFR ligands correlated with each other, as well as the expression levels of the four receptors of the EGFR family. Also, the expression levels of the ligands significantly correlated to the expression levels of the receptors, corroborating the existence of an autocrine signaling loop between them. Furthermore, significant correlations were found between the expression of EGFR ligands and the sensitivity towards cetuximab, in contrast to erlotinib. This reflects the distinct mechanisms of action of these EGFR targeting drugs. The gene copy number (GCN) of BRAF, EGFR, KRAS, NRAS and c-MET correlated positively and significantly with sensitivity towards both EGFR inhibitors. This suggests that PDX tumors which are addicted to a certain pathway therefore respond to its blockade. The mutational status of pathway effectors downstream of EGFR reflected the correlations encountered in clinical studies: activating mutations in KRAS and BRAF were predictive for resistance towards EGFR inhibition. Furthermore, PDX models with wildtype KRAS, BRAF and PIK3CA showed significantly higher sensitivity towards the two EGFR pathway inhibiting substances compared to PDX models carrying a mutation in one or more of these genes.

In order to further study the molecular mechanism of cetuximab resistance, two novel cetuximab resistant PDX models were generated *in vivo*. In these PDX an increase in the expression of the EGFR ligands BTC and TGFα was observed. An increase in HER2 and HER3 expression, coupled to a decrease in expression of EGFR, was found in one of them. This demonstrates that PDX models can be further used to elucidate acquired resistance mechanisms to cetuximab *in vivo* and to develop strategies for overcoming resistance.

In summary, the established 49 PDX models reflect the heterogeneity of CRC and show a high similarity to the original patient tumors. Mechanisms of resistance towards EGFR-inhibitors were well reflected in the PDX panel. Overall, these PDX models represent an appropriate tool for *in vivo* development and optimization of cancer therapies and for correlative analyses regarding biomarker expression and therapy response.

Table of contents

1. Introduction

1.1 Cancer

In 2012 about 14.1 million new cases of cancer were diagnosed globally and it caused about 8.2 million deaths or 14.6% of all deaths [1].

Even though cancer is a term used for a group of more than 100 diseases, two main features distinguish cancer cells from normal cells. Abnormal cells divide without control, evading control mechanisms of cell growth and division, and are malignant, meaning able to invade other tissues. Cancer cells can spread to other parts of the body through the blood and lymphatic system, generating distant metastases, which significantly limit the therapeutic options [2].

Cancers are classified by the type of cell they derive from. The ones developing in the breast, prostate, lung, pancreas, and colon are carcinomas, they develop from epithelial cells. About 80% of human cancers are carcinomas; since most of the cell proliferation in adults occurs in epithelia, which at the same time are the tissues most exposed to cancer inducing damage. Cancers which develop from mesenchymal cells outside the bone marrow or connective tissue (i.e. bone, fat, nerve), are called sarcomas. Besides these two main categories, lymphoma and leukemia are two classes of cancer that arise from hematopoietic cells. Further cancer types are germ cell tumors, and blastomas, which derive from precursor cells or embryonic tissue.

Acquisition of a malignant phenotype depends on an accumulation of genomic alterations, which include mutations, chromosomal imbalance or instability resulting in amplification, overexpression or inappropriate expression of a particular gene; loss of a gene or its fusion with another gene resulting in a chimeric protein with altered function; epigenetic modifications such as aberrant methylation of cytosine in CpG islands and altered patterns of histone acetylation. Developing cancer cells select mutations having two basic functions: they increase the activity of oncogenes or inactivate the function of tumor suppressor genes [3]. Mutations which confer a selective advantage to cancer cells are termed “driver” mutations, while the remainder of mutations are “passengers”, and do not confer growth advantage [4]. There is a strong correlation between the number of stem cell divisions and the incidence for cancer development in a tissue, showing, that replication of the stem cells is essential in the multistep process of selecting malignant clones during carcinogenesis [5]. Patients with familiar adenomatous polyposis (FAP) are 30 times more

likely to develop colorectal cancer (CRC) than duodenal cancer, since there are 150 times more stem cell divisions in the colon than in the duodenum. The incidence for colon cancer would be very low if colonic epithelial cells were not constantly dividing [5].

These genetic alterations result in the malignant phenotype, whose main features were summarized by six hallmarks of cancer [6, 7]:

- Self-sufficiency in growth signaling: normal cells are unable to proliferate in the absence from stimulatory signals, in contrast to malignant cells. Exogenous growth stimulation is usually given by the overexpression or activation of growth factors or their receptors, as well as activation of downstream signaling cascades [8, 9]. Alternatively, cancer cells may send signals to stimulate normal cells within the supporting tumor-associated stroma, which as response will supply the cancer cells with paracrine growth factors [10].
- Insensitivity to anti-growth signals, in most cases caused by the disruption of the retinoblastoma protein (Rb) circuits, controlled mainly by TGFβ, can make a cancer cell elusive to cell cycle control [11–13]. During colon carcinogenesis, inactivation of the APC/ß-catenin pathway serves to block the egress of enterocytes in the colonic crypts into a differentiated, post-mitotic state [14].
- Tumor cells evolve a variety of strategies to attenuate or circumvent apoptosis. Most common is the loss of the tumor suppressor function of p53. Alternatively, tumors may show an increased expression of antiapoptotic regulators or survival signals, or a downregulation of proapoptotic factors [15, 16].
- Limitless replicative potential is required for a tumor to reach an invasive growth. Telomerase protects the telomeres from the erosion inherent to cell doubling by adding repeat segments to the ends of telomeric DNA, thus protecting the cell population from entering into senescence or crisis. It is almost absent in non-immortalized cells but expressed at functionally significant levels in ca. 90% of spontaneously immortalized cells, including human cancer cells [17].
- Induction and sustainment of angiogenesis: normally quiescent, angiogenesis is transiently turned on during physiologic processes such as wound healing. During tumor progression, an ‘‘angiogenic switch’’ is almost always activated and remains on, causing the vasculature to continually and aberrantly develop [18–20].
- The expression of genes encoding cell-to-cell and cell-to-ECM (extracellular matrix) adhesion molecules is altered in some highly aggressive carcinomas. Those

genes favoring cytostasis are typically downregulated, while adhesion molecules normally associated with cell migration are often upregulated, in some cases triggering a process called epithelial-to-mesenchymal transition (EMT) [7, 21].

The tumor associated stroma also undergoes changes during carcinogenesis and plays a crucial role in maintaining cancer proliferation [7].

1.2 Colorectal cancer

CRC is the third most diagnosed cancer worldwide (10.0% in men and 9.2% in women), and 1.36 million new cases were diagnosed in 2012. It is the fourth most common cause of death due to cancer worldwide and the second in Europe [22–25].

CRC occurs when tumors form in the lining of the large intestine, also called the large bowel. These cancers can also be referred to separately as colon cancer or rectal cancer. More than 95% of CRCs are a type of cancer known as adenocarcinomas. Other, less common types of tumors may also start in the colon and rectum. These include: carcinoid tumors (start from specialized hormone-producing cells in the intestine), gastrointestinal stromal tumors (GISTs) that start from specialized cells in the wall of the colon called the interstitial cells of Cajal, lymphomas (typically start in lymph nodes) and sarcomas [26]. The prognosis and choice of treatment depend strongly of the stage the tumor is diagnosed.

1.2.1 Staging and Grading and survival rates of colorectal cancer

Staging and grading are universal systems used to describe, evaluate and compare a cancer disease and its treatment. Currently, the primary method considered the most precise and descriptive for assessing prognostic differences among CRC patients is the tumor-node-metastasis (TNM) staging system [27]. **T** stands for tumor and the depth to which it has penetrated the colon wall, **N** stands for lymph node involvement, and **M** refers to metastases. The numbers 0 through 4 that appear after T, N, and M evaluate each of these factors and indicate increasing severity [27, 28].

The tumor stage is expressed in numbers from stage I (the least advanced) to stage IV (the most advanced). The stage of a tumor relates to its prognosis and treatment. In stage I the cancer is limited to the lining of the colon. In stage II it may penetrate the wall of the colon into the abdominal cavity or other adjacent organs but does not invade any local lymph nodes. Stage III is characterized by invasion of one or more local lymph nodes without spreading to other distant organs. In Stage IV, the tumor has spread to distant sites (liver,

lungs, bones, etc.). A recurrent/relapsed stage has set on when CRC has progressed or returned following initial treatment [27]. The stages of CRC and their main features are summarized in *Table 1* and *Figure 1*.

The WHO grading system is the most widely used and defines the histological grade of CRC based on the percentage of gland formation [29]. Well differentiated tumors have over 95% glandular structures and are designated grade 1 (G1), moderately differentiated tumors with 50-95% gland formation are grade 2 (G2), poorly differentiated tumors with 5-50% gland formation are grade 3 (G3) and undifferentiated tumors with less than 5% gland formation are defined as grade 4 (G4) [30] . The grade is often simplified as either low grade (G1 or G2) or high grade (G3 or G4). Low-grade cancers grow and spread slower and their prognosis is better than high-grade cancers of the same stage. This distinction is often used to help decide whether a patient should get adjuvant treatment after surgery.

ANATOMIC STAGE/PROGNISTIC GROUPS			
Stage	**T**	**N**	**M**
0	Tis	N0	M0
I	T1	N0	M0
	T2	N0	M0
IIA	T3	N0	M0
IIB	T4a	N0	M0
IIC	T4b	N0	M0
IIIA	T1-T2	N1/N1c	M0
	T1	N2a	M0
IIIB	T3-T4a	N1/N1c	M0
	T2-T3	N2a	M0
	T1-T2	N2b	M0
IIIC	T4a	N2a	M0
	T3-T4a	N2b	M0
	T4b	N1-N2	M0
IVA	Any T	Any N	M1a
	Any T	Any N	M1b

cTNM is the clinical, pTNM is the pathologic classification. The y prefix is used for these cancers that are classified after neoadjuvant pretreatment. The r prefix is to be used for those cancers that have recurred after a disease free interval (rTNM).

Table 1: Colon and Rectum Cancer Staging, according to the American Joint Committee on Cancer (AJCC), 2009. Copyright: AJCC

The 1-year and 5-year relative survival rates for patients with CRC are 83.4% and 64.9%, respectively and continue to decline to 58.3% at 10 years after diagnosis. When detected at early stage, the 5-year relative survival rate is 90%, but is as small as 12.5% when diagnosed in stage IV [31]. About 20 - 30% of patients with stage II disease and 50 - 80% of patients with stage III disease will relapse [32].

1.3 Molecular biology of colorectal cancer

Knowledge of the molecular basis of CRC has advanced significantly in recent years, mostly due to the progress in the field of genomic medicine and DNA sequencing technologies. The increased use of targeted therapies demands treatment regimens tailored to the mutation profile of individual tumors, which in turn makes understanding the molecular genetics of colorectal carcinogenesis crucial.

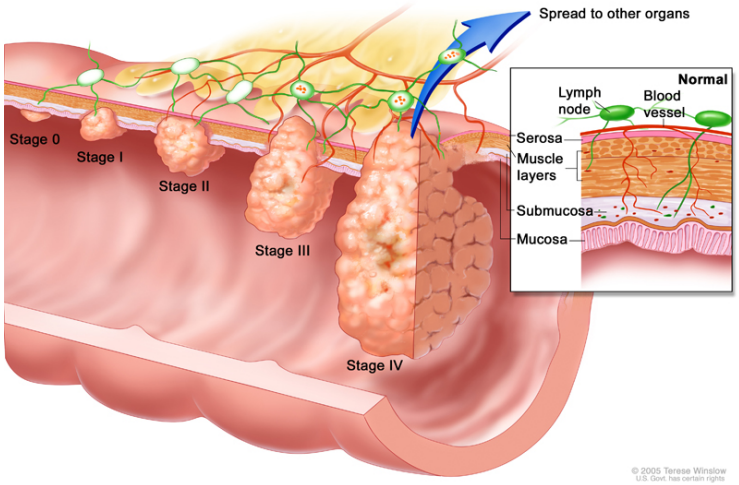

Figure 1: Stages of colorectal cancer and main pathological features. Copyright: NCI, NIH; 2005

CRC arises as a result of the accumulation of genetic and epigenetic changes. After the adenoma-carcinoma-sequence model, proposed by Vogelstein [33], has been revisited and refined, it is now established that colorectal carcinogenesis progresses by at least two well-recognized pathways (*Figure 2*). Most colorectal adenocarcinomas arise either via the tumor suppressor (chromosomal instability) or serrated neoplasia (mutator) molecular pathway.

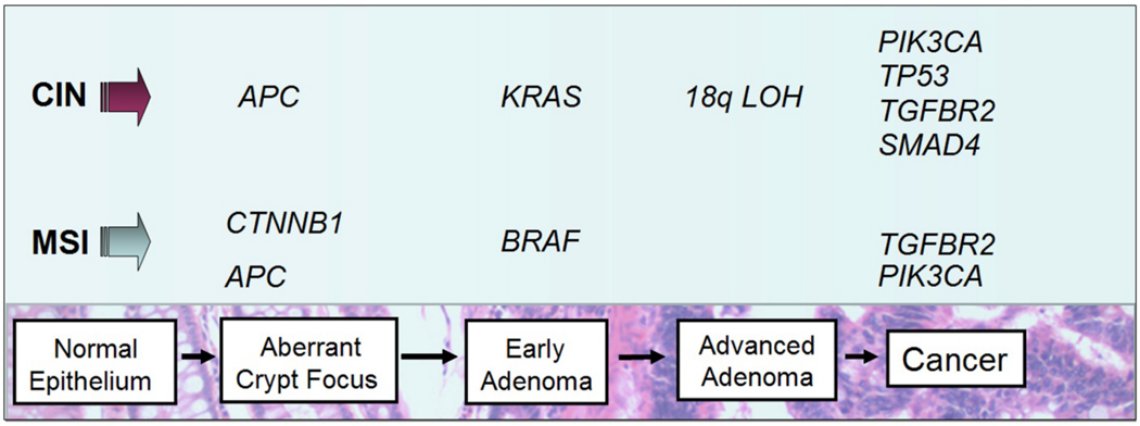

Figure 2: Colorectal carcinogenesis progresses by at least two well-recognized pathways. The main genetic alteration events are summarized according to their correlation to the carcinogenic stages in CRC. From Pritchard *et al.*, published in Gut, 2011 [34].

The chromosome instability pathway (CIN), defined as the presence of structural aberrations or changes in chromosome copy number, but usually stable karyotype, is found in up to 85% of CRCs [34]. During the CIN pathway (also termed "classical" pathway), normal glandular epithelial cells transform into benign neoplasms (adenomas) and subsequently into invasive carcinomas [35]. This pathway is characterized by classic

tubular adenoma histology and the early acquisition of mutations in the adenomatous polyposis coli (APC) gene, which mainly lead to an expression of a truncated, inactive version of the tumor suppressor protein and occur in 80% of CRC. Inactivation of APC leads to deregulated WNT signaling, which results in altered apoptosis and cell-cycle control, which drives the neoplastic cell proliferation [36, 37].

Frequent activating mutations of the Kirsten rat sarcoma-2 viral oncogene homolog (KRAS*)* oncogene at the early adenoma stage, loss of heterozygosity at chromosome 18q (18qLOH) in late adenomas, and inactivating mutations of the tumor suppressor p53 that facilitate the transition to invasive carcinomas, are further events of this pathway. The p53 protein has a regulatory role in mediating cell-cycle arrest and cell death and is mutated in about 50% of all CRC [34].

But not only tubular and tubulovillous adenomas have the potential to progress to invasive adenocarcinoma. In an alternative pathway for carcinogenesis, through which 15 - 30% of CRC tumors evolve, a subset of hyperplastic polyps progress to serrated adenomas and ultimately a smaller fraction to carcinomas [38]. Premalignant serrated polyps more frequently arise in the proximal colon and are associated with microsatellite instability (MSI) as a result of inactivation of genes responsible for DNA mismatch repair (MMR), aberrant DNA methylation at CpG islands and BRAF V600E mutations [39, 40].

Pathways exhibiting oncogenic mutations in CRC include the epidermal growth factor receptor (EGFR), mitogen-associated protein kinase (MAPK) pathway and the phosphatidylinositol 3-kinase (PI3K) pathway. EGFR activation triggers intracellular phosphorylation cascades through downstream effectors RAS and BRAF, which is amplified through the MAPK or PI3K pathway to promote cell growth. Activating mutations promoting CRC have been found for the RAS (mainly KRAS) and BRAF genes in a number of human cancers. Mutations in KRAS are found in about 40% of CRCs as an early event in the adenoma-carcinoma sequence and mutations in BRAF were detected in 13% of CRC patients [41, 42], [34]. Mutations of the phosphatidylinositol-4,5-bisphosphate 3-kinase, catalytic subunit alpha (PIK3CA), present in approximately 15-20% of CRCs, lead to upregulation of PI3K signaling that inhibits apoptosis of tumor cells [43]. Mutations in PIK3CA and KRAS or BRAF may coexist within the same tumor , but KRAS and BRAF mutations appear to be mutually exclusive [44–49].

Although somatic mutations that inactivate PTEN, a phospholipid phosphatase that mediates dephosphorylation of PIP_3 to $PIP_{2,}$ are found in roughly 10% of CRCs, some

studies suggest that PTEN protein expression may be lost in approximately 15 - 20% of CRCs [50, 51]. Similar to PIK3CA oncogenic mutations, PTEN inactivation probably acts to enhance effects downstream of KRAS protein [50].

1.4 Colorectal cancer therapy

Treatment for patients with CRC is dependent on tumor location and stage at diagnosis. Surgery is the most common treatment of early-stage (stage I and II) colon (98%) and rectal (88%) cancer. A colostomy (creation of an abdominal opening for elimination of body waste) is more commonly used for rectal cancer (29%) than for colon cancer (12%). For patients with stage III and some stage II CRCs, surgery is followed by approximately six months of chemotherapy to lower the risk of recurrence. In contrast, patients with stage II and III rectal cancers are often treated with neoadjuvant chemotherapy combined with radiation therapy [31]. Chemotherapy alone, or in combination with radiation therapy, is often given to patients at late-stage disease (50 - 70%) before or after surgery [52]. Three targeted monoclonal antibody therapies approved by the US Food and Drug Administration (FDA) to treat patients with metastatic CRC (mCRC) are bevacizumab, cetuximab, and panitumumab [52]. Most patients with stage IV cancer receive chemotherapy and/or targeted therapies to control the disease. Often, two or more of these drugs are combined to increase treatment effectiveness.

1.4.1 Classical chemotherapy

Cytotoxic chemotherapeutic agents act by interfering with cell division and include alkylating agents, platinum analogs, antimetabolites, topoisomerase-interacting agents, cytotoxic antibiotics, and microtubule stabilizing agents. Although some chemotherapeutic agents are associated with organ-specific toxicity, most induce myelosuppression and exhibit dose-dependent cytotoxicity against a range of proliferating normal cells [53].
There was a 35% reduction in the risk of death and a median survival of 11.7 months in patients treated with chemotherapy compared with a median survival of 8.0 months in patients who received best supportive care alone [54]. The chemotherapeutic drugs used as first line therapy for the treatment of CRC include 5-flourouracil (5-FU) and its second generation analogue capecitabine, irinotecan and oxaliplatin.

1.4.1.1 5-fluorouracil (5-FU)

5-FU is an analog of uracil and is rapidly incorporated into the cells using the same transport system as uracil [55]. Subsequently, 5-FU is converted into active metabolites which disrupt the action of thymidylate synthetase (TS) and RNA synthesis [56].

5-FU has been the main choice for treatment of CRC since its introduction into clinical practice 40 years ago. 5-FU based therapies are well established for patients with stage III disease in an adjuvant setting as well as for treatment of advanced metastatic disease [57, 58]. The overall response rate to 5-FU in advanced CRC is limited to 10-15%. Biochemical modulation of 5-FU cytotoxicity by combination with the vitamin-like drug leucovorin (LV, also called folinic acid), methotrexate, alpha interferon, PALA or other modulators have improved the response rate up to 30%.

Usually, 5-FU is combined with oxaliplatin or irinotecan as the first-line treatment for advanced CRCs, which improved the response rates to 40 - 50% and prolonged overall survival, although the toxicity increased [59, 60].

Capecitabine (Xeloda®) is a pro-drug of fluorouracil, developed to improve tolerability and intratumor drug concentrations through the specific conversion to 5-FU. It is used to treat stage III CRC in an adjuvant setting and as first-line treatment in mCRC [61].

1.4.1.2 Irinotecan (Camptosar®)

Irinotecan, a water-soluble, semisynthetic derivative of camptothecin, is a key component of first- and second-line treatment regimens for mCRC. Irinotecan, a pro-drug, is converted to its biologically active metabolite 7-ethyl-10-hydroxy-camptothecin (SN-38) by a carboxylesterase-converting enzyme. SN-38 is one thousand-fold more potent than the pro-drug in inhibiting topoisomerase I activity by stabilizing the cleavable complex between topoisomerase I and DNA, resulting in DNA breaks that inhibit DNA replication and trigger apoptotic cell death [62, 63]. Because ongoing DNA synthesis is necessary for irinotecan to exert its cytotoxic effects, it is classified as an S-phase-specific agent.

The use of irinotecan as a second-line treatment was approved by the FDA in 1996, and in 2000 as first-line treatment for mCRC combined with 5-FU/LV [59, 64, 65].

1.4.1.3 Oxaliplatin (Eloxatin®)

Active oxaliplatin (trans-/-diaminocyclohexane oxalatoplatinum) derivatives (monoaquo- and diaquo-DACH platinum) alkylate macromolecules, forming inter- and intra-strand DNA crosslinks as well as DNA-protein crosslinks, which result in inhibition of DNA

replication and apoptosis [66]. *In vitro*, *in vivo*, and clinical studies indicate that it is synergistic with 5-FU and LV [67, 68]. Oxaliplatin was first approved by the FDA in 2002 for use in combination with 5-FU/LV as second-line therapy for the treatment of recurrent mCRC. In 2004 it was also approved for use for advanced CRC and stage III carcinoma in an adjuvant setting.

About 30 - 45% of patients (whose disease progressed upon fluorouracil-based therapy) responded to second-line combination therapy with oxaliplatin and 5-FU/LV. Objective responses were achieved in 20 and 24% of patients in two trials of first-line oxaliplatin monotherapy and in 10% of patients given the drug as a second-line option [60, 69].

The combinations most commonly used to treat CRC are FOLFOX (LV, 5-FU, and oxaliplatin), FOLFIRI (LV, 5-FU, and irinotecan) and CapeOX (capecitabine and oxaliplatin). These regimens are also increasingly combined with the targeted agents cetuximab/panitunumab and avastin/regorafenib.

1.4.2 Targeted therapies

While standard chemotherapy affects all rapidly dividing cells in the body, targeted therapies use drugs or other substances (e.g., synthetic antibodies) that block the growth and spread of cancer cells by interfering with specific molecules that are involved in the growth, progression, and migration pathways. The aim is to better protect normal cells in association with fewer side effects than standard chemotherapy. Hence, targeted therapies are often cytostatic (they block tumor cell proliferation); whereas standard chemotherapy agents are cytotoxic (they kill tumor cells). The targeted therapies that have been approved for cancer treatment include hormone therapies, signal transduction inhibitors, gene expression modulators, apoptosis inducer, angiogenesis inhibitors, immunotherapeutics, and toxin molecules. Mainly two modalities of targeted therapies are approved for the use in CRC, such as angiogenesis inhibitors (bevacizumab) and EGFR inhibitors (cetuximab and panitumumab), additionally, the TK inhibitor regorafenib was approved in 2012.

1.4.2.1 Bevacizumab (Avastin®)

The expression of vascular endothelial growth factor A (VEGF-A) is upregulated in a wide range of human tumors and has been associated with a worse prognosis and an increased incidence of disease recurrence [70, 71]. VEGF-A binds tyrosine kinase (TK) receptors on angioblasts and endothelial cells, which activates the signal transduction cascade resulting in angiogenesis, or the formation of new blood vessels [72]. Bevacizumab is a partially

humanized monoclonal antibody that binds to VEGF-A and inhibits its receptor binding, thereby preventing the growth and maintenance of tumor blood vessels impairing tumor growth. Phenotypic changes associated with angiogenesis inhibition include changes in vessel structure, vascular permeability, partial pressure of oxygen and a decrease in interstitial fluid and in tumor blood perfusion and volume [73].

In 2004, the FDA approved bevacizumab as a first-line treatment for patients with mCRC [74]. When added to irinotecan/5-FU/LV (IFL) regimen, the overall response rate to the treatment was 45% compared to 35% for the control arm [74–76].

1.4.2.2 Erlotinib (Tarceva ®)

Two main strategies can be used to inhibit the EGFR. Monoclonal antibodies such as cetuximab and panitunumab are mainly used in CRC and head and neck carcinoma. Small molecules, TK inhibitors such as erlotinib and gefitinib are used in lung and renal cancer.

The anticancer drug erlotinib is considered a standard therapy for patients with advanced non-small cell lung cancer (NSCLC) refractory to chemotherapy. It was first approved by the FDA in 2004 for the treatment of locally advanced or metastatic NSCLC, and in 2005 for the treatment of patients with locally advanced, unresectable or metastatic pancreatic carcinoma (PC) in combination with gemcitabine.

Erlotinib hydrochloride, also known as CP-358,774, OSI-774 and Tarceva®, is an orally active selective inhibitor of the EGFR-TK. Erlotinib is a potent, direct-acting, reversible, ATP-competitive inhibitor of EGFR tyrosine phosphorylation (TKI). This leads to inhibition of mitogenesis, inhibition of tumor cell division, and cell cycle arrest. In some cell types, such as the CRC cell line DiFi, erlotinib was proven to induce concentration-dependent apoptosis *in vitro*. Specificity analysis indicated a more than 1000-fold selectivity against other TKs, such as $pp60^{v\text{-}src}$, $pp145^{c\text{-}abl}$, ErbB-2, and ErbB-4 [77, 78]. Erlotinib has significant duration of action and the degree of inhibition of phosphorylation correlates with the degree of growth inhibition of subcutaneous (s.c.) xenografts [79].

The response rate to erlotinib among NSCLC patients is 8.9% and was associated with the presence of activating EGFR mutations localized to a small region in the EGFR gene that encodes the TK-domain [80]. In the trials OPTIMAL und EURTAC only patients with activating EGFR mutations were enrolled and response rates between 83% and 58% could be reached [81, 82]. In a phase II study of erlotinib in mCRC, treatment achieved inhibition of pEGFR and pERK, but no objective response could be observed [83].

1.4.2.3 Cetuximab (Erbitux ®)

Cetuximab (C225, IMC-C225) is a human/mouse chimera IgG_1 monoclonal antibody (mAb). It consists of a human immunoglobulin G (IgG) constant region gene segment and its variable fraction blocks the ligand-binding site of the EGFR and was derived from the mouse myeloma cell line 225. The antibody binds specifically to the extracellular domain of the human EGFR on both normal and tumor cells, and competitively inhibits the binding of its natural ligands, due to its higher affinity (K_d= 0.1-0.2 nM) to the EGFR [84–86]. The binding of cetuximab to the EGFR blocks phosphorylation and activation of receptor-associated kinases, resulting in inhibition of cell growth, induction of apoptosis, and decreased matrix metalloproteinase and VEGF production, as well as inhibition of invasion and metastasis [87–89]. Synergistic cytotoxicity with chemotherapy and radiotherapy, as well as induction of antibody dependent cellular toxicity (ADCC), are further advantages of a cetuximab treatment [90, 91].

The FDA approved Erbitux® in 2004 for use in combination with irinotecan for the treatment of EGFR-expressing mCRC in patients resistant to irinotecan-based chemotherapy and in 2012, also for use in combination with FOLFIRI in this subset of patients. Cetuximab is also approved for the treatment of locally or regionally advanced squamous cell carcinoma of the head and neck (SCCHN).

When cetuximab was used as monotherapy in two different studies comparable results were achieved (8.8% and 10.8% response), and a strong improvement of the response rate upon combination with irinotecan was observed. EGFR inhibition by cetuximab may overcome resistance to irinotecan by abrogating drug efflux, restoring apoptosis, or impairing DNA-repair activity [90, 92–94].

The status of EGFR positivity of the tumor cells and the staining intensity did not appear to correlate with the clinical response in either of the studies and EGFR inhibiting antibodies even showed activity in patients with EGFR-negative immunohistochemistry (IHC) [95] .

Somatic mutations in the EGFR TK domain are associated with sensitivity to EGFR-TKIs, but not to cetuximab [96, 97]. In contrast, several studies have demonstrated that an increased EGFR gene copy number (GCN) could be associated with sensitivity of anti-EGFR mAb-based therapy in mCRC [98–102]. The response rates in patients with skin reactions after cetuximab treatment were higher than those in patients without skin reactions (25.8% vs. 13.0%; $p = 0.005$) [103, 104].

Several studies have indicated that the presence of activating KRAS mutations is associated with a lack of response to EGFR mAbs like cetuximab [46, 105–109]. Also mutations in BRAF, NRAS and PIK3CA, as well as the loss of PTEN, result in continuous activation of the downstream RAS/MAPK or PI3K pathways, regardless of whether the EGFR is activated or pharmacologically blocked [110, 111]. These factors have also been associated with acquired resistance to cetuximab in more recent studies [112–114]. The overexpression of the EGFR ligands epiregulin and amphiregulin showed to be predictive of antitumor activity of cetuximab [115, 116]. c-MET, the receptor for Hepatocyte Growth Factor (HGF), and its ligand HGF, have been previously implicated in acquired resistance to targeted therapies and mCRC patients became resistant to anti-EGFR antibodies as a result of the emergence of MET amplification in their tumors [117].

The target of erlotinib and cetuximab: the EGF Receptor

The ErbB family of tyrosine kinases comprises 4 transmembrane receptors: Erbl (EGFR or HER1), Erb2 (HER2 or neu), Erb3 (HER3), and Erb4 (HER4). These receptors transmit signals from the cell surface into the cytoplasm and nucleus regulating cell growth. In normal cells, EGFR expression ranges from 40,000 to 100,000 receptors per cell [118]. Overexpression of EGFR is detected in many human cancers including CRC.

The four ErbB receptors have different ligand binding properties. ErbB2 has a functionless ligand binding domain, while ErbB3 has a defective tyrosine kinase activity [119]. The four receptors share an overlapping downstream signaling network. Upon binding of ligands, the ErbB receptors form homodimers or heterodimers with other ErbB family members and are then internalized and autophosphorylated on their intracellular tyrosine residues. Phosphotyrosine residues then activate, either directly or through adaptor proteins, downstream components of signaling pathways including the MAPK, PI3K/Akt, STAT and mTOR pathways [120, 121]. Despite overlap in the molecules recruited to the different receptors, the ability of individual ErbBs to preferentially bind some effector proteins leads to specificity in their signaling potential.

ErbB ligands (13 are currently known) begin as cell membrane anchored proteins that are proteolytically processed to release soluble molecules [122]. The ligands of the ErbB receptors have different receptor specificity, which together with such characteristics as redundant signaling, differential processing and variable tissue expression patterns add to the signaling diversity of the EGF pathway.

1.5 Preclinical models in the development of anticancer agents

Cell culture (*in vitro*) and animal studies (*in vivo*) are critical steps in determining the efficacy, mechanism of action, and pharmacodynamics of novel anti-cancer drugs and represent essential prerequisites before clinical studies can be initiated.

1.5.1 *In vitro* models for cancer research

1.5.1.1 Established cell lines

Tumor cell lines are established cultures of (immortalized) tumor cells that proliferate indefinitely. The use of tumor cell lines allows testing of anticancer agents under highly controlled and reproducible conditions and studying the effect of a drug candidate on proliferation, migration, invasion and on signaling mechanisms.

The Developmental Therapeutics Program (DTP) of the National Cancer Institute (NCI) was initiated in 1955 as a public resource to facilitate the evaluation of novel chemicals as potential cancer chemotherapeutics and has played a decisive role in the development of more than 40 FDA-approved agents, including paclitaxel, bortezomib, fluorouracil and cetuximab. The original idea behind this project was that the elucidation of empirically defined antitumor activity in a model would translate into activity in human cancers.

Starting in 1985, the human tumor cell line panel comprised of 60 different cell types, including mainly solid malignancies from nine different origins (brain, breast, colon, hematopoietic cells, kidney, lung, melanocytes, ovary and prostate) was implemented to screen up to 20.000 compounds per year for anticancer activity. Although the endpoints are growth rate and cytotoxicity, the combined data from the cell lines provides information also on drug mechanism of action and response patterns [123–126]. The *in vitro* screen avoids the use of animals, saves on the amount of material required and accelerates data acquisition, but is unsuitable for the testing of prodrugs and immune modulators.

The use of cell lines in two dimensional cell culture systems has shown in retrospective studies to be able to predict drug-response in some fast growing tumor entities like childhood leukemia, but does not reflect the complexity of solid tumors in patients [127]. The propagation of cells that have been maintained for decades in enriched growth media, grown as monolayer cultures and under non-physiological oxygen tensions, result in the artificial selection of primarily undifferentiated tumor cell clones with high proliferative potential lacking the genetic and epigenetic heterogeneity of the original primary tumor and showing accumulation of additional genetic and epigenetic changes, e.g. higher levels

of DNA methylation accompanied by decreased gene expression in cell lines compared with primary tumors [128–130]. Using primary cells may circumvent these problems; however, obtaining sufficient amounts of cells fully reflecting tumor diversity represents a significant challenge. Nevertheless, cell lines contributed greatly to sorting out the driver from the passenger mutations in cancer, as tests for functionality and genetic manipulations are difficult if not impossible to perform in tumor tissues or animal models [131].

These *in vitro* selected tumor cell lines often show rapid and predictable ectopic xenograft growth *in vivo*, but result in tumor models with limited phenotypic, histological, and genotypic similarities to most primary human cancers. Moreover, the metastatic rates from s.c. or intramuscular (i.m.) tumor xenografts in murine hosts have been low or nonexistent [132]. Consequently, reliance upon cell line derived s.c. and systemic tumor xenograft models alone to study therapeutic impact on tumor growth, metastasis, vascularization, and emergence of tumor resistance, has limited predictability for clinical outcomes, particularly for targeted therapeutics versus traditional cytotoxic anti-cancer agents [133, 134].

1.5.1.2 3D cultures

Tumor cells in a tumor interact closely with the ECM and with other cells of the tumor stroma and microenvironment, including endothelial cells, fibroblasts and immune and inflammatory cells which affects cell polarity, nuclear organization and gene expression. Three dimensional (3D) or organoid cell culture models are being increasingly developed, aiming to mimic the interaction of these components [135]. Cells grown in 3D cultures have different growth characteristics and responses to chemotherapeutic drugs compared with cells grown in two dimensional culture systems [135–137]. Thus, they provide a compromise between the reductionist approach which isolates cancer cells as a 2D monolayer and the complexity of growing human tumors in xenogeneic hosts.

3D culture models range from simple cancer cell spheroids to models comprising multiple cell lines, or multicellular tumor spheroids (MCTS). They can be studied in suspension in bioreactors or in 3D matrices and closely resemble cell-cell and cell-matrix interactions. The spheroids consist of actively proliferating cells on the outside, with quiescent cells in the inner, nutrient-deprived zone. Therefore, their size is limited to 400-600 μm as with increasing size the cells inside the spheroid become necrotic [138,139]. However, nutrient restriction and lack of oxygen may better reflect the tumor microenvironment than a fully oxygenated and nourished cell monolayer. Spheroids display cell-cell interactions, proved

by the presence of E-cadherin, and development of ECM. CRC spheroids gave rise to well-differentiated adenocarcinomas and did not give rise to tumors following single-cell implantation [140]. The main application of 3D culture is the testing of chemotherapeutic agents, particularly of novel drug delivery systems. Scaffolds have been adapted as matrices (e.g. collagen, hyaluronic acid, etc.) and can be designed to meet specific requirements, however, cell behavior will also depend on their chemical properties [135]. The major advantage of 3D models is that they model tumor physiology more closely, but, their limited resource and life span do not allow long term genetic manipulations [131].

1.5.2 *In vivo* models for cancer research

Two main *in vivo* animal models are used for the evaluation of drug activity: tumors grafted in syngeneic (genetically identical) host animals and human xenografts implanted in immunodeficient animals (mostly mice or other rodents).

1.5.1.3 Syngeneic models

In a syngeneic model, murine cell lines are injected mostly s.c. in immune competent murine hosts, thus avoiding the deficiencies of the immune system relevant in other *in vivo* models. The syngeneic models allow working in a reproducible manner with a variety of well characterized cell lines. However, there is a poor correlation to the therapeutic activity in humans, mostly due to innate differences in the biology of human and murine cells. Another caveat of these models is the poor variety of available tumor types and rapid tumor growth, with average of tumor doubling times of 2 days, which is not representative of most human solid tumor growth kinetics [141]. Syngeneic mouse models helped to identify 35 therapeutic agents until the early 1980s, but the classes of anticancer drugs identified were mainly DNA damaging agents, also toxic to the bone marrow, and novel structures had not been discovered for over 20 years [141]. Syngeneic models are also fairly unsuited for the testing of humanized antibodies, nowadays widely used for targeted cancer therapies, or require their production in a species-directed way [142]. However, the syngeneic mouse tumor model is especially valuable for immunotherapy experiments in which an intact immune system is required for the evaluation of therapies that target specific components of blood vessels or the ECM [141].

1.5.1.4 Xenograft models

Xenograft models of cancer are established by injection or implantation of human tumor cells or primary tumor fragments into immunodeficient mice.

Immunodeficient mouse strains used in cancer research

Commonly used immunodeficient mice include nude mice (*Foxn1*^{nu}), severe combined immunodeficiency (*scid*) mice (*Prkdc*^{scid}), RAG1 or RAG2-deficient mice, and NOD-*scid* and NOD-*Rag1*$^{-/-}$ mice [143]. Nude mice have a spontaneous deletion in the FOXN1 gene, which causes lack of a thymus and normal T cell development. These mice lack of body hair, which gives it the name "nude". They were the first genetically immunodeficient mouse model reportedly used for xenotransplantation of a human tumor in 1969 [144]. T-cell deficiency is not complete and these mice have increased NK cell activity, though. As a result, only about 20 - 40% of human tumor cell lines grow in nude mice [143].
In SCID mice the *Prkdc*^{scid} mutation affects the DNA-dependent protein kinase complex that is necessary for the DNA recombination events during B- and T-cell development. Therefore, these mice lack B- and T-cells, but have an intact innate immune system [145]. RAG1 and RAG2 are required for gene segment recombination in the generation of B- and T-cell receptors and immunoglobulin and *Rag1*$^{-/-}$ and *Rag2*$^{-/-}$ mice lack B- and T-cells as well. The level of innate immune system activity is lower in mice crossed onto the non-obese diabetic (NOD) background. As a result, NOD-*scid* and NOD-*Rag1*$^{-/-}$ mice are more receptive to xenografts. Because development of diabetes mellitus in NOD mice is T-cell dependent, these moce do not develop diabetes. A further level of immunosuppression is achieved by crossing T- and B-cell-deficient mice with mice in which the common cytokine receptor chain IL2RG is knocked out. This causes in addition absence of NK cells, which leads to a high success rate of engraftment of xenografts.

Table 2: Immunodeficient mouse strains and their main characteristics

Strain	Nomenclature	Immune Characteristics
nude	*Foxn1*^{nu}	Reduced T-cell number
scid	Prkdc^{scid}	Lack of B and T cells, high NK cell activity, some Ig leakiness
Rag1$^{-/-}$ *Rag2*$^{-/-}$	*Rag1tm*^{1Mom} *Rag2tm*^{1Fwa}	Lack of B and T cells, high NK cell activity, no Ig leakiness, reduced radiation sensitivity compared to *scid*
NOD-*scid*	NOD.*Prkdc*^{scid}	Lack of B and T cells, as well as reduced NK cell activity, some leakiness due to *scid* mutation
NOG	NOD.Cg-*Prkdc*^{scid} *Il2rg*^{tm1Sug}/JicTac	Lacks B and T cells, further reduction in NK, macrophage and dendritic cell activity compared to NOD-*scid*
NSG	NOD.Cg-*Prkdc*^{scid} *IL2rg*^{tm1Wjl}	Similar to NOG mice but contains a complete null mutation of the IL2rg gene

Ectopic xenograft models

Since the early 1970s, when it was demonstrated that human tumor tissues could be successfully propagated in athymic nu/nu mice, ectopic tumor xenografts have been widely used for cancer research. Ectopic tumor xenograft models employ mostly s.c., but also intraperitoneal (i.p.), or i.m. implantation of tumor cell lines or tissue explants into immunocompromised rodents.

Mainly s.c. xenograft models derived from established cell lines are extensively used because of the ease of handling and measurement of tumor mass. Growth of solid tumors is monitored using *in situ* caliper measurements and activity of a drug is defined by tumor growth delay, optimal % T/C (treated tumor mass / control tumor mass) or net log cell kill. Tumor growth delay is the difference in days for treated versus control tumors to reach a specified volume, usually 1 cm^3. These models are useful in assessing anti-tumor efficacy and overall tolerability *in vivo* in the early screening of new substances due to their reproducibility and cost- and time-effectiveness.

A review of the *in vitro* and *in vivo* screening of the 60 NCI human cell line panel elucidated, that the correlation between the results from xenografts and human Phase II clinical studies for 39 agents was generally poor [134]. When T/C-values obtained for xenografts were compared with response rates in patients with the same tumor indication, clinical activity could not be predicted for breast and colon histology, but was predictive for NSCLC and ovarian cancers when panels of xenografts were used [133]. Exceptions to these limitation are tumor lines whose growth is highly dependent upon specific ‘‘driver mutations’’. In this case, the responses obtained in traditional ectopic xenograft models have shown to be representative of the clinical responses observed in cancer patients treated with targeted therapies directed against this mutated oncogenic proteins. The responsiveness of NSCLC ectopic xenografts with activating mutations in EGFR to EGFR TKI, or xenografts bearing the acquired T790M mutation in EGFR to second-generation inhibitors of EGFR and HER2, were consistent with the clinic [146]. Similarly, ectopic xenograft models of melanoma harboring activating BRAF mutations respond to BRAF inhibitors as well as subsets of malignant melanoma patients bearing the same mutations; in contrast, in there is a marked discordance between outcomes in BRAF mutated ectopic xenografts and BRAF mutated patient subpopulations in CRC [147, 148].

The relatively low clinical predictability of tumor cell line based ectopic xenograft models is a consequence of their limited pathological relevance. This is reflected by histological

features such as loss of tumor architecture, altered genetic profiles, loss of inter- and intra-tumor heterogeneity, non-physiological growth location in the host, and the absence of critical stromal and micro environmental spatial and paracrine interactions with host non-cancerous cells and tissues, including endothelial cells, inflammatory cells, tumor-associated fibroblasts, and matrix proteins. Nevertheless, virtually every clinically approved anti-cancer drug has been evaluated in human ectopic xenograft models [149].

Orthotopic xenograft models

The widely used s.c. xenograft does not reflect the normal complex interactions between tumor cells and the original tumor microenvironment. Thus, an alternative approach is to inject or implant tumor cells or tumor tissue orthotopically, i.e. in the same mouse organ or tissue from which the human tumor cells were derived. Compared to the s.c. xenograft model, orthotopic tumor implantation more closely simulates the natural environmental milieu of the original tumor, and orthotopically implanted tumors tend to metastasize more frequently than s.c. tumors [150]. Therefore orthotopic models provide an opportunity for studying the mechanisms of pathogenesis as well as tumor proliferation, angiogenesis, local invasiveness and distant metastasis dissemination behavior of the original tumor. Orthotopic models, particularly when utilized in immune-competent syngeneic in bred mouse strains (e.g. CT-26 colon carcinomas in Balb/c mice), can have considerable translational impact in the mid-later stages of a drug discovery project and in the pharmacological characterization of a drug in a host with an intact immune system [132].
However, orthotopic injection or implantation is technically more demanding and time consuming, with caveats such as highly variable tumor take rates, development times, and animal morbidity associated with surgical implantation or injection of cells. Moreover, the tumors are not easily accessible in live animals, and tumor cells must be transfected with green fluorescent protein, luciferase or another label that allows *in vivo* imaging, in order to monitor tumor growth [151]. The implantation site has been demonstrated to affect the response of tumors to chemotherapeutic agents in xenograft studies [152]. Although orthotopic models are more relevant regarding tumor biology, they have a limited use for widespread screening and initial evaluation of new anticancer substances.
When generated from established tumor cell lines versus primary tissue explants, orthotopic models can present the same limitations of ectopic xenografts, like poorly

differentiated, largely homogeneous tumor cell populations, histological and genetic dissimilarities with original tumor tissue, and the loss of tumor heterogeneity.

Transgenic and genetically engineered mouse models (GEMMs)

The genetic profile of mice can be altered so that one or several genes thought to be involved in transformation or malignancy are mutated, deleted or overexpressed. The effect of these genetic alterations and /or therapeutic responses can be studied over time *in vivo*. The expression patterns of specific genes can be regulated systemically or in a tissue- and time-specific manner in germ-line transgenic and conditional transgenic models, respectively. Thus, tet-regulated or CRE-inducible alleles can regulate the timing, duration, and tissue compartment of gene expression or inactivation. These technologies can also be combined, resulting in GEMMs with specific cancers that overexpress or lack genes of interest in all cells or in a specific tissue and/or developmental stage. The tumors develop spontaneously and undergo stages of progression similar to those observed in human tumors, in the appropriate tissue, in an immunocompetent host [132]. These are the main features that distinguish GEMMs from traditional ectopic human tumor xenografts, and which they to some degree share with orthotopic xenografts in syngeneic mice.

Cancer agents can be evaluated with focus on the dynamics of the immune response, local invasion, angiogenesis and systemic metastatic spread. The use of GEMMs can more faithfully model the features of the development and progression of specific cancers and has significantly contributed to our understanding of cancer pathogenesis. At the same time, the fact that most GEMMs rely on the change of a single, potent oncogene to drive the tumor, not always entirely representative for this disease when put into context, is the main disadvantage of using these models for translational research. A further disadvantage of GEMMs is the low penetrance and heterogeneity with respect to tumor formation frequency, latency for tumor development, and growth of the mainly murine tumors. The use of out-bred murine strains with a non-uniform genetic background can influence tumor development and impact outcomes in drug efficiency studies. Furthermore, GEMMs do not incorporate the heterogeneity inherent to tumor initiation, progression, and metastasis, and systemic disease is rarely observed [132].

GEMMs are best suited for testing of hypothesis obtained from drug discovery, translational biology and biomarker studies, rather than a high throughput *in vivo* screen to be used early in drug discovery research. Overall, GEMMs have rarely been used to test

novel anti-cancer therapeutics with the goal of accurately predicting clinical responses. The few studies that have compared GEMMs using clinically effective agents have not been encouraging. Thus, GEMMs have not yet demonstrated a role in drug discovery [150].

Humanized mice

Perhaps the most fundamental concern with xenotransplantation is that the recipient mice lack a functional immune system. Studies over the past decade have clearly demonstrated the importance of the innate and adaptive immune system in preventing the outgrowth of tumors and in selection of tumor cells that escape the immune response [153]. The immune response does also play an important role in the effect of cancer therapies. For example, chemotherapy and radiotherapy were less effective in nude mice than in immune competent mice with syngeneic tumors, due to the activation of e.g. dendritic cells [154]. Furthermore, the screening of the new immunotherapies for cancer is a challenge that is addressed by humanized mouse models, bringing them increasingly into focus.

The term humanized mice describes numerous animal models, including immunodeficient mice reconstituted with human stem cells or lymphocytes [155]. This approach has also been combined with the transplantation of human thymus and/or bone marrow before stem cell injection to provide human stromal environment. Humanized mice can be challenged with human tumor xenografts or viruses to study the effect of immunity on tumor growth or the role of interactions between xenogeneic human stroma and tumors in tumor progression and metastasis.

Another definition of humanized mice involves the insertion of a human gene into the mouse genome. Such GEMMs are used to study species-associated differences in phenotypes, including responses to drugs or tumor antigens.

Patient-derived xenograft (PDX) models

PDX models represent a powerful, experimentally rigorous and more clinically predictive and relevant approach to oncology, drug discovery and development. They aim to preserve and stabilize the genotypic and phenotypic features of the original tumor of different entities, including CRC.

In the PDX approach, also referred to as personalized mouse model, a portion of a patient's tumor, obtained by surgical resection, is transplanted (mostly s.c.) in immunodeficient mice and allowed to propagate without any *in vitro* manipulation.

Subsequent PDX passages are then used for drug testing purposes aiming at the possibility to guide patient therapy. Typically, the third passage (P3) is used for drug testing, although earlier passages may also be used for this purpose [156]. The employment of PDX to drug efficacy and safety studies is referred to as xenopatient trial. Studies conducted in the 1980s already showed a high degree of correlation between clinical response to cytotoxic agents in patients with NSCLC and in PDX models generated from their respective tumor tissue [157]. Similar observations were made in studies of childhood rhabdomyosarcomas [158]. PDX models have also been used to conduct preclinical phase II studies with classic chemotherapeutics [159]. A correct prediction of clinical outcome was observed for both tumor resistance (97%) and tumor sensitivity (90%) in a large panel of PDX [141].

Successful implantation of the tumor is decisive for PDX establishment and depends on a number of factors including tumor type, site of transplantation, mouse strain used, and usually takes between two and four months [160]. PDX models have a reported primary tumor take rate of 40 - 60 % under ideal conditions, although engraftment rates as high as 64 - 87% have been reported for CRC PDX and much lower rates of 3 - 27% were reported for breast carcinoma (BC) or NSCLC [161–164]. For CRC PDX models the interval between CRC tumor implantation and palpable growth is relatively short (ca. four weeks). In some cases short time for PDX establishment might allow intervention studies to be performed within the time of patient's recovery time from tumor surgery [165–167]. These models can be used to simultaneously test multiple drugs or combinations in an *in vivo* system that closely approximates the human tumor [168]. Initial tumor transplantation to mice is the moment at which the most genetic variations can arise, mainly concerning the expression of genes associated with stromal gene ontology annotations, due to loss of the human stroma in PDX. Subsequent minor genetic changes occurring with each passage to a new mouse host are thought to represent genomic rearrangements intrinsic to tumor progression [169]. Therefore, most authors recommend using PDX models with a low passage number (< 10), since impact and degree of genetic alterations that occur with each tumor passage remains unclear [170].

A great advantage of PDX models is the absence of *in vitro* selection of tumor cells, maintenance of the primary tumor cell architecture and the retention of the inherent genetic heterogeneity of the original tumor [164, 171]. PDX retain the DNA methylation pattern of the original tumor and may more faithfully mimic the response of human tumors to cancer

drugs [128]. Indeed, even in early stage CRC tumors exhibiting chromosomal instability, establishment and propagation as PDX conserves the intratumoral heterogeneity, chromosomal instability, and histology of the patient tumor for up to 14 passages [172]. Concordance between the engrafted PDX tumors and the original patient tumors have been established in several cancer models such NSCLC, small cell lung cancer (SCLC), PC and also CRC [161, 166, 173, 174]. In comprehensive analysis of NSCLC and BC PDX and their respective patient tissue, unsupervised hierarchical clustering of microarray gene expression data showed that serially-transplanted PDX clustered with the original patient tumor [163, 164].

Although most PDX models are established as s.c. tumors, the orthotopic implantation of primary tumor fragments offers the additional advantage and physiological relevance of maintaining tumor clinical markers and histopathologies, while frequently recapitulating clinically relevant patterns of metastasis [175].

In recent years there has been renewed interest in the development of PDX models from different tumor entities as the preferred preclinical tool to improve and to accelerate the drug development process. Recent studies confirmed and expanded the observations of similarities between patient outcome and PDX responses. In this context, high concordance was observed between the clinical response and the corresponding PDX model in two different studies of BC PDX [176, 177]. Similar observations were made for other solid malignancies including high-grade serous ovarian cancer for cisplatin sensitivity [178]. First reports of using PDX models to guide therapy include a pilot study in 14 patients with refractory advanced cancer. The patient's treatments were selected on the basis of chemosensitivity testing in their respective PDX. Most importantly, selected chemotherapies were not necessarily the first choice for the conventional second- or third-line treatment of the respective tumor type. The objective response rate was 88% for treatments that showed activity in the PDX models and were then applied to the respective patients [175]. In a cohort of 15 CRC PDX, established and characterized by Fichtner *et al.*, very encouraging results were obtained. Most importantly, for 5 PDX where clinical data were available, the response correlated with the patient outcome [165].

CRC PDX studies have been conducted to cross-validate and evaluate the role of known predictive biomarker such as KRAS mutations regarding resistance to EGFR antibodies [161, 179]. This led to the identification of mechanisms of acquired resistance to targeted

therapies, e.g. the identification of c-MET or HER2 amplifications in tumors resistant to cetuximab and signatures for resistance to mTOR inhibitors in CRC [162, 179, 180]. Further, PDX studies have been successfully used for identifying novel targets and testing of alternative therapies for tumors based on their molecular characteristics, among others the use of trametinib in pancreatic carcinoma and selumetinib in CRC [181, 182]. The screening for novel therapy approaches was also extended to the testing of gene therapy using CRC PDX [183, 184]. These and other studies emphasize the potential impact of combining molecular data and the PDX models with a closely associated clinical translation to accelerate drug development and predictive biomarker identification and validation in CRC and other diseases. Further, treatments tailored to a patient's specific tumor genotype and/or phenotype can be pursued. This allows personalized medicine in a time frame that could use data to selectively adjust therapy regimen for the patient. Therefore, PDX models are important for improved therapy response prediction and for identification of novel biomarkers.

For the thorough analyses of PDX models, availability of respective comprehensive clinical data sets and access of detailed molecular analysis data is essential. Therefore this study aimed to establish our own PDX panel as basis for further molecular correlation analyses and the generation of resistance models. By such PDX models, mechanisms of chemosensitivity and the development of resistance towards particular treatments can be better analyzed and used for the development of novel treatment strategies.

Aim of the study

Preclinical models that closely recapitulate heterogeneity of human tumors are needed to efficiently promote drug development in oncology. Due to the high incidence of CRC, CRC PDX models have reportedly been used and showed an important role in panel oriented approaches for validation of novel targets and biomarkers in CRC. In spite of this, the high cost of privately developed models and restricted transfer regulations between academic and commercial entities have slowed the implementation of this methodology in a wide range. The lack of standardized quality criteria and validated response evaluation criteria for PDX explains the need to develop own, well characterized CRC PDX models.
The aim of this study was the establishment and molecular characterization of PDX from colorectal carcinomas that can be used for screening of known and of novel drugs and for biomarker research. The high attrition rate of cancer therapies demands for accurately predictive cancer models. Furthermore, the emergence of targeted therapies entailed the urgent need for predictive biomarkers, so that the right patient populations can profit from individualized and also from novel and less toxic therapies.

In this study a set of 49 stably passageable CRC PDX models was established and characterized. In this regard the current study was in particular aiming at:

- Analyses of the PDX models regarding their histopathological and biological characteristics in comparison to the original patient samples.
- Determination of the stability of the PDX models regarding maintenance of histology and genetic characteristics over passages.
- Analyses of their most important molecular characteristics and sensitivity to targeted and cytostatic drug treatments currently used in the clinic.
- The dynamics of the EGFR pathway in the PDX to confirm their fidelity of reproducibility in the mouse model.
- The correlation of molecular characteristics of the models to the drug response, and especially to EGFR inhibitors to elucidate resistance/sensitivity markers in the PDX model.
- Finally, the generation of cetuximab resistant PDX models to further aid the understanding of the mechanisms of resistance to EGFR-inhibiting therapies in PDX models and to correlate dynamics of this pathway in human CRC.

2. Material and Methods

2.1 Material

Animals

Strain	Common name
NOD.Cg-*Prkdc*^{scid} *Il2rg*^{tm1Wjl}/SzJ	NOD-*scid* gamma (NSG)
Crl:NMRI-*Foxn1*^{nu}	NMRI:*nu/nu*

Equipment

Device	Manufacturer
Analytical Balance	Sartorius
BioPhotometer	Eppendorf
Cryostat CM1900	Leica
Electrophoresis power supply, Consort EV265	Sigma-Aldrich
Gel casting System Horizon 58	GibcoBRL
Microplatereader Infinite M200	Tecan Group Ltd.,
Microscope Axioskop40	Zeiss
MiSeq Desktop Sequencer	Illumina
NanoDrop	Thermo Scientific
PCR-System GeneAmp 9700	Applied Biosystems
PowerPac HC Power Supply	Bio-Rad
StepOnePlus Real-Time PCR System	Applied Biosystems
Thermomixer Comfort	Eppendorf
TissueLyser II	Qiagen
Vortex Mixer	Snijders
Centrifuge 5403	Eppendorf

Consumables

Product	Manufacturer
Coverglass, 25x60mm	Menzel GmbH & Co KG
Cuvettes UVette®	Eppendorf
MicroAmp® 8 Cap-Strip	Applied Biosystems
MicroAmp® Fast Optical 96-well Reaction Plate	Applied Biosystems
MicroAmp® Optical Adhesive Film	Applied Biosystems
MicroAmp® Reaction Tubes	Applied Biosystems
Microscope slide SuperFrost® Plus,25x75x1.0 mm	Menzel GmbH & Co KG
Nunc-Immuno™ Plates, Maxi-Sorp, F96	Nunc GmbH und Co. KG
Rotilabo® Embedding Cassettes	Roth

Chemicals

Product	Manufacturer
Animal Research Kit	Dako
Bio-Rad Protein Assay Dye Reagent Concentrate	Bio-Rad
Bovine Serum Albumin, ≥98%	Sigma-Aldrich
Citric Acid Monohydrate	Sigma-Aldrich
DAPI	Roth
Dulbecco's PBS (10x), (-) $CaCl_2$, (-) $MgCl_2$	Gibco
Eosin G Solution	Merck
Ethanol	Serva
Formalin solution, neutral buffered, 10%	Sigma-Aldrich
Glycerol	Roth
Hematoxylin	Dako
Peroxidase block	Vector Laboratories
Peroxidase Substrate Kit AEC	Vector Laboratories
Phosphatase Inhibitor cocktail 1 and 2	Sigma-Aldrich
Phosphate buffered saline (10x)	Invitrogen
Protease Inhibitor cocktail	Sigma-Aldrich
Substrate Reagent Pack	R&D Systems
Roticlear I and II	Roth
Streptavidin-Biotin blocking kit	Vector Laboratories
Trisodium citrate dihydrate	Sigma-Aldrich
Tween® 20	Carl Roth GmbH & Co KG
VectaMount AQ Aqueous Mounting Medium	Vector Laboratories
Xylene, histological grade	Roth

Antibodies

Antibodies and ELISA Kits	Clone / Code	Manufacturer
Primary antibodies and ELISA Kits		
anti-human-Ki-67-antibody, M7240	MIB-1	Dako
Anti-Nuclei antibody, MAB4383C3, cy3-labeled	3E1.3	Merck Millipore
DuoSet® ELISA, human AREG	DY262	R&D Systems
DuoSet® ELISA, human BTC	DY261	R&D Systems
DuoSet® ELISA, human EGF	DY236	R&D Systems
DuoSet® ELISA, human EGFR	DY231	R&D Systems
DuoSet® ELISA, human TGFα	DY239	R&D Systems
EGFR	sc-03	Santa Cruz
ELISA Kit for human EREG	E91945Hu	USCN Life Science
EpCAM, 804-330-C100	VU1-D9	Enzo Life Sciences
p53	DO-7	Dako
Anti-PCNA	D3H8P	Cell Signaling
Secondary antibodies and labeled streptavidin		
Cy2-conjugated Goat anti-Rabbit IgG (H+L)		Dianova
Cy3-conjugated Streptavidin		Dianova
HRP-conjugated Streptavidin		Dianova

2.2 Methods

2.2.1 Establishment of PDX and sample collection

The majority of the tumor samples was obtained from the Charité Comprehensive Cancer Center (CCCC), Berlin and the Evangelisches Lungenklinikum (ELK) Berlin-Buch providing primary tumors, in limited cases adjacent normal tissue, as well as lung metastases of colorectal carcinoma. Approval of the local ethical committees was given and informed consent was obtained from all patients by the respective hospital prior to sample acquisition and experimentation. The first 15 PDX of this set were established by Fichtner *et al.* [165], and included in the further analysis carried out in this study.

All animal experiments were carried out in accordance to the German Animal Welfare Act as well as the UKCCCR (Guidelines for the Welfare of animals in Experimental Neoplasia). Approval of local authorities (Tiergenehmigungsnummer G0124/09) was given.

The resected patient tumor material was processed to contain as much vital tumor tissue as possible (hence, be free of necrosis, fat, muscle or other connective tissues). The tissue was immediately transferred into a tube with sterile transport medium (RPMI 1640) and transported to the animal facility. The fresh tumor fragments (approximately 3 x 3 x 3 mm in size) were transplanted subcutaneously into the left flank of anaesthetized NSG mice. The mice were observed for maximum 120 days and maintained under sterile and controlled conditions (22°C, 50% relative humidity, 12 h light–dark cycle, autoclaved food and bedding, acidified drinking water). Tumor growth was measured in two dimensions with a caliper. Tumor volumes (TV) were determined by the formula:

$$TV = (width^2 \times length) \times 0.5$$

When tumors reached a TV of approximately 1 cm^3 they were routinely passaged. Starting at passage 1, NMRI*:nu/nu* mice were used for further experimentation. The aim of this procedure was to reach a stable and passageable xenograft growth in the less immunosuppressed NMRI*:nu/nu* mice.

Starting at passage 0 (P0), samples of tumor xenograft material were snap frozen in liquid nitrogen and stored at -80°C for further experimentation. Fresh tissue was also collected and immediately fixed in formalin to be later processed to formalin fixed, paraffin embedded (FFPE) blocks for histopathological evaluation.

2.2.2 Chemosensitivity testing of the PDX

The sensitivity of the PDX regarding three cytostatic agents, one angiogenesis inhibitor and two EGFR-inhibitors was determined *(Table 3)*. Groups of five mice were randomized to receive either solvent as control or one of the respective substances. Tumors of low passages were used (between P3 and P5) and treatment was started at palpable tumor size of approx. 5 x 5 x 5 mm.

The injection volume was 0.2 mL/20 g body weight. *Table 3* summarizes the treatments used in this characterization.

Table 3: Treatment schedules used for determining the sensitivity profile of the PDX. Application route, schedule and dose used are summarized. Application route: i.p. = intraperitoneal; p.o. = per os, orally. Schedule: Q*A*D*x*B – every *A* days, for *B* cycles; BIW=twice a week.

Treatment	Application route	Schedule	Dose [mg/kg/inj.]
NaCl	i.p.	QDx5	
5-FU	i.p.	Q7Dx2	100
Irinotecan	i.p.	QDx5	15
Oxaliplatin	i.p.	QDx5	5
Avastin	i.p.	BIWx2	5
Erlotinib	p.o.	QDx5x4	50
Cetuximab	i.p.	Q7Dx2	50

Tumor size was measured twice weekly in two dimensions using calipers (see *2.2.1*). The body weight of the mice was determined twice weekly and the change in body weight (BWC) given as a percentage was used as a measure of toxicity. The animals were observed for a period of four weeks after first treatment or until the TV of the control group reached a size of approx. 1.5 cm^3.

For evaluation of therapeutic efficacy, the ratio of the mean TV of the treated group (T) and the control group (C) was expressed as the T/C-value in percentage. The optimal T/C-value (optT/C) was chosen for final evaluation. The following sensitivity scores were used: negative =T/C>50%; +=T/C 36–50%; ++=T/C 21–35%; +++=T/C 6–20%; ++++=T/C≤5%. Subsequently, a two-tailed ANOVA-test was used to verify if the treated group was statistically different from the respective control group.

Antitumor activity was also defined on the basis of the Response Evaluation Criteria in Solid Tumors (RECIST) [185]. To assess the relative tumor volume (RTV) the TVs at

three weeks of treatment were related to the first treatment day. Tumor growth of ≥ 20% (hence, an RTV > 1.2) was classified as progressive disease (PD), analog as it would be in a clinic situation. An RTV of 0.7-1.2 was classified as stable disease (SD), an RTV lower than 0.7 (30% decrease of TV due to treatment) was classified as partial response (PR) and a complete disappearance of the tumor was classified as complete response (CR).

2.2.3 Generation of cetuximab-resistant PDX sub-lines

In order to address mechanisms of cetuximab resistance, two cetuximab sensitive PDX were chosen and chronically treated with cetuximab for 10 passages in order to generate PDX sub-lines resistant to the substance. Co7596 (which initially had an optT/C of 0.7%) and Co10718 (which initially had an optT/C of 23%) were chosen. Co10718 is not part of the PDX collection established for this study, it was characterized during a similar project. Groups of five tumor bearing mice were initially treated with 50 mg/kg cetuximab once a week, and control animals received vehicle. The TVs were evaluated after every treatment. When PDX in one of the groups reached a TV ≥ 1.5 cm^3, PDX were passaged. In the initial passages, the cetuximab dose remained stable in the treated group and treatment was stopped when tumor growth was inhibited by more than 50% in comparison to the last measurement or PDX tumors were ≤ 0.2 cm^3. Gradually, the cetuximab dose was raised to 75 mg/kg and later to 100 mg/kg. For every passage of the cetuximab treated group, the individual PDX that reached the highest RTV (normalized to the TV on the first treatment day) was chosen for passage. In the case that the tumor material from the mouse with the highest RTV was not suitable for transplantation (necrotic, cystic or unsterile tumors), it was replaced by another tumor from the same treated group, opting for PDX with the higher TVs or RTVs. For the control group, individual tumors were chosen, whose TVs and RTVs were in the middle of the range of values. The corresponding untreated PDX was passaged in parallel as control. PDX tissue samples from every passage were taken and immediately shock frozen in liquid nitrogen and stored at -80°C. *Figure 3* exemplarily describes the procedure used for the generation of PDX Co7596_cetux. The same procedure was used to generate Co10718_cetux.When the PDX subline chronically treated with cetuximab reached comparable growth rate as the untreated PDX, the PDX was propagated to 10 mice and tumors were again characterized regarding their sensitivity to cetuximab. This step was undertaken to corroborate, that PDX specifically resistant to cetuximab and not just faster growing PDX were selected during the passaging process.

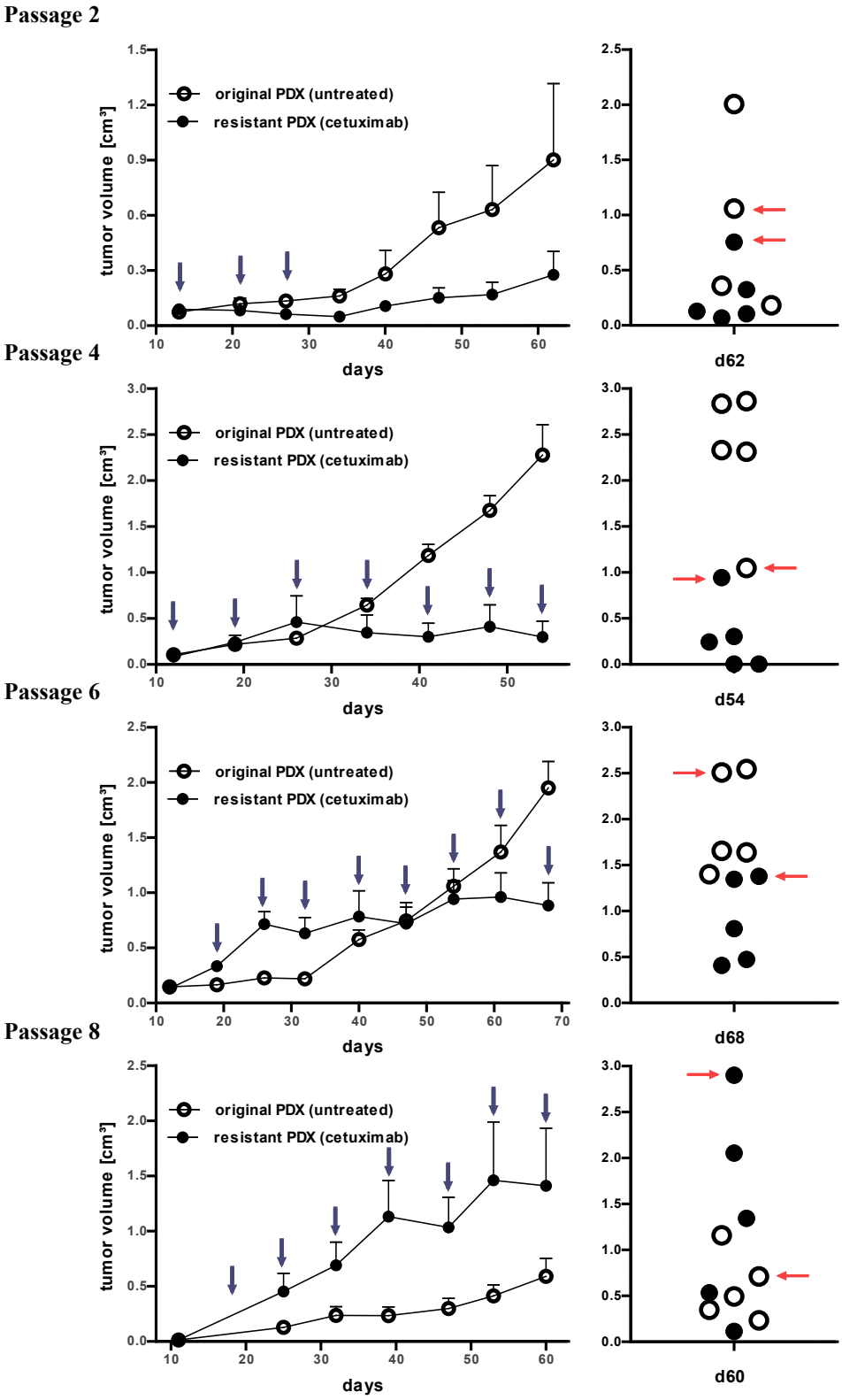

Figure 3: Experimental procedure used to generate the cetuximab-resistant PDX subline Co7596_cetux. Growth curves from even passages are depicted on this graph. Groups of 5 tumor bearing mice were treated chronically with cetuximab for several passages. The PDX with the highest RTV / TV was passaged and underwent chronic treatment as well. Corresponding untreated PDX were passaged as control. The blue arrows represent days, treatment was administered. Red arrows point to the individual tumor chosen for passaging.

2.2.4 Genetic analysis of PDX

2.2.4.1 Total DNA extraction from tissues

The isolation of total DNA from xenograft tissue samples and patient samples was carried out using a commercial purification column-based kit from QIAGEN (DNeasy Blood and Tissue Kit) following the manufacturer's instructions. Tissue pieces of app. 3 x 3 x 3 mm in size were lysed overnight at 56°C on a Thermomixer (Eppendorf) in ATL buffer (supplied with the kit). In the final step DNA was eluted from the column using 200 µl of distilled H_2O.

The DNA concentration was measured by NanoDrop at 260 nm, assuming that an A_{260} absorbance value of 1.0 corresponds to a concentration of 50 µg/µl. The ratio of the absorbance at 260 and 280 nm ($A_{260/280}$) was used to assess sample purity. The samples with a ratio between 2.0 and 2.2 were chosen for further analysis.

2.2.4.2 DNA sequencing

The DNA samples from selected patients and all 49 established PDX (see *2.2.1*) were analyzed with the Illumina TruSeq® Amplicon – Cancer Panel, which targets 212 amplicons from 48 oncogenes in a multiplexed one-tube reaction. All reagents were supplied in the TruSeq® Amplicon – Cancer Panel Kit (Catalog#FC-130-1008) from Illumina. Then, 250 ng of high quality genomic DNA ($A_{260/280}$ = 1.8 - 2.0) were hybridized to a custom pool of oligos specific to the targeted regions of interest on a hybridization plate. Unbound oligos were removed using a filter capable of size selection by repeated washing. Afterwards, extension-ligation of bound oligos was performed, which resulted in the formation of products containing the regions of interest flanked by sequences required for amplification. The extension-ligation products were amplified using primers that add index sequences for sample multiplexing as well as common adapters required for cluster generation. This step was followed by library normalization, to ensure equal representation of each sample in the pooled library. For cluster generation and sequencing, equal volumes of normalized library (including control DNA) were combined, diluted in hybridization buffer and heat denatured prior to MiSeq sequencing.

MiSeq sequencing was carried out on Illumina MiSeq Desktop Sequencer, which relies on sequencing by synthesis. The library fragments act as a template, and as fluorescence labeled nucleotides incorporate into the growing DNA strand, they are digitally recorded as

sequence. Illumina Variant Studio 2.1 was used for sample analysis. For correlation analysis, known SNPs were excluded and only somatic mutations, which occur with an allelic frequency > 5 % were considered.
One sample from all established 49 PDX was analyzed. For the models Co9587, Co9775 and Co10925, corresponding patient tumor and normal tissue, as well as tissue from the first 3 - 5 passages was sequenced, as well as tissue from the cetuximab-resistant sub-lines Co7596_cetux and Co10718_cetux.
This analysis was carried out by Dr. Annika Wulf-Goldenberg.

2.2.4.3 Gene Copy Number Analysis

Gene deletion and gene duplication are genomic variations that can affect cell function or phenotype. Gene copy number of BRAF, EGFR, KRAS, NRAS and c-MET was analyzed in the PDX samples using real-time quantitative PCR with commercial TaqMan® Copy Number Assays and a TaqMan® Copy Number Reference Assay from Applied Biosystems (*Table 4*). The Copy Number Assay contains two primers and a FAM™ dye-labeled minor groove binder (MGB) probe to detect the genomic DNA target gene or genomic sequence of interest, and the Reference Assay containing two primers and a VIC® dye-labeled TAMRA™ probe to detect a genomic DNA reference sequence that is known to exist in two copies in a diploid genome (for this analysis the human RNaseP H1 RNA gene was chosen).
20 ng of high quality genomic DNA ($A_{260/280}$ = 1.8 - 2.0) was combined with the TaqMan® Copy Number Assay, TaqMan® Copy Number Reference Assay, and TaqMan Universal PCR Master Mix, without Amperase. The real-time PCR reaction was set up on the Applied Biosystems Real-Time PCR System StepOnePlus™ using universal PCR cycling conditions: 95°C for 10 min as a denaturation step, followed by 40 cycles of 95°C for 15 s for denaturation and an annealing/ extension step at 60°C for 1 min. The number of copies of the target sequence in each test sample was determined by relative quantitation (RQ) using the comparative threshold cycle (ΔC_T) method [186]. This method measures the C_T difference (ΔC_T) between target and reference sequences, and then compares the values of test samples to a calibrator sample known to have two copies of the target sequence ($\Delta\Delta C_T$), calculates $RQ = 2^{(-\Delta\Delta CT)}$ and the copy number of the target is calculated to be two times the relative quantity. Applied Biosystems CopyCaller™ Software was used for post-PCR data analysis of copy number quantitation experiments.

Table 4: Assays from Applied Biosystems used to analyze copy number of BRAF, EGFR, KRAS. NRAS and c-MET in the PDX samples

Assay	Assay ID number
TaqMan® Copy Number Assay, BRAF	Hs04988196_cn
TaqMan® Copy Number Assay, KRAS	Hs06949804_cn
TaqMan® Copy Number Assay, EGFR	Hs04960197_cn
TaqMan® Copy Number Assay, c-MET	Hs04992084_cn
TaqMan® Copy Number Assay, NRAS	Hs05807163_cn
TaqMan® Copy Number Reference Assay, human, RNase P	

2.2.5 Gene expression analysis in PDX

2.2.5.1 Total RNA extraction from tissues

The isolation of total RNA from xenograft tissue samples was carried out using a commercial purification column-based kit from QIAGEN (RNeasy Mini Kit) following the manufacturer's instructions. Tissue pieces of app. 3 x 3 x 3 mm in size were lysed with the TissueLyzer from QIAGEN (3 min, 15 Hz) and the RNA was eluted from the column using 50 µl of H_2O.

The RNA concentration was measured by NanoDrop at 260 nm, assuming than an A_{260} absorbance value of 1.0 corresponds to a concentration of 40 µg/µl. The ratio of the absorbance at 260 and 280 nm ($A_{260/280}$) was used to assess sample purity.

2.2.5.2 cDNA synthesis

A commercially available Kit was used to generate cDNA from the RNA samples obtained in *2.2.5.1*. The Reverse-Transkriptase-Kit (Applied Biosystems) was used according to manufacturer's instructions to generate a master mix or 1x RT-buffer, containing 500 µM dNTP's, 5.5 mM $MgCl_2$, 2.5 µM random hexameres, 0.4 U/µl RNase inhibitor und 1.25 U/µl MultiScribe-Reverse-Transkriptase. 200 ng of high quality RNA ($A_{260/280}$ = 1.8 - 2.0) were diluted in 10 µl 1xRT-buffer and the RT-PCR reaction was conducted at 25°C for 10 min, 48°C for 30 min und 95°C for 5 min. If not used immediately, the products were stored at -20°C.

2.2.5.3 Gene expression analysis using real-time PCR

The expression of several EGFR ligands (AREG, BTC, EGF, EREG and TGFα), as well as the EGFR receptor family (HER1 - HER4) was analyzed in the cDNA using real-time PCR with commercially available, pre-designed TaqMan® gene expression assays (*Table 5*). Each assay includes a single FAM™ dye-labeled TaqMan® probe with a minor groove binder (MGB) moiety and two unlabeled oligonucleotide primers. 200 ng of cDNA, TaqMan® Fast Master Mix and TaqMan® Gene Expression Assays were combined in a total volume of 20 µl according to manufacturer's instructions. The real-time PCR was carried out on a StepOnePlus™ System and was conducted at 95°C for 20 s as a denaturation step, followed by 40 cycles of 95°C for 1 s for denaturation and an annealing/extension step at 60°C for 20 s. For every sample the cDNA of interest was run in duplicate and an assay for a house keeping gene sequence (for this study β-actin was chosen) was run in duplicate as well.

For the analysis, the obtained fluorescence based amplification plots were evaluated with the StepOne™ Software Version 2.3. The baseline was set between cycles 3 and 15 and a threshold value of 0.2 was chosen for the used to determine the C_T. C_T of the gene of interest was normalized to the C_T of β-actin and the ΔC_T-values were used to compare the expression between samples. High C_T-values, hence a high ΔC_T, point to a low concentration of the cDNA of interest in the sample.

Table 5: Gene expression assays from Applied Biosystems used to analyze the expression of the EGFR receptor family molecules (HER1 – HER4) and selected EGFR ligands in the PDX samples

Assay	Assay ID number
TaqMan® Copy Number Assay, AREG	Hs 00155832_m1
TaqMan® Copy Number Assay, BTC	Hs 01101203_m1
TaqMan® Copy Number Assay, EGF	Hs 00153181_m1
TaqMan® Copy Number Assay, EREG	Hs 00154995_m1
TaqMan® Copy Number Assay, TGFα	Hs 00177401_m1
TaqMan® Copy Number Assay, EGFR	Hs 00193306_m1
TaqMan® Copy Number Assay, HER2	Hs01001582_m1
TaqMan® Copy Number Assay, HER3	Hs00951455_m1
TaqMan® Copy Number Assay, HER4	Hs00171783_m1
TaqMan® Copy Number Assay,ACTB	Hs 99999903_m1

2.2.6 Biochemical analysis

2.2.6.1 Paraffin embedding and sectioning of tissue samples

Freshly dissected tissue (ca. 5 x 5 x 5 mm) was fixed with 10% formalin for 24 - 48 h at room temperature (RT). Subsequently the paraffin embedding of the PDX samples was carried out by the Haider lab in Berlin. Shortly, the tissue was dehydrated with ethanol, incubated in xylene and several changes of paraffin and finally embedded in paraffin in a tissue embedding cassette. The paraffin tissue blocks can be stored at RT for years.
To prepare staining sections the paraffin-embedded tissue block was sectioned at 5 - 8 µm thickness on a microtome and the sections were floated in a 40°C water bath containing distilled water to be transferred onto glass slides suitable for immunohistochemistry. Slides were allowed to dry overnight and at RT.

2.2.6.2 Deparaffinization, rehydration and antigen retrieval of paraffin sections

For deparaffinization slides were incubated in Roticlear I Solution and then in in Roticlear II solution (both from Roth), both for 8 min. Then, the slides were immersed in two changes of 96% ethanol for 2 min, rehydrated in descending ethanol (80%, 70%) and incubated for 30 s in tap water.
For antigen retrieval slides were placed in Coplin jars with citric acid buffer (10 mM Citric Acid, 0.05% Tween 20, pH 6.0) at 95 - 100°C, cooked for 10 min in a microwave and allowed to cool down to RT for 40 - 45 min.

2.2.6.3 HE staining

HE staining was performed for patient and corresponding PDX tissue. Shock frozen tissue was cut in 4 - 5 µm sections and slides were stored at -20°C until use. Slides from paraffin blocks were prepared as described in *2.2.6.2*. Shock frozen tissue sections were fixed in 96% ethanol for 5 min prior to staining.
In the following step, specimens were stained with hematoxylin for 5 min and washed with deionized water. This was followed by 5 min incubation with eosin. After that sections were differentiated with 70% ethanol and submitted to incubation in ascending concentrations of ethanol (70%, 80%, and 95%). Finally the sections were mounted with xylene.
Pictures were taken using an Axioskop 40 and the software *AxioVision 4.5* (Zeiss).

2.2.6.4 Immunohistochemical / immunofluorescent staining

Human nuclei staining

After antigen retrieval on FFPE specimens, slides were washed in phosphate buffered saline (PBS) and permeabilized in 0.1% Triton-X for 7 min. After a further PBS wash step, slides were incubated with a Cy3-labeled Anti-Nuclei antibody from Merck Millipore (dilution 1:300), 1 h at 37°C in a humid chamber. Slides were then washed for 20 min in PBS and mounted in a 1:1 mixture of glycerol and PBS containing 5 µg/ml DAPI. This antibody stains nuclei of all human cell types resulting in a diffuse nuclear staining pattern.

Immunofluorescence (IF) staining for EGFR

Frozen sections were dried at RT and fixed with 4% formalin for 20 min. After a 5 min washing step in PBS, sections were blocked with 20% goat serum for 30 min at RT and again washed in PBS. Anti-EGFR antibody (Santa Cruz) was applied to the slides for 1 h at RT in a 1:75 dilution. Sections were then washed in PBS for 20 min and incubated with a Cy3-labeled goat-anti rabbit secondary antibody (Dianova) for 1 h at RT in a 1:800 dilution. After that the slides were washed with PBS for 20 min and mounted in a 1:1 mixture of glycerol and PBS containing 5 µg/ml DAPI.

Immunohistochemical (IHC) staining for EpCAM, Ki-67 and p53

Frozen sections were dried at RT and fixed with 4% formalin for 20 min. After a 5 min washing step in PBS, sections were blocked with Peroxidase block according to manufacturer's instructions, washed in PBS and blocked with a Streptavidin-Biotin block (both from Vector Laboratories) according to manufacturer's instructions. Afterwards the sections were blocked with 20% goat serum for 30 min at RT. In the next step, the slides were incubated with the primary antibodies. As the antibodies used were monoclonal with mouse as host, all antibodies were biotinylated prior to use in order to avoid cross reaction from the secondary antibody with the murine fraction of the PDX. The Animal Research Kit from Dako was used according to manufacturer's instructions for this procedure. The slides were then incubated with the primary antibodies: p53 antibody (1:50, overnight, 4°C), Ki-67 antibody (1:50, 2 h, RT), both from DAKO, or EpCAM antibody (1:200, 2 h, RT) from Enzo Life Sciences and washed in PBS for 20 min. After that incubation with horse radish peroxidase (HRP) labeled streptavidin (1:800, 20 min, RT) was carried out.

After that staining was visualized with 3,3'-Diaminobenzidine (DAB) substrate (Dako) according to manufacturer's instructions and the sections were counterstained with hematoxylin. Finally the slides were mounted with VectaMount® Aqueous Mounting Medium.

2.2.6.5 Protein isolation from PDX tissue

Protein lysates were generated from PDX tissue in order to analyze the concentration of EGFR and its ligands AREG, BTC, EGF, EREG and TGFα in the samples. Pieces of tissue of app. 4 x 4 x 4 mm were homogenized with a pistil in 200 µl T-PER™ Tissue Protein Extraction Reagent (Life Technologies) supplemented with protease and phosphatase inhibitors (Sigma-Aldrich). Then, samples underwent three freeze and thaw cycles and centrifuged for 15 minutes at 4°C at 13000 x g to separate the tissue debris from the protein. The supernatants were handled on ice from this point on or stored at -80°C if not to be used immediately.
The protein concentration in the PDX protein lysates was measured with the Bio-Rad Protein Assay (Bio-Rad) and a BSA standard curve on a microplate reader according to manufacturer's instructions.

2.2.6.6 Enzyme Linked Immunosorbent Assay (ELISA)

Commercial ELISA assays (R&D Systems and USCN Life Science) that use the "sandwich" ELISA method, were chosen to measure the concentration of EGFR and its ligands in protein lysates from PDX tissues. The Sandwich ELISA quantifies antigens between two layers of antibodies (capture and detection antibodies directed towards different epitopes of the target molecule), which makes this method highly efficient for antigen detection, especially important when measuring molecules that are at a low concentration in the samples.
Prior to analysis, protein concentration was measured and adjusted with PBS to 4 µg/µl and each sample was diluted 1:5 with Reagent Diluent (1% BSA in PBS, pH 7.2) for the analysis of the ligands and 1:50 for the analysis of EGFR. Experiments with selected PDX samples were undertaken prior to this measurement to find the appropriate protein concentration of the sample in order to work were in the dynamic detection range of the assays and rule out murine background.

The DuoSet® ELISA Assays to measure the concentration of EGFR, AREG, BTC, EGF, EREG and TGFα were used according to manufacturer's instructions. 96-well Maxi-Sorp® plates were coated with the capture antibody and incubated at RT overnight. Plates were washed with wash buffer (0.05% Tween in PBS, pH 7.2) and blocked with reagent diluent for 1 h. Following, samples were applied to the plate and incubated. A biotinylated secondary antibody was applied and incubated for 2 h. Subsequently, the plate was incubated with HRP-labeled streptavidin and a chromogen substrate (R&D Systems) was applied and incubated for 15 min in a dark chamber. The reaction was stopped with 2 N H_2SO_4. All steps were performed at RT and the plate was washed 4 times with wash buffer after every step. All plates contained a standard curve with at least seven known concentrations of the molecule of interest.

For the analysis of epiregulin concentration a sandwich ELISA system from USCN Life Science was used. The assay contained a 96-well plate pre-coated with the capture antibody. The kit was used according to manufacturer's instructions and samples were incubated on the plate at 37°C for 2 h.

The optical density of each well was determined using a microplate reader set to 450 nm with a wavelength correction at 540 nm.

For the calculation of the concentration of the molecules analyzed, standard curves were calculated using a four-parameter curve fit with the software Graph Pad Prism 5. A threshold was calculated for every set of samples evaluated, and only samples with a higher OD were regarded as positive. The threshold was calculated as follows:

$$CutOff = \mu\,(blank\ values) + 3 \bullet \sigma\,(blank\ values)$$

$$\mu = average;\ \sigma = \text{standard deviation}$$

The calculated concentrations were then normalized to the total protein concentration in the samples.

All samples were measured in duplicate. For the measurement of the cohort, tissue from three different PDX (preferably from different passages) was analyzed (n = 3). For the comparative measurements of the cetuximab resistant PDX, tissue from all mice of the passage chosen was analyzed (n = 5).

2.2.6.7 Statistical analysis

All statistical analyzes were performed with Graph Pad Prism 5.

For the response evaluation in the sensitivity characterization, two way ANOVA testing was used. A p value of < 0.05 was considered as statistically significant.

Correlation analysis was performed as Spearman rank-order correlation with a two tailed p-value. The Spearman Rho (r_S), as well as the obtained p values were taken into account to evaluate the strength of possible correlations. A p-value of < 0.05 was considered as significant.

Statistical analyzes were also performed to compare the generated cetuximab resistant PDX sub-lines with their sensitive counterparts regarding the expression of the EGFR receptor family and its ligands, as well as GCNs from key players of the EGFR network. In this case a Mann-Whitney-U-Test was performed. A p-value of < 0.05 was considered as significant.

3. Results

3.1 Standarization of the PDX models

87 surgical samples from CRC patients were transplanted subcutaneously into immunodeficient mice in order to establish a set of PDX representative of this disease. The engraftment and growth behaviour of the PDX was studied and several histological and molecular analyzes of the patient samples and corresponding PDX samples were carried out in order to prove the stability of the models and the resemblance between the original patient samples and the corresponding PDX. These criteria have to be fulfilled in order to use the models for drug screening or translational studies.

First engraftment was measured (P0) when the subcutaneously growing PDX tumors reached a TV of 0.5 cm^3 or higher. The tumors were serially passaged, replacing the NSG mice for NMRI:*nu/nu* mice as hosts. If growth was stably detected until passage 3, this means if tumors reached a TV of 0.5 cm^3 or higher in a comparable or shorter time than the previous passage, the models were considered as passageable.

3.1.1 Histology and analogy to original patient samples

In order to validate that only human tumor cells engrafted, samples of tumor tissue (shock frozen or FFPE) were taken from every passage. HE staining of patient primary tumor tissue paired with corresponding PDX tissue were carried out and evaluated by a pathologist *(Figure 4a,b)*. This evaluation revealed that all of the patient samples that yielded stably passageable PDX were staged as adenocarcinomas and the PDX derived thereof displayed adenocarcinoma-like histology. Immunofluorescence (IF) staining of samples of the PDX models was performed with an antibody that specifically detects human nuclei *(Figure 4c)*. When the IF and HE staining was compared, it was observed, that the cells in the PDX that build the adenocarcinoma-like structures were human and the surrounding stroma was murine. Macroscopic observation of a tendency towards a higher ratio of proliferating tissue in a PDX compared to the patient sample was observed. This observation was confirmed by Ki-67 and proliferating-cell-nuclear antigen (PCNA) staining of selected PDX and demonstrated, that mainly epithelial tumor cells were proliferating, while murine stroma was largely mitotically inactive *(Figures 4a,b and 5)*.

In order to further confirm the origin of the adenocarcinoma-like cells in the PDX tissue, samples were stained for EpCAM (epithelial cell adhesion molecule), which is exclusively expressed in epithelia and epithelia derived neoplasms [187]. In all PDX samples, EpCAM was detected in the same cells that were recognized as human by the anti-nuclei IF staining. The *Figure 4* shows the above mentioned staining for four representative PDX models (two PDX derived from primary tumors, and two different metastases from liver and lung) and demonstrates that a PDX tumor tissue is composed of human tumor cells. The stroma cells are of murine origin, which replaced the human stroma cells.

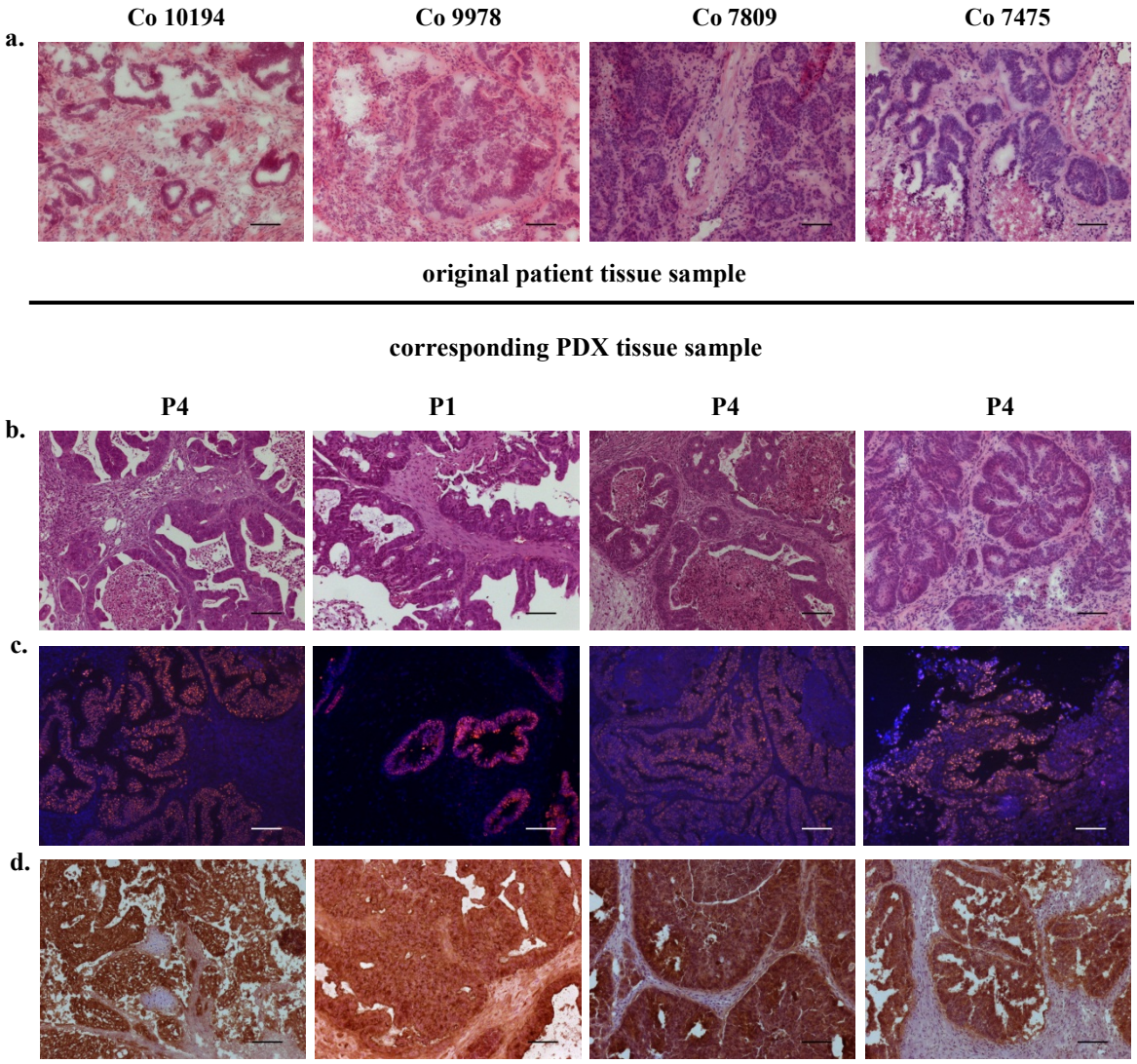

Figure 4: Staining of the original patient tissue paired to the corresponding PDX tissue. Representative patient/PDX pairs were chosen: Co10194 is derived from a primary colon carcinoma samples, Co9978 from a rectum sample, Co7809 was derived from a liver metastasis and Co7475 is derived from a lung metastasis. **a.** HE staining of original patient tissue; **b.** HE staining of PDX tissue; **c.** IF staining for human nuclei, DAPI=blue; human nuclei=orange (Cy3); **d.** IHC staining for EpCAM. Scale bar represents 100µm.

Only PDX in which human tumor cells were detected by positive staining for human nuclei and EpCAM, that retained adenocarcinoma histology as confirmed by a pathologist were regarded as established CRC PDX.

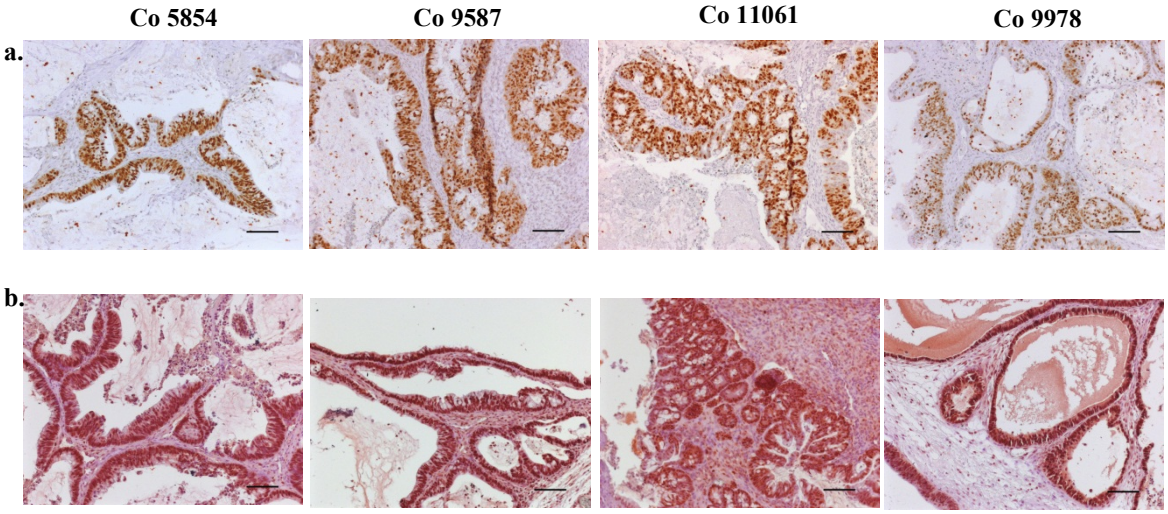

Figure 5: Ki-67 and PCNA staining of representative PDX models. **a.** IHC staining for Ki-67 **b.** IHC staining for PCNA. Scale bar represents 100 µM

3.1.2 Stability of histology and genetic profile of the PDX models in serial passages

Stability and therefore comparability of the PDX models with the primary tumor tissue is important in order to obtain reproducible results and use the PDX as a preclinical tool for studying CRC. Thus, it had to be confirmed, that the histological and molecular characteristics of the PDX stay unchanged through the passaging process. Therefore samples from serial passages of PDX tumors, paired with corresponding patient tissue, were evaluated regarding their histology and genetic profiling.

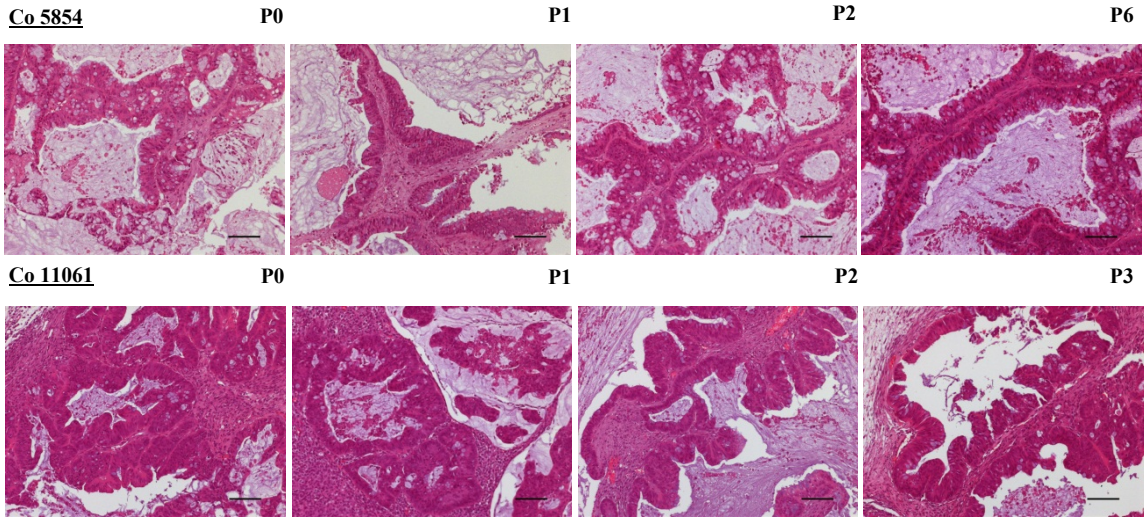

Figure 6: Representative HE staining of consecutive passages of PDX Co5854 and Co11061 demonstrate that the phenotype reflects the features of human colorectal adenocarcinoma. Scale bar represents 100 µm.

The phenotype of the adenocarcinoma histology, assessed by HE staining, was confirmed in several passages of the respective PDX. The expression of selected key biomarkers for colorectal carcinoma (EpCAM, mentioned in *3.1.1*, p53 and EGFR) were studied in serial passages by IHC or IF *(Figures 6 and 7)*.

Figure 6 shows HE staining of consecutive passages of two representative PDX models. In these two examples, as well as in all other established PDX models, the histopathological phenotype remained stable through the passages. In order to confirm these observations, presence of the human marker proteins EpCAM, p53 (IHC) and EGFR (IF) were evaluated. The expression of these molecules was similar in PDX tissue samples originating from different passages of the same PDX model *(Figure 7)*.

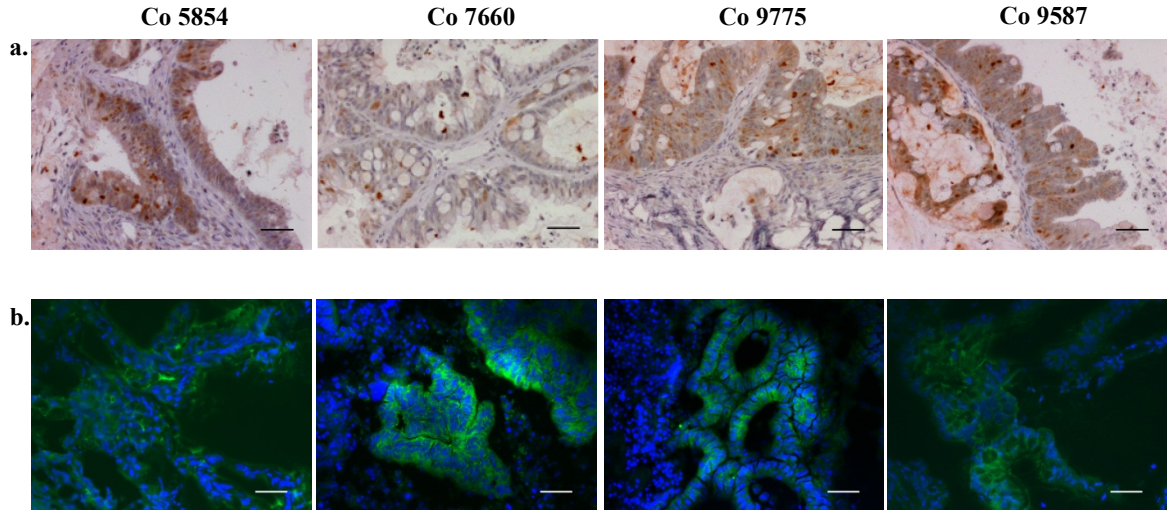

Figure 7: a. IHC staining for p53 for representative PDX models. **b.** IF staining for EGFR for representative PDX models. Scale bar represents 50µm.

To further evaluate if the PDX models were representative for the patient tissue they were derived from, and if their characteristics were stable along the passages, the genetic profile of three representative models was analyzed. A sample of patient tumor tissue, paired with a sample of normal tissue from the same patient, as well as tissue from at least three different passages of the respective PDX model, were sequenced using the TruSeq® Amplicon – Cancer Panel, where 48 oncogenes are targeted with 212 amplicons *(Table 6)*. The oncogenes targeted are listed in *Annex I*.

Table 6: Patient tumor and matched normal tissue, paired with tissue from different, sequential passages of the corresponding PDX models was sequenced using the TruSeq® Amplicon – Cancer Panel. 212 amplicons in 48 oncogenes were targeted. The results obtained for the main oncogenes are summarized in this table.

	Mutation detected (alternate variant frequency [%], AA mutation)							
Patient or PDX, passage	***APC***	***BRAF***	***EGFR***	***KRAS***	***MET***	***PIK3CA***	***PTEN***	***TP53***
Co 9587, *normal tissue*	-	-	-	-	-	-	-	-
Co 9587, *patient tumor*	n.a.	n.a.	n.a.	n.a., G12D	n.a.	n.a.	n.a.	n.a.
Co 9587, P0	59, ins 1554; 30, R876X	-	-	51, G12D	-	51, del 104	-	-
Co 9587, P1	57, ins 1554; 29, R876X	-	-	50, G12D	-	49, del 104	-	-
Co 9587, P2	58, ins 1554; 29, R876X	-	-	48, G12D	-	50, del 104	-	-
Co 9587, P3	72, ins 1554; 33, R876X	-	-	56, G12D	-	49, del 104	-	-
Co 9587, P4	65, ins 1554; 22, R876X	-	-	45, G12D	-	49, del 104	-	-
Co 9775 *normal tissue*	-	-	-	-	-	-	-	-
Co 9775, *patient tumor*	-	-	-	5, G12D	-	-	-	4, G245S
Co 9775, P0	-	-	-	63, G12D	-	-	-	99, G245S
Co 9775, P1	-	-	-	42, G12D	-	-	-	95, G245S
Co 9775, P3	-	-	-	57, G12D	-	-	-	99, G245S
Co 9775, P4	-	-	-	63, G12D	-	-	-	99, G245S
Co 10925 *normal tissue*	-	-	-	-	-	-	-	-
Co 10925, *patient tumor*	39, E1379X	-	-	-	-	-	-	-
Co 10925, P1	97, E1379X	-	-	-	-	-	-	-
Co 10925, P2	96, E1379X	-	-	-	-	-	-	-
Co 10925, P4	97, E1379X	-	-	-	-	-	-	-

n.a. = not analysed due to poor DNA quality

No mutations in the 48 targeted oncogenes were detected in the normal patient tissue samples. Mutations in the genes APC, KRAS, PIK3CA and TP53 were detected in the patient tumor tissue and all analyzed passages of the matched PDX tissue. The mutations found in PDX tissue were congruent with the ones found in patient tumor tissue, no gain or loss of mutations was observed through the xenografting process. The ratio of mutated DNA (alternate variant frequency) in the PDX samples was usually around 50% or 100%, reflecting a hetero- or homozygote genotype concerning those genes. The ratio of mutated DNA was lower in the patient tumor samples analyzed. As can be observed in *Figure 4*, the PDX tissue displayed a higher ratio of tumor cells and the stroma was of murine origin. Thus, only the DNA of the human tumor cells was targeted in these PDX by the TruSeq® Amplicon – Cancer Panel. The patient tissue did not undergo micro-dissection, due to the

already very limited tissue available before xenotransplantation. For the method applied, a micro-dissection of PDX tissue is optional, as shown by the results in *Table 6*.

3.1.3 Proliferation and engraftment rate of the PDX models

A further requirement for a PDX model is stable passaging. Since this set of PDX models was intended to be used for drug screening in the future, also a stable engraftment in NMRI*:nu/nu* mice was an essential prerequisite.

After transplantation of patient tissue in NSG mice, a positive engraftment was defined by TV of 0.5 cm³. This initial engraftment (P0) required between 18 and 90 days. The average duration of an initial engraftment (TV = 0.5 cm³) was 49.4 ± 19.5 days. In the passages P1 to P2, the PDX were transplanted to NMRI*:nu/nu* mice, since this strain has a higher tolerability for cytotoxic substances, a characteristic relevant for the chemosensitivity testing experiments anticipated for these models.

In case of a positive engraftment in NMRI*:nu/nu*, this mouse strain was preferred for further passaging. For all the established PDX models a stable engraftment in NMRI*:nu/nu* was achieved by passage P2. A tendency towards an increase of growth ratio between passages P0 and later passages was observed in some of the models (see *Figure 8*). This difference can be explained by the fact that the original patient tissue contained different amounts of vital tumor tissue available for xenotransplantation. By contrast, reproducibly and almost exclusively vital tumor tissue could be prepared and used for transplantations for the serial passages from mouse to mouse. The growth rate (as well as ratio of human tissue) was then similar amongst passages higher than P2. PDX in passages P3 to P5 were used for the characterization experiments carried out in NMRI*:nu/nu* mice. In these passages the time for the PDX to reach a TV = 0.5 cm³ was 32.0 ± 10 days.

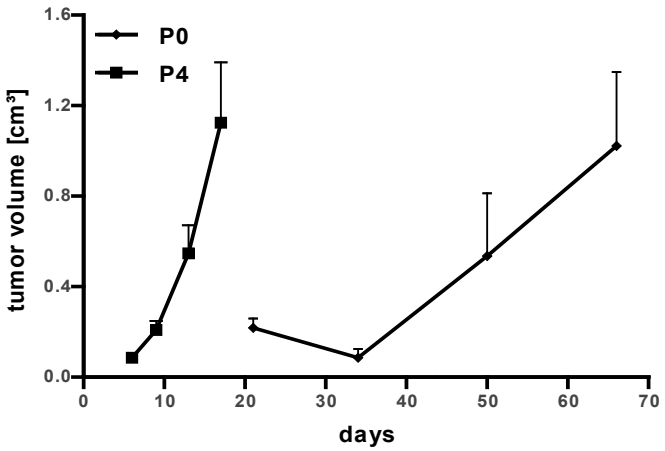

Figure 8: Growth curves of P0 and P4 of CRC PDX Co10377. This graph summarizes the results of two independent experiments.

Figure 9 summarizes the tumor doubling times (TDTs) of the 49 PDX models that were established (see also *Annex II*). The mean TDT of the CRC PDX in passages between P3 and P5, used for the chemosensitivity characterization experiments, was 9.96 ± 4.73 days. The TDT values were distributed among a rather wide range between 2.5 and 30.5 days; nevertheless, the TDT of half of the models lied in a moderate range of 7.1 to 11.7 days.

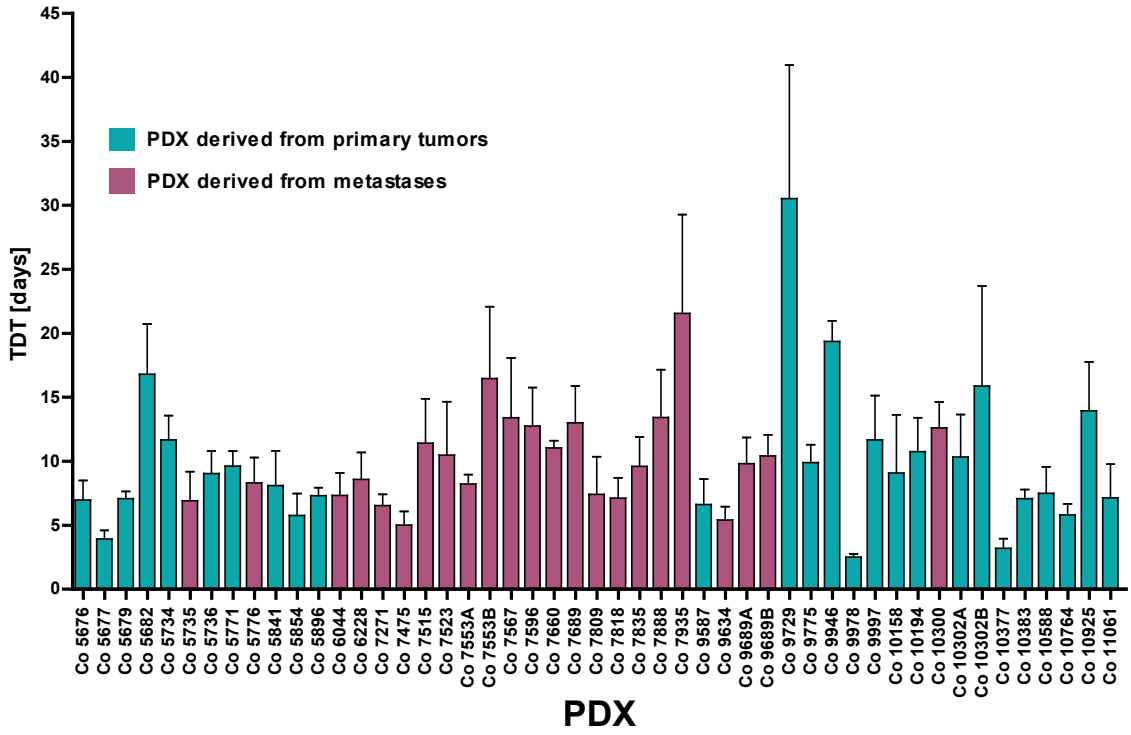

Figure 9: The tumor doubling times (TDT) of the PXD models are summarized in this graph. The tumor doubling time was measured once the models were considered as stably passageable or established.

When the TDT from PDX derived from primary tumor samples versus PDX derived from metastases (see *Tables 7* and *8*) were compared, no significant differences were determined. There were also no significant differences in the growth ratio between primary tumors that already formed metastases at time of tissue collection or did not so (M0 vs. M1). Also when the TDTs of the PDX were grouped according to their site of tumor origin (colon vs. rectum), no significant differences were observed neither in the PDX derived from primary tumors nor metastases. There was also no significant difference in the TDT between PDX derived from metastasis of the liver or lung. The grading of the tumor tissue was obtained for 33 patient samples, from which 21 were G2 and 12 were G3. Also this criterion had no impact on the growth ratio of the PDX models.

Finally the following characteristics had to be fulfilled in order for a PDX model to be regarded as established:

- positive detection of human cells in the tumor PDX tissue
- resemblance between original patient tumor tissue and PDX tumor tissue demonstrated by adenocarcinoma-like histology assessed in both by a pathologist
- expression of EpCAM (and other biomarkers of CRC) in PDX tumor tissue
- stable passageability of PDX in NMRI*:nu/nu* mice.

Of 87 patient samples that were transplanted, 49 fulfilled these criteria, representing an engraftment rate of 56%.

3.1.4 General characteristics of the patients

Clinical data of those patients whose tumor tissue yielded stably passageable PDX was available. Only main relevant characteristics could be gathered for reasons of patient's privacy. *Table 7* summarizes the distribution of the characteristics of the patients whose tissue showed a positive engraftment.

Table 7: Summary of patient characteristics for the corresponding engrafted PDX.

	Number	ratio of PDX [%]
Patients	**44**	
male	*28*	
female	*16*	
generated PDX	**49**	
PDX derived from colon carcinoma	**27**	**55**
PDX derived from rectum carcinoma	**22**	**45**
PDX derived from primary tumors	**26**	**53**
PDX derived from metastases	**23**	**47**
liver	*11*	**22**
lung	*11*	**22**
lymph node	*1*	**2**

Table 8 summarizes the main clinical data of the patients. Male patients were higher represented in this set of 49 PDX (61%). The ages at resection were between 27 and 81 years.

Table 8: Main clinical data corresponding to the patients whose tumor samples yielded passageable PDX.

PDX	Patient characteristics		Tumor sample characteristics					
	Gender	Age	TNM-Status	Grading	Classification	Primary site	Metastasis	
							Type	Site
Co 5676	f	67	T3aN0M0	G2L0V1R0	primary	rectum		
Co 5677	m	71	T4bN1M0	G2L0V0R0	primary	colon		
Co 5679	f	51	T3N2M1	G3L1V1R0	primary	colon		
Co 5682	f	78	T4bN2M0	G2L0V1R0	primary	rectum		
Co 5734	m	79	T3bN0M0	G2L0V0R0	primary	colon		
Co 5735	m	84	T3N0M1	G2	metastasis	rectum	met	liver
Co 5736	f	77	T4N0M0	G2L0V0R0	primary	rectum		
Co 5771	m	49	T3N1M0	G2LxV0R0	primary	rectum		
Co 5776	m	55	yT3N1M1	G3L1V1R0	metastasis	rectum	syn	liver
Co 5841	m	55	T3N2M1	G3L1V1R0	primary	rectum		
Co 5854	f	52	T4N2M0	G3L1V1R0	primary	colon		
Co 5896	m	71	T2N0M0	G2L0V0R0	primary	rectum		
Co 6044	m	53	T4N2M1	G2L0V1R2	metastasis	rectum	syn	lymph
Co 6228	f	60	rpTxNxM1	GxLxVxR0	metastasis	colon	met	liver
Co 7271[1]	f	66	pT2pN1	G3L0V1R0	metastasis	colon	syn	lung
Co 7475	f	68	pT2pN0	G2	metastasis	rectum	met	lung
Co 7515	m	53	pT3 pN0M0	L0V0 R0	metastasis	rectum	met	lung
Co 7523	f	64	pT3pN1cM0	n.a.	metastasis	colon	met	lung
Co 7553A[2]	m	77	T3pN1M0	G3	metastasis	colon	met	lung
Co 7553B[2]	m	77	T3pN1M0	G3	metastasis	colon	met	lung
Co 7567	m	75	pT3pN0M1	R0	metastasis	colon	syn	lung
Co 7596	f	72	pT3NxcM0C2	n.a.	metastasis	rectum	met	lung
Co 7660[1]	f	67	pT2pN1	G3L0V1R0	metastasis	colon	met	lung
Co 7689	f	58	pT3N2M0	G2c	metastasis	rectum	met	lung
Co 7809	m	67	yrp TxNxM1	R0LxVxG3	metastasis	colon	syn	liver
Co 7818	m	68	rpTxNxM1	R0LxVxG2	metastasis	colon	syn	lung
Co 7835	m	75	rpTxNxM1	R0LxVxG2	metastasis	colon	syn	lung
Co 7888	m	73	yrepTxNxM1	R0LxVxGx	metastasis	rectum	syn	liver
Co 7935	m	65	rpTxNxM1	R0LxVxG2	metastasis	rectum	syn	liver
Co 9587	f	80	pT3pN0(0/16)	G2R0L1V0	primary	colon		
Co 9634	f	61	pT3C4pN1C4c	L0V0	metastasis	colon	met	liver
Co 9689A[3]	m	53	pT3pN2cM1	L1V1	metastasis	rectum	met	liver
Co 9689B[3]	m	53	pT3pN2cM1	L1V1	metastasis	rectum	met	liver
Co 9729	m	68	pT3pN1c	G3L1V0	primary	rectum		
Co 9775	m	67	pT3pN2apM1	G2R0L0V0	primary	colon		
Co 9946	m	81	pT4bpN0	G2R0	primary	colon		
Co 9978	f	50	pT4apN1bpM	G2R0L1V1	primary	rectum		
Co 9997[4]	f	27	pT4apN2b	G3R0L1V1	primary	rectum		
Co 10158	m	67	pT4apN0	G2R0L0V0	primary	colon		
Co 10194	m	78	pT3pN0	G2R0L0V0	primary	colon		
Co 10300[4]	f	27	pT4apN2b	G3R0L1V1	metastasis	rectum	syn	liver
Co10302A[5]	m	64	pT4b(m)pN1b	G2RXL1V0	primary	colon		
Co10302B[5]	m	64	pT4b(m)pN1b	G2RXL1V0	primary	colon		
Co 10377	m	50	ypT3ypN0	RxL0V1G2	primary	colon		
Co 10383	m	51	pT2pN0pM1	G3R0L0V0	primary	rectum		
Co 10588	m	72	pT3pN0	G2R0	primary	colon		
Co 10764	m	62	yrpT4bpN1ap	n.a.	primary	colon		
Co 10925	m	73	pT3pN2bcM0	R0	primary	colon		
Co 11061	f	81	pT3pN0	G2R0L0V0	primary	colon		

[1 -5] PDX models were derived from the same patient
syn = synchronous metastasis
met = metachronous metastasis

Regarding the primary tumor site (colon or rectum), and the sample collection site (primary or metastasis) of the 49 PDX established, 27 (55%) were derived from tumors of the colon as the primary tumor site (regardless whether primary tumor or metastasis was sampled) and 45% originated from tumors of the rectum (primary or metastasis). The ratio of PDX derived from samples from primary tumors was balanced to that derived from metastases (53% to 47%), which were also evenly distributed between lung and liver. This kind of statistics could not be made for the patients whose tissue did not show positive engraftment, since their data were not available. Therefore no comparison between the patients' characteristics of engrafted versus non engrafted PDX could be performed.
For five patients, PDX pairs could be established. Co10302A and Co10302B were primary tumors derived from the transverse and the sigmoid colon, respectively. The pairs Co7553A and Co7553B, as well as Co9689A and Co9689B, were also obtained simultaneously and represented metastases pairs from different lung (Co7553) or liver (Co9689) locations resected on the same day. Co7271 and Co7660 were also both lung metastases from the same patient, resected 14 months apart. Among the established PDX there was also a primary tumor and liver metastasis pair (Co9997 and Co10300), resected in a 4 month period of time.

Of 87 patient samples transplanted into NSG mice, 56% showed positive engraftment in this strain, and later in NMRI*:nu/nu*. Growth rate of established PDX was stable and histological and molecular characteristics remained conserved along the passages. PDX tissue from several passages was compared to patient tissue regarding its histology and genetic profile, drawing the conclusion, that human tumor cells form adenocarcinoma like structures surrounded by mouse stroma *in vivo*, and this tumor tissue conserves the genetic profile of the patient tumor cells. Due to the summarized findings the models were regarded as suitable to be used for further studies, like comprehensive molecular profiling and drug screening.

3.2 Characterization of the PDX models

Once the set of PDX models was established, the models were extensively characterized at the molecular level. The mutational profiling, as well as gene expression and alterations in the number of copies of selected genes or gene copy number (GCN), were analyzed. A comprehensive genetic profiling is indispensable to elucidate tumor relevant oncogene pathways or draw correlations to the response to drugs.

3.2.1 Mutational profiling of the PDX

For mutational profiling DNA from PDX material was extracted and prepared with the Illumina TruSeq® Amplicon – Cancer Panel and the sequencing was performed on the MiSeq. In a multiplexed reaction, 212 amplicons from 48 oncogenes were targeted (see *Annex I* for complete list of oncogenes). The results obtained for selected genes, chosen for their relevance in CRC carcinogenesis or sensitivity towards treatment, are summarized in *Table 9*.

Table 9 summarizes all genetic alterations and amino acid exchanges detected in each sample. The ratios of mutated DNA detected in the samples allowed discriminating between homozygote and heterozygote mutations. *Table 9* further summarizes the results obtained for all 49 PDX. The genes most frequently mutated in the 49 PDX were APC (67%), KRAS (55%) and TP53 (53%). Models carrying a PI3KCA (16%) and BRAF (10%) mutation were also moderately represented in the set of the 49 PDX. In all five PDX pairs derived from the same patient, the mutational profile of these genes was identical, except for a difference in the APC mutational status between Co10300A and Co10300B.

The TDT of PDX models carrying a mutation in one of the genes whose mutational status is summarized in *Table 9* was compared to the TDT of PDX models with a wildtype variant of this gene. The mutational status of the above mentioned molecules was not relevant for the TDT, except for mutated PIK3CA. Models with a mutation in PIK3CA (n = 8) had a mean TDT = 7.1 ± 2.8 days, compared to a TDT = 10.5 ± 4.8 days (n = 41) in the models with wildtype PI3KCA ($p = 0.019$). Thus, an activating mutation in PIK3CA conferred a faster growth rate in this set of PDX models. An activating mutation in this gene, leading to upregulation of PI3K signaling, confers a PDX the capacity to grow faster *in vivo*.

Table 9: Mutational profiling of the PDX models was performed with Illumina TruSeq® Amplicon – Cancer Panel, where 212 amplicons of 48 oncogenes were analyzed. This table summarizes the mutational status of the most relevant oncogenes in colorectal cancer assessed with this method.

PDX	APC	BRAF	EGFR	KRAS	NRAS	PIK3CA	PTEN	TP53
	AA mutation							
Co 5676								Indel^{HO}
Co 5677								Indel^{HO}
Co 5679	E1451X^{HE}			G13D^{HO}				R273H^{HO}
Co 5682	Indel^{HO}			G12S^{HO}				G206C^{HO}
Co 5734								V172F^{HO}
Co 5735	Indel^{HE}							L194R^{HO}
Co 5736	Indel^{HO}			G12V^{HE}				
Co 5771	S1392X^{HE}			Q61H^{HE}		Q546K^{HE}		
Co 5776	E1306X^{HO}			A146T^{HE}				V173F^{HO}
Co 5841	Q1123X^{HE}			G12D^{HE}				R196X^{HO}
Co 5854	E1538X^{HO}	V600E^{HE}				E542K^{HE}	G293V^{HO}	
Co 5896	Indel^{HE}			G12S^{HE}				P278L^{HO}
Co 6044	S1356X^{HO}							
Co 6228								R175H^{HO}
Co 7271[1]	Indel^{HO}			G12A^{HO}				R175H^{HO}
Co 7475	Indel^{HO}			A146T^{HE}		E545K^{HE}		
Co 7515	Indel^{HO}						R335X^{HO}	R267X^{HO}
Co 7523		G466R^{HE}			G12E^{HE}			
Co 7553A[2]								
Co 7553B[2]								
Co 7567	Q1406X^{HO}			G12A^{HE}				R175H^{HO}
Co 7596	R876X^{HO}							R243W^{HO}
Co 7660[1]	Indel^{HO}			G12A				R175H^{HO}
Co 7689				G12D^{HE}				
Co 7809	Indel^{HO}			G12D^{HE}				R273C^{HO}
Co 7818		G469V^{HE}						R248Q^{HO}
Co 7835	K1308X^{HO}			G12D^{HE}		E545G^{HE}		R273C^{HO}
Co 7888				A146V^{HO}				R248Q^{HO}
Co 7935	E1322X^{HO}							
Co 9587	R876X^{HE}			G12D^{HE}		del104^{HE}		
Co 9634				Q61H^{HO}		C420R^{HE}; R88Q^{HE}		
Co 9689A[3]	Q1378X^{HE}							R248W^{HO}
Co 9689B[3]	Q1378X^{HE}							R248W^{HO}
Co 9729	E1397X^{HE}			G12V^{HO}				
Co 9775				G12D^{HE}				G245S^{HO}
Co 9946	ins1414^{HE}				Q61R^{HO}	N345I^{HO}		R306X^{HO}
Co 9978	E1322X^{HE}			G12V^{HE}				
Co 9997[4]	Q1429X^{HE}; del904^{HE}			G12A^{HE}				
Co 10158	99, Q1429X			A146T^{HO}				
Co 10194	A876X^{HE}; E1306X^{HE}							
Co 10300[4]	Q1429X^{HE}; del904^{HE}			G12A^{HE}				
Co10302A[5]	E1521V^{HE}	V600E^{HE}						
Co10302B[5]		V600E^{HE}						
Co 10377	Q1406X^{HO}			A146T^{HE}		del106^{HE}		R248W^{HO}
Co 10383				G12C^{HE}				
Co 10588				G12V^{HO}				E211X^{HE} Y163X^{HE}
Co 10764				G13D^{HO}				R196X^{HO}
Co 10925	E1379X^{HO}							
Co 11061	del1412^{HE}						del321^{HE}	
%*mut*PDX	**67.3**	**10.2**	**0.0**	**55.1**	**4.1**	**16.3**	**6.1**	**53.1**

^{HE} = heterozygous; ^{HO} = homozygous; [1-5] PDX models were derived from the same patient

3.2.2 Sensitivity towards conventional cytostatics and targeted drugs

In order to better characterize the models, and with the aim to use this set as a tool for validation and discovery of new drugs, the sensitivity of the models to drugs routinely used in the clinic was assessed.

3.2.2.1 Sensitivity towards standard of care cytostatic agents

The sensitivity of the PDX models towards the three cytostatic agents mainly used in the clinic for the treatment of CRC was tested in a monotherapy setting. The lowest or optimal respective T/C-value (optT/C) was chosen for measuring the sensitivity towards a specific drug and the values were grouped in ranges, or "scores" (see *2.2.2*). The RTV reflects the gain of TV in three weeks after treatment start and is a more comparable read-out to the RECIST criteria, used in the clinic.

Table 10: Summary of the response of the PDX to standard of care cytostatic agents. A responder PDX was defined as a model with a T/C-value < 50%, where the TVs of the treated group are significantly lower than the TVs of the control group. RTV was recorded 3 weeks after treatment start.

[%] PDX	5-FU	Irinotecan	Oxaliplatin
optT/C-value < 50%	45.83	91.67	36.73
RTV < 1.2 (SD+PR)	6.25	50	8.16
fulfill both criteria	6.25	50	4.08

SD = stable disease; PR = partial remission; CR = complete remission; PD = progressive disease

The PDX models displayed differential responsiveness to the treatment with 5-FU or oxaliplatin. Response ratios of 37% and 46%, respectively, were obtained when models with a tumor growth inhibition higher than 50% were regarded as responder. In 4% and 8% of the PDX an SD or PR could be reached through the treatment with 5-FU or oxaliplatin, respectively. Irinotecan reached the highest response rates from all treatment groups. 92% of the PDX were inhibited in their growth by more than 50% by irinotecan and 50% of them reached SD or PR according to the adapted RECIST criteria. The sensitivity profiles were similar for PDX derived from the same patient.

The individual response of every PDX model to the treatment with cytostatic agents is summarized in *Table 11*. The response rates did not correlate to any of the patients' characteristics, nor to the derivation site of the tissue.

Table 11: Sensitivity of the PDX models towards standard of care cytostatic agents. Groups of 5 tumor-bearing mice were treated with the maximum tolerated dose of the substances. Tumor response score: - negative: 100-50% T/C-value; +, 35-50% T/C-value; ++, 21-35% T/C-value; +++, 6-20% T/C-value; ++++, 0-5% T/C-value. RTV was evaluated approximately 3 weeks after treatment begin.

PDX	5-FU			Irinotecan			Oxaliplatin		
	opt T/C [%]	score	RTV	opt T/C [%]	score	RTV	opt T/C [%]	score	RTV
Co 5676	47.6	+	1.9	16.6	+++	0.6	60.61	-	2.03
Co 5677	64.5	-	2	18.8	+++	0.3	107.3	-	8.9
Co 5679	35.5	+	2.1	14.8	+++	0.8	95.3	-	10.2
Co 5682	43.6	+	1.4	49.1	+	1.2	60.3	-	1.7
Co 5734	31	++	1.1	30.9	++	1.1	57.8	-	4.8
Co 5735	21.6	++	1.4	9.9	+++	0.7	9.8	+++	1.8
Co 5736	73.1	-	2	46.2	+	1.3	60.8	-	6.2
Co 5771	54	-	3.1	11.5	+++	0.6	59.2	-	3.6
Co 5776	47.6	+	1.9	6.37	+++	1.25	18.5	+++	3
Co 5841	47.1	+	2.32	34.1	++	2	22.6	++	3.6
Co 5854	93.7	-	5.2	31.8	++	1.6	25.9	++	5.3
Co 5896	74.32	-	2.85	47.46	+	1.6	44.7	+	4.9
Co 6044	21.3	++	1.7	5.6	+++	0.5	14.2	+++	1.5
Co 6228	74.14	-	3.9	22.41	++	1.46	43.8	(+)	5.4
Co 7271[1]	21.2	++	1.6	6.1	+++	0.7	86.6	-	9.1
Co 7475	12.38	+++	1.53	1.9	++++	0.27	88.1	-	8.8
Co 7515	50.53	-	3.05	25.26	++	1.21	34.6	++	3.5
Co 7523	41.8	+	1.56	24.59	++	1.09	55.8	-	3.6
Co 7553A[2]	42.86	+	3.28	11.43	+++	0.75	58.8	-	6.6
Co 7553B[2]	55.71	-	3.58	18.45	+++	0.93	63.5	-	1
Co 7567	54.39	-	1.22	31.34	++	1	80.2	-	3.1
Co 7596	52.38	-	4	7.14	+++	0.47	138.7	-	8.9
Co 7660[1]	n.a.	n.a.	n.a.	n.a.	n.a.	n.a.	75.1	-	2.4
Co 7689	77.12	-	5.37	12.14	+++	1.42	19.1	+++	1.2
Co 7809	88.75	-	7.87	2.1	++++	0.28	26.3	++	1.3
Co 7818	71.43	-	10.33	10.22	+++	1	41.4	+	4.2
Co 7835	33.59	++	5.95	3.98	++++	0.6	42	+	5.7
Co 7888	52	-	2.63	11.11	+++	0.38	60.7	-	2.6
Co 7935	82.73	-	3.37	27.85	++	1	63.1	-	2.1
Co 9587	54.9	-	1.3	74.8	-	1.6	58.4	-	1.2
Co 9634	39.3	+	10.7	12.4	+++	1.6	48.1	+	10.8
Co 9689A[3]	64.9	-	4.2	31.7	++	2.2	54.3	-	3.6
Co 9689B[3]	103.8	-	5.5	9.1	+++	0.6	67.2	-	4.8
Co 9729	106.1	-	2.1	118.3	-	2.1	94.5	-	1.7
Co 9775	30.4	++	2	18.5	+++	1.5	51.8	-	3.9
Co 9946	86.9	-	2	71.1	-	1.4	79.1	-	1.5
Co 9978	20.6	++	15.8	13	+++	3.6	38.2	+	19.5
Co 9997[4]	52.4	-	3	27.4	++	1.6	97.6	-	6.6
Co 10158	18.3	+++	3.1	11.1	+++	2	20.6	++	3.5
Co 10194	85.7	-	4.9	9.6	+++	0.7	38.9	+	1.9
Co 10300[4]	56.3	-	2	26.2	++	1.3	97.2	-	3.6
Co10302A[5]	46.9	+	2.1	37.4	+	1.7	72.4	-	3.6
Co10302B[5]	44.6	(+)	1.9	25.7	++	1.5	72.7	-	1.9
Co 10377	126.4	-	32.1	2.2	++++	1.5	69.6	-	15.7
Co 10383	8.8	+++	1.2	5.6	+++	1	70	-	9.8
Co 10588	188.4	-	12.2	53.3	-	3.5	133	-	4.4
Co 10764	40.7	+	3.4	28.8	++	2.2	48.5	+	3.6
Co 10925	17.8	+++	0.8	11.6	+++	0.5	25.2	++	1.2
Co 11061	21.9	++	1.8	24	++	2.3	42.5	+	4.1

[1 -5] PDX models were derived from the same patient; n.a.= not analysed; (+) = not significant

Figure 10 shows the growth curves from the characterization experiments of two representative PDX models. The PDX model Co9689B was resistant to 5-FU and oxaliplatin, but its growth could be inhibited by irinotecan. The PDX model Co10925 was sensitive to all three treatments.

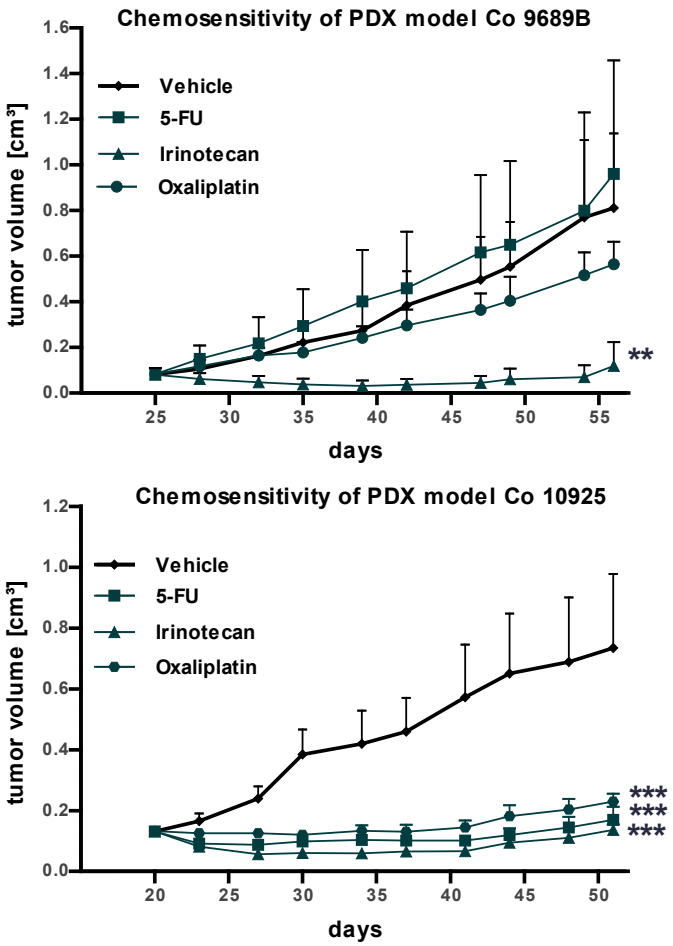

Figure 10: Growth curves from two representative sensitivity screenings of the models Co9689B and Co10925. Animals were randomized in groups of five and treated either with vehicle or standard of care cytostatic agents. When statistical significance was reached, *p < 0.05; **p < 0.01;*** p < 0.001

No significant correlations (r_S) between the sensitivity values to the different treatments could be found, reflecting their different tumor growth suppression mechanisms. The opt/C-values for these agents correlated significantly to the RTV of the untreated PDX.

In the clinical situation, 5-FU and oxaliplatin given as monotherapy reached response rates between 10% - 20%, and irinotecan had response rates between 15% - 30%, which makes the chosen cut off for optT/C-value probably a weak criterion. Nevertheless, the values obtained by calculating the RTV yielded lower response rates for 5-FU and oxaliplatin.

3.2.2.2 Sensitivity towards targeted agents

The sensitivity to two targeted agents approved for clinical use in CRC, cetuximab and bevacizumab, was tested in the PDX models. Erlotinib was included in the sensitivity testing in order to explore its possible role in the treatment of CRC and to better explore the dynamics of the EGFR pathway in the context of targeted treatments. The same evaluation criteria as mentioned in *3.2.2.1* were used. *Figure 11* depicts the growth curves of two representative characterization experiments.

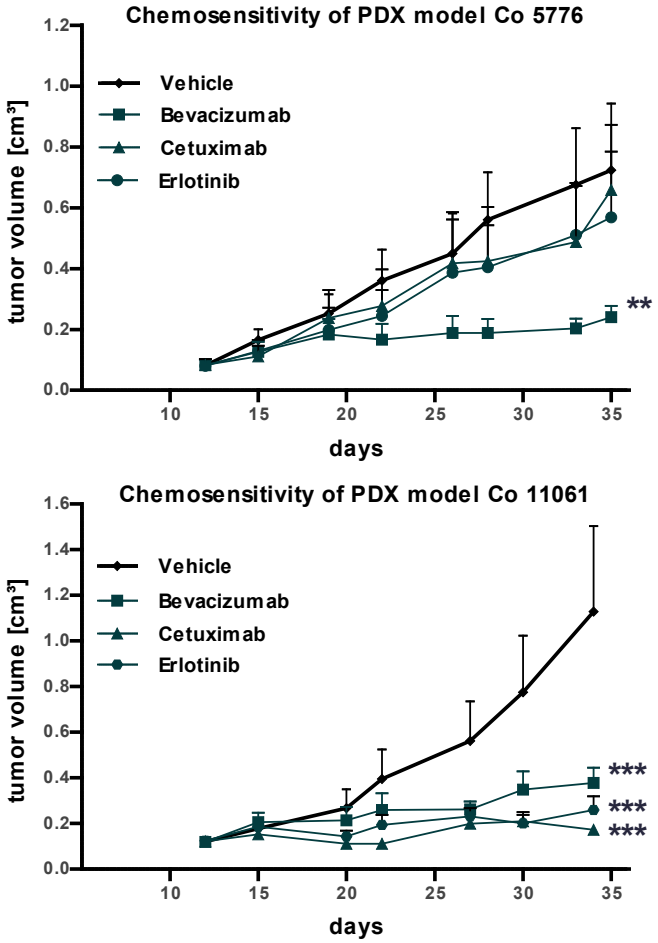

Figure 11: Growth curves from two representative sensitivity screenings of the models Co5776 and Co11061. Animals were randomized in groups of five and treated either with vehicle or targeted agents. When statistical significance was reached, *p < 0.05; **p < 0.01;*** p < 0.001

Table 12 summarizes the individual response of each PDX model to the three targeted drugs cetuximab, bevacizumab and erlotinib.

Table 12: Sensitivity of the PDX models towards the targeted agents erlotinib, cetuximab and bevacizumab. Groups of 5 tumor-bearing mice were treated with the maximum tolerated dose of the substances. Tumor response score: - negative: 100-50% T/C-value; +, 35-50% T/C-value; ++, 21-35% T/C-value; +++, 6-20% T/C-value; ++++, 0-5% T/C-value. RTV was evaluated approximately 3 weeks after treatment begin.

PDX	Bevacizumab			Cetuximab			Erlotinib		
	opt T/C [%]	score	RTV	opt T/C [%]	score	RTV	opt T/C [%]	score	RTV
Co 5676	48.8	+	4.1	0.57	++++	0.12	53.1	-	4.7
Co 5677	79.2	-	5.2	96.9	-	5.7	103.8	-	8
Co 5679	44.8	+	6.6	38.6	+	6.2	151.2	-	8.7
Co 5682	21.5	++	0.9	45.2	+	1.3	78.1	-	3.7
Co 5734	33.8	++	1.8	12.1	+++	1.4	29.6	++	1.2
Co 5735	15.9	+++	2.6	22.5	++	3.0	39.9	+	3.8
Co 5736	107.3	-	12.2	92.4	-	12	51.4	-	6
Co 5771	14.7	+++	1.1	25.5	++	1.7	36.6	+	2.6
Co 5776	30.1	++	3.3	72.3	-	7.1	72.2	-	6.7
Co 5841	23	++	1.5	44.2	+	1.6	27.4	++	3.6
Co 5854	38.9	+	8.2	73.7	-	16.8	34	++	7.2
Co 5896	39.6	+	3.6	44.3	+	4.2	92.9	-	7.3
Co 6044	75.5	-	6.4	102.4	-	12.2	81.6	-	5.7
Co 6228	27.8	++	5.2	74.4	-	3.6	78	-	12.7
Co 7271[1]	45.7	+	4	15.9	+++	1.6	56.1	-	5.8
Co 7475	15.9	+++	5.7	38.5	+	7.7	97.1	-	5.5
Co 7515	40.4	+	2.9	20.5	++	2.2	42.2	+	4.3
Co 7523	57.8	-	3.8	20.8	++	1.2	73.7	-	5.7
Co 7553A[2]	36.9	+	3.8	8.3	+++	0.8	26.9	++	2.4
Co 7553B[2]	36.5	+	1.2	8.7	+++	0.8	36	+	0.7
Co 7567	72.5	-	2	94.5	-	2.2	141.4	-	3.3
Co 7596	31.2	++	2.2	0.7	++++	0.2	29.2	++	1.6
Co 7660[1]	26.9	++	0.7	28.8	++	0.7	76.9	-	1.7
Co 7689	63.7	-	4	58.2	-	4.6	73.4	-	3.5
Co 7809	11.7	+++	2.2	60.3	-	8.4	85.3	-	10.9
Co 7818	37.9	+	3.7	36.4	+	3.6	38.9	+	3.2
Co 7835	24.5	++	2.9	44.4	+	6.4	45.5	+	5.8
Co 7888	59.5	-	1.9	29.1	++	1.1	63.9	-	3.4
Co 7935	67.4	-	1.5	21.1	++	0.9	23	++	1
Co 9587	65.9	-	1.5	75.4	-	2	42.7	+	1
Co 9634	41.9	+	5.2	64.1	-	7.8	72.6	-	8.2
Co 9689A[3]	33	++	1.9	14.5	+++	0.8	51.9	-	2.9
Co 9689B[3]	25	++	2.3	8.4	+++	0.9	32.7	++	2.7
Co 9729	109.7	-	2.3	103.9	-	2	119.6	-	2.2
Co 9775	25.1	++	1.7	49.7	(+)	3.3	47.5	+	3.7
Co 9946	50.2	-	1	57.2	-	1.1	72.3	-	1.6
Co 9978	20.2	++	9.2	14.7	+++	10.6	18	+++	8.8
Co 9997[4]	55.8	-	3.3	42.2	+	2.2	52.8	-	3.2
Co 10158	24	++	3.6	42.1	+	6.1	40.2	+	6.1
Co 10194	64.2	-	3.1	0.6	++++	0.1	33.5	++	2
Co 10300[4]	71.3	-	2.7	55	-	2.3	65.8	-	2.8
Co10302A[5]	100.7	-	4.7	190.4	-	9.5	88.5	-	4.2
Co10302B[5]	108.8	-	2.3	87.7	-	3.7	53.4	-	2.2
Co 10377	44.3	+	8.5	69.3	-	13.6	106	-	23.3
Co 10383	16.3	+++	1.9	15.9	+++	2.1	60.5	-	8.4
Co 10588	100.2	-	6.9	171.8	-	10.7	206	-	14.8
Co 10764	38.1	+	2.8	39.5	+	2.8	51.6	-	3.6
Co 10925	21.9	++	1.1	6.8	+++	0.4	32.2	++	1.5
Co 11061	33.6	++	3.1	15.2	+++	1.6	22.9	++	2.3

[1 -5] PDX models were derived from the same patient; (+) = not significant

Table 13 summarizes the response ratios of the PDX models to the targeted drugs. The best response rates evaluated by calculating the optT/C or RTV, were obtained with cetuximab (63% of PDX with optT/C < 50%) and bevacizumab (67% of PDX with optT/C < 50%). Erlotinib showed a slightly lower responder rate of 41%. The PDX model pairs derived from tissue samples of the same patient showed similar sensitivity profiles also regarding targeted drugs (*Table 12*).

Table 13: Summary of the response of the PDX to three targeted agents, the angiogenesis inhibitor bevacizumab, and the EGFR inhibitors cetuximab and erlotinib. A responder PDX was defined as a model with a T/C-value < 50%, where the TVs of the treated group are significantly lower than the TVs of the control group. RTV was recorded 3 weeks after treatment start.

[%] PDX	Bevacizumab	Cetuximab	Erlotinib
optT/C-value < 50%	66.67	62.50	40.82
RTV < 1.2 (SD+PR)	12.50	27.08	8.16
fulfill both criteria	10.42	25.00	8.16

SD = stable disease; PR = partial remission; CR = complete remission; PD = progressive disease

To elucidate, if the PDX responsive to one of the drugs show a tendency to be sensitive to another (possibly demonstrating a similar mechanism of action of the drugs in the PDX tumors), Spearman Rho (r_S) linear correlation coefficients were built between the response panels for every drug. The optT/C-values towards bevacizumab showed a moderate correlation towards the optT/C-values obtained with the EGFR-inhibitors cetuximab and erlotinib; $r_S = 0.463$, $p = 0.001$ and $r_S = 0.354$, $p = 0.013$, respectively. The optT/C-values for the two EGFR-inhibitors, cetuximab and erlotinib, strongly correlated with each other ($r_S = 0.643$, $p < 0.001$). This is also depicted by the growth curves in *Figure 11*. Models that could be inhibited in their growth by the erlotinib treatment, were inhibited to stronger extent by the treatment with cetuximab. The high correlation coefficient reflects the similar mechanism used by both drugs to inhibit tumor growth and depicts that there is a group of PDX that is more likely to be inhibited by EGFR-pathway blockade.

Generally, the response rates towards targeted drugs could generate higher responder rates as the cytostatics in this set of PDX. In this case, the evaluation made with the modified RECIST criteria reflected the response rates found in the clinic more closely than in the case of cytostatics.

3.2.3 Characterization of the dynamics of the EGFR-pathway in the PDX models with focus on EGFR inhibition

The molecules that participate in the EGFR pathway and some of the signaling cascades triggered by its activation were examined in the PDX. The expression level at mRNA and protein level for ligands and co-receptors from EGFR were measured, as well as copy number and mutational status of some key molecules were determined. The results of these measurements were correlated to the sensitivity profiles of the two different EGFR-inhibitors used.

3.2.3.1 Expression of ligands of EGFR

The expression of the five main EGFR ligands amphiregulin (AREG), betacellulin (BTC), epidermal growth factor (EGF), epiregulin (EREG) and transforming growth factor α (TGFα) was measured at mRNA- and protein level. The expression of the molecules was measured and correlations were built to better depict the dynamics of the EGFR pathway in the PDX models. Cetuximab binds to EGFR impairing the binding of its ligands and inhibiting the signaling through this pathway. For this reason it was verified if there are correlations between the expression of ligands and the response to EGFR inhibitors.

The mRNA expression was measured using real-time RT-PCR, and the ΔC_T values were obtained when the C_T values for the genes of interest were normalized with the C_T values for ß-actin. The protein expression of the molecules was measured by ELISA assay, where the concentrations of the measured molecules were normalized with the total protein (T_P) content in the PDX-tumor lysate. For both methods, three different PDX samples were used (n = 3). The values for each PDX model are summarized in *Annex III*.

Amphiregulin

Figure 12 summarizes the expression values obtained for AREG. The ΔC_T-values ranged between 0.7 (highest expression) and 8.7 (lowest expression). In order to better represent the proportions between the models, for the graph, the ΔC_T-values obtained were subtracted from 40 (the total number of cycles used for the Real-time RT-PCR). The protein concentrations for AREG ranged between 196 pg/mg_{TP} and 6525 pg/mg_{TP}, and were the highest detected among all ligands measured.

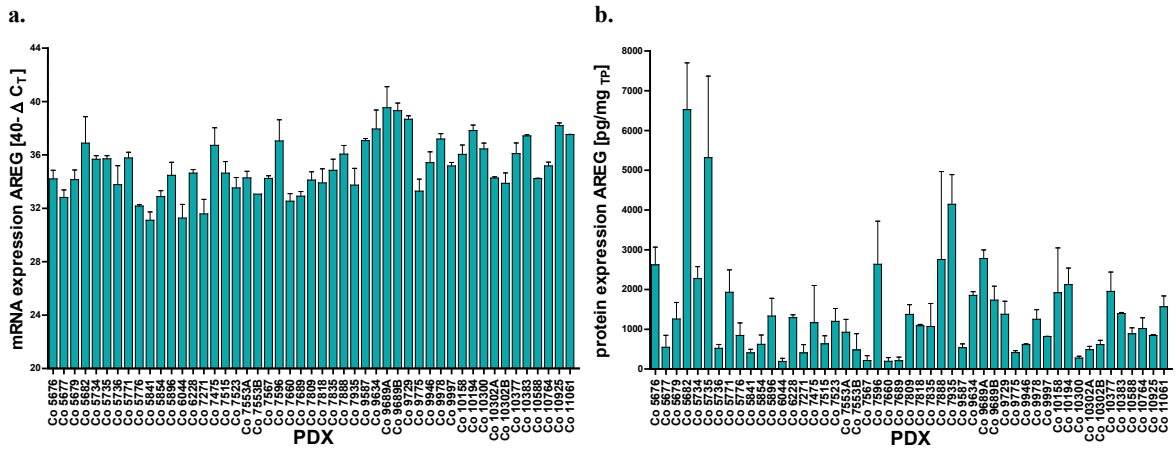

Figure 12: AREG expression was measured at **(a.)** mRNA- (real-time RT-PCR) and **(b.)** protein level (ELISA) in the PDX models. The mRNA expression levels are described by the inverse of ΔC_T, normalized to the β-actin C_T. The protein concentrations have been normalized to the total protein content in the sample. Three PDX samples from different passages were measured (n = 3).

In order to determine if the measured values for AREG at mRNA and protein level correlated with each other, a r_S was calculated using a regression curve (*Figure 13*). The r_S between the ΔC_T-values and protein concentrations in PDX tissue was $r_S = -0.594$, $p < 0.001$, which means that the measured values significantly correlated with each other, thus, models with a high mRNA expression tendentially showed a higher protein expression of the molecules, suggesting no further regulation of the expression of AREG.

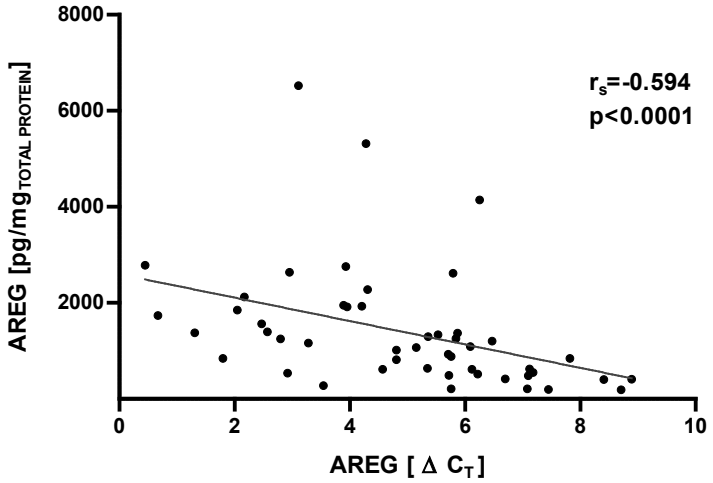

Figure 13: Correlation analysis of mRNA- and protein-expression levels of AREG in the PDX; Spearman Rho (r_S) was calculated.

Betacellulin

Figure 14 summarizes the expression values obtained for BTC. The ΔC_T-values ranged between 6.5 (highest expression) and 15.0 (lowest expression), and were clearly higher than the values obtained for AREG, which points to a lower mRNA expression of BTC in the PDX models. The ΔC_T-values were processed in the same procedure as AREG for the graph in *Figure 12*. The protein concentrations for BTC were also clearly lower as those measured for AREG and ranged between 13 pg/mg$_{TP}$ and 147 pg/mg$_{TP}$.

The r_S between the ΔC_T-values and protein concentration of BTC in the PDX samples (r_s = -0.635, $p < 0.001$) also demonstrated a strong correlation of the values.

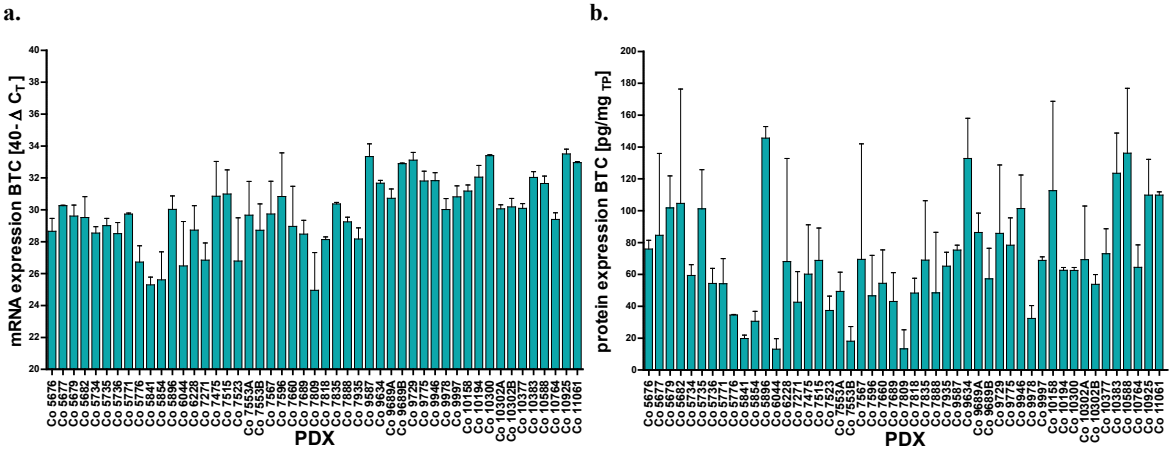

Figure 14: BTC expression was measured at **(a.)** mRNA- (real-time RT-PCR) and **(b.)** protein level (ELISA) in the PDX models. The mRNA expression levels are described by the inverse of ΔC_T, normalized to the β-actin C_T. The protein concentrations have been normalized to the total protein content in the sample. Three PDX samples from different passages were measured (n = 3).

EGF

In the case of the mRNA measurement for EGF, not every sample reached a C_T. As a consequence a ΔC_T-value could not be calculated. The amount of EGF mRNA in these samples was below the detection range of the assay used. The lowest ΔC_T-values for EGF obtained were ΔC_T = 3.8. Except for sample Co9634, (77.5 pg/mg$_{TP}$), the EGF concentrations in the samples ranged between 0 pg/mg$_{TP}$ and 32 pg/mg$_{TP}$. Also in this case a significant r_S = 0.745, $p < 0.001$, showed that the results of both measurements correlated with each other, similar to AREG.

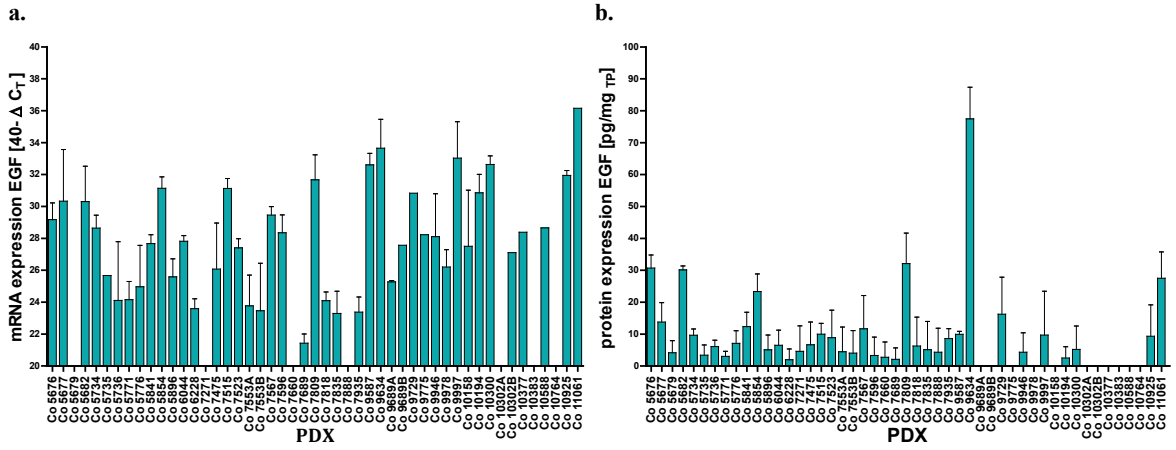

Figure 15: EGF expression was measured at **(a.)** mRNA- (real-time RT-PCR) and **(b.)** protein level (ELISA) in the PDX models. The mRNA expression levels are described by the inverse of ΔC_T, normalized to the β-actin C_T. The protein concentrations have been normalized to the total protein content in the sample. Three PDX samples from different passages were measured (n = 3).

Epiregulin

As depicted in *Figure 16* the range of the ΔC_T-values for EREG was similar to those from AREG (1.6 and 9.7). The protein concentrations of EREG in PDX tissue measured by ELISA ranged between 13 pg/mg$_{TP}$ and 188 pg/mg$_{TP}$. The r_S between the ΔC_T-values and protein expression values was $r_s = -0.661$, $p < 0.001$.

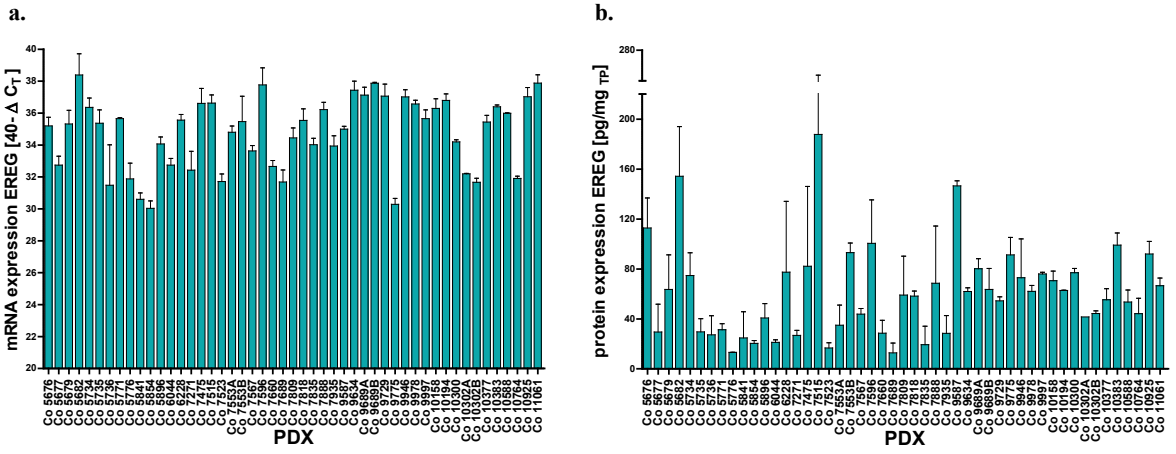

Figure 16: EREG expression was measured at **(a.)** mRNA- (real-time RT-PCR) and **(b.)** protein level (ELISA) in the PDX models. The mRNA expression levels are described by the inverse of ΔC_T, normalized to the β-actin C_T. The protein concentrations have been normalized to the total protein content in the sample. Three PDX samples from different passages were measured (n = 3).

TGFα

The ΔC_T-values for TGFα showed the lowest variation and smallest expression range in the PDX models amongst all EGFR ligands. The values ranged between 4 and 9.8. The highest protein expression value was detected in Co9729 (159 pg/mg$_{TP}$), for the remaining PDX the values ranged between 9 pg/mg$_{TP}$ and 86 pg/mg$_{TP}$. The correlation coefficient between the mRNA and protein expression values was also the lowest among all EGFR-ligands (r_s = -0.449, p = 0.001).

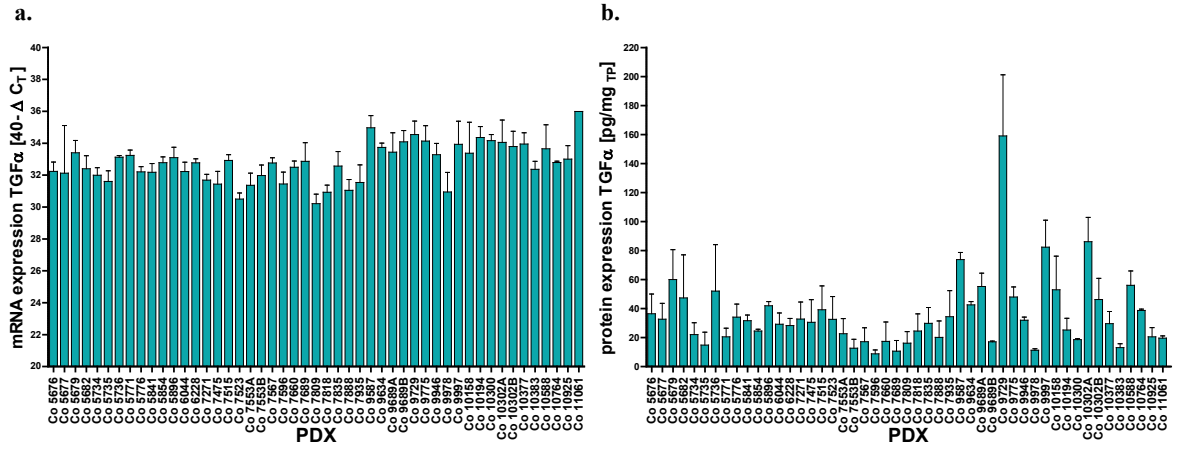

Figure 17: TGFα expression was measured on **(a.)** mRNA- (real-time RT-PCR) and **(b.)** protein level (ELISA) in the PDX models. The mRNA expression levels are described by the inverse of ΔC_T, normalized to the β-actin C_T. The protein concentrations have been normalized to the total protein content in the sample. Three PDX samples from different passages were measured (n = 3).

Differential expression of the five ligands of EGFR (AREG, EREG, EGF, BTC and TGFα) was determined in the PDX. The highest values were obtained for AREG and EREG, on mRNA and protein level, even though AREG showed the highest (and most differential) protein expression. BTC expression was lower than the expression of AREG and EREG, but still high when compared to EGF and TGFα. The lowest expression was detected for EGF and TGFα, on both, mRNA and protein levels, suggesting that these two ligands are less involved in the signaling in this set of CRC than AREG and EREG.

Analysis of the correlation of expression between ligands of EGFR

The ΔC_T-values and protein concentrations of the EGFR ligands were compared to each other at mRNA and protein levels and r_S were calculated to determine if the expression of the molecules significantly correlated with each other. The expression of the EGFR ligands, and its binding to the EGFR receptor, induce several anti-apoptotic and survival signaling cascades. It also stimulates the expression and secretion of further ligands in

order to promote tumor growth. Linear correlations were built between the expression of the EGFR ligands to corroborate that this relationship is also depicted by the PDX.

Table 14 summarizes the correlation coefficients calculated for the ΔC_T-values of the five molecules. For every pair of molecules, Spearman Rho linear correlation coefficients were built between the expression values. Except for EREG and TGFα, significant r_S were calculated between all molecules analyzed, demonstrating a positive correlation to each other between the amount of mRNA coding for the EGFR ligands in the PDX models. The strongest correlation coefficient were observed for AREG with EREG or BTC.

Table 14: Correlation coefficients (r_S) of the mRNA expression of the ligands of EGFR amongst each other.

mRNA Expression	ΔC_T AREG		ΔC_T EREG		ΔC_T BTC		ΔC_T EGF		ΔC_T TGFα	
	r_S	p-value	r_S	p-value	r_S	p-value	r_S	p-value	r_S	p-value
ΔC_T AREG	-	-	0.824	<0.001	0.750	<0.001	0.415	0.010	0.379	0.007
ΔC_T EREG	0.824	<0.001	-	-	0.580	<0.001	0.370	0.022	0.156	n.s.
ΔC_T BTC	0.750	<0.001	0.580	<0.001	-	-	0.449	0.005	0.676	<0.001
ΔC_T EGF	0.415	0.010	0.370	0.022	0.449	<0.001	-	-	0.452	0.004
ΔC_T TGFα	0.379	0.007	0.156	n.s.	0.676	<0.001	0.452	0.004	-	-

n.s. = not significant

The expression of the ligands at protein level did not correlate as strong with each other as at the mRNA level. EGF only showed a moderate correlation to TGFα and its expression did not correlate to the rest of the ligands. The closest correlation was between TGFα and BTC (0.424, p = 0.002), followed by the r_S between AREG, EREG and BTC, which ranged between 0.314 and 0.382, summarized in *Table 15*. The expression of ligands seems to induce further expression, or common mechanisms of regulation of expression. This is particularly notable in the case of BTC, AREG and EREG. The high correlation coefficients between these molecules suggest a strong interaction and relevance for the EGFR related signaling.

Table 15: Correlation coefficients (r_S) of the protein expression of the ligands amongst each other.

Protein expression	AREG		EREG		BTC		EGF		TGFα	
	r_S	p-value	r_S	p-value	r_S	p-value	r_S	p-value	r_S	p-value
AREG	-	-	0.314	0.028	0.320	0.025	0.040	n.s.	-0.030	n.s.
EREG	0.314	0.028	-	-	0.382	0.007	0.176	n.s.	0.039	n.s.
BTC	0.320	0.025	0.382	0.007	-	-	0.271	n.s.	0.424	0.002
EGF	0.040	n.s.	0.176	n.s.	0.271	n.s.	-	-	0.374	0.021
TGFα	-0.030	n.s.	0.039	n.s.	0.424	0.002	0.374	0.021	-	-

n.s. = not significant

3.2.3.2 Expression of EGFR and the HER receptor family

The expression of EGFR was assessed by IHC during the initial characterization of the models described in *3.1*. However, no detectable differences in the expression level of EGFR in the PDX models using this method (IHC) could be reliably measured. To obtain more accurate expression values, the expression level of EGFR was measured at the mRNA level using real-time RT-PCR (see *Annex IV*) and by ELISA to determine the amount of EGFR in the protein lysates of PDX models.

The ΔC_T-values were similar to those obtained for AREG and EREG, and ranged between 1.4 and 6.0, pointing to a moderate to high expression of EGFR in the PDX models. The protein concentration in protein lysates of PDX ranged between 0.8 ng/mg$_{TP}$ and 11.5 ng/mg$_{TP}$, and was clearly higher as the concentrations measured for the ligands by several folds and was highest in the PDX models Co7271, Co7809 and Co10764.

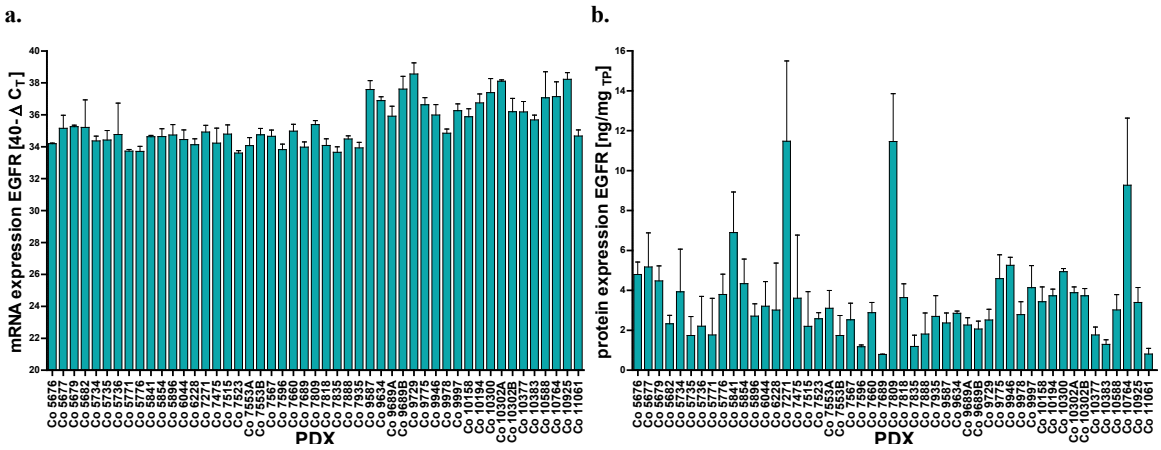

Figure 18: EGFR expression was measured at **(a.)** mRNA- (real-time RT- PCR) and **(b.)** protein level (ELISA) in the PDX models. The mRNA expression levels are described by the inverse of ΔC_T, normalized to the β-actin C_T. The protein concentrations have been normalized to the total protein content in the sample. Three PDX samples from different passages were measured (n= 3).

The r_S between the ΔC_T-values for EGFR and the protein concentrations measured in the PDX tissue were not significant, so there was no correlation between the mRNA and protein expression levels for EGFR in the 49 PDX models. The protein level measured by ELISA did not correlate with the ΔC_T-values obtained with real-time RT-PCR , suggesting that the models with high amounts of EGFR mRNA are not necessarily the ones with a high protein expression. This could mean that further posttranscriptional regulation mechanisms are active during the expression of EGFR.

Expression of HER2, HER3 and HER4

The EGFR receptor family comprises three further receptors, HER2, HER3 and HER4. These receptors participate in the EGFR signaling, have differential binding affinities towards the EGFR ligands and are able to build heterodimers with EGFR (or HER1) or with each other, and so activate signaling cascades downstream of EGFR. Their expression, possible correlations to the expression of the EGFR ligands and possible influence regarding EGFR-inhibition sensitivity were studied as well. The values obtained for each PDX models are summarized in *Annex IV*.

The mRNA expression levels of HER2, HER3 and HER4 are summarized in *Figure 19*. A high expression, comparable to that of EGFR, could be measured for HER2 and HER3, whose ΔC_T-values ranged between ΔC_T = 0.5 - 5.7 and ΔC_T = -1.3 - 4.3, respectively. HER4 mRNA could not be detected in 2/49 PDX. For the remaining PDX models the ΔC_T-values ranged between ΔC_T = 10.5 and ΔC_T = 19.8. The mRNA expression levels for HER4 were explicitly lower than for the rest of the members of the EGFR receptor family, which indicated that HER4 is not as strongly expressed by the PDX as HER2 and HER3.

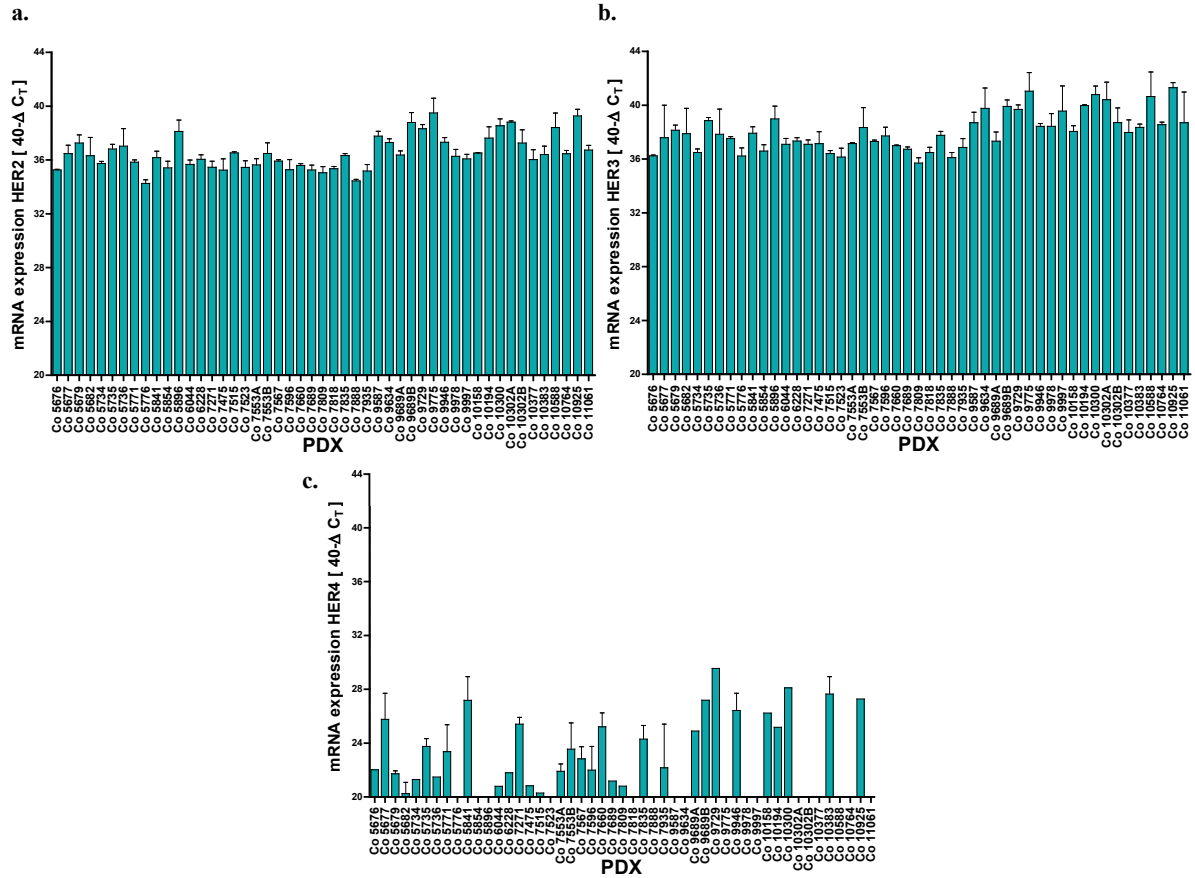

Figure 19: mRNA expression levels of **(a.)** HER2, **(b.)** HER3 and **(c.)** HER4. The mRNA expression levels are described by the inverse of ΔC_T, normalized to the β-actin C_T, measured with the real-time RT-PCR method. The protein concentrations have been normalized to the total protein content in the sample. Three PDX samples from different passages were measured (n = 3).

Analysis of the correlation of expression between HER receptors

Table 16 summarizes the results obtained in the correlation analysis of the ΔC_T-values of the HER receptors, where r_S for each receptor pair was calculated. For building the r_S between the ΔC_T-values for HER4 and the other receptors, only PDX with detectable mRNA expression values were taken into account (n = 23). Significant correlation coefficients between $r_S = 0.572$ and $r_S = 0.820$ were calculated, meaning that the mRNA expression levels of the receptors positively correlated with each other, similarly than in the case of the ligands. In comparison, the correlations between the receptors on mRNA level were stronger to those of the ligands. The strong correlation coefficients reflect the interconnection between the EGF-receptors also observed by several other studies.

Table 16: Correlation coefficients (r_S) of the mRNA expression of the EGFR family receptors.

mRNA expression	ΔC_T EGFR		ΔC_T HER2		ΔC_T HER3		ΔC_T HER4	
	r_S	p-value	r_S	p-value	r_S	p-value	r_S	p-value
ΔC_T EGFR	-	-	0.748	<0.001	0.678	<0.001	0.655	<0.001
ΔC_T HER2	0.748	<0.001	-	-	0.820	<0.001	0.572	0.004
ΔC_T HER3	0.678	<0.001	0.820	<0.001	-	-	0.577	0.004
ΔC_T HER4	0.655	<0.001	0.572	0.004	0.577	0.004	-	-

The measurement of protein concentration of EGFR in tumor lysates of the 49 PDX did not correlate significantly with the mRNA expression levels of any of the receptors from the EGFR receptor family. These results stay in line with the previous observation that the expression values for EGFR at mRNA and protein level did not correlate with each other, either did the protein levels of EGFR correlate to the expression of HER2 - 4. On the other hand, the expression levels among the HER receptors significantly correlated with each other at mRNA level, possibly pointing to shared regulation of transcription.

3.2.3.3 Correlation analysis of the expression of HER receptors and ligands

Table 17 summarizes the correlation analysis between the mRNA expression levels (expressed by ΔC_T) of the receptors (HER1 - HER4) and the expression levels of the EGFR ligands AREG, EREG, BTC, EGF and TGFα (ΔC_T and concentration in PDX tissue). Similar to the previous evaluations, only the HER4 values above the detection threshold could be considered.

The mRNA expression of EREG did not correlate with any of the receptors. EGF only correlated with EGFR and HER2, while the ΔC_T-values for HER4 only significantly correlated to those of BTC. All other receptor – ligand pairs examined in *Table 17* significantly correlated with each other at mRNA level, displaying moderate to high r_S. Significant correlations between the ΔC_T-values of the receptors and the protein expression of the EGFR ligands showed, that the protein expression levels measured for BTC negatively correlated with the ΔC_T-values for HER1 and HER3. Also the mRNA expression level of EGFR significantly correlated to the measured protein expression of the ligands in the 49 PDX. The negative correlation coefficients that were calculated between the ΔC_T-values of HER1 and HER4 and the ligands still point to a positive correlation, since the ΔC_T-values behave inversely to the amount of mRNA in the sample. The measured protein concentrations of EGFR in the PDX models did not correlate with the expression of any of the ligands on mRNA or protein level.

Table 17: Correlation coefficients (r_S) of the expression of EGFR ligands of and the EGFR receptor family.

mRNA expression	**ΔC_T AREG**		**ΔC_T EREG**		**ΔC_T BTC**		**ΔC_T EGF**		**ΔC_T TGFα**	
	r_S	**p-value**	**r_S**	**p-value**	**r_S**	**p-value**	**r_S**	**p-value**	**r_S**	**p-value**
ΔC_T EGFR	0.411	0.003	0.234	n.s.	0.623	<0.001	0.640	<0.001	0.679	<0.001
ΔC_T HER2	0.377	0.008	0.201	n.s.	0.703	<0.001	0.377	0.020	0.733	<0.001
ΔC_T HER3	0.480	<0.001	0.247	n.s.	0.740	<0.001	0.298	n.s.	0.692	<0.001
ΔC_T HER4	0.273	n.s.	0.034	n.s.	0.533	0.009	0.456	n.s.	0.460	0.027
Protein to mRNA expression	**AREG**		**EREG**		**BTC**		**EGF**		**TGFα**	
	r_S	**p-value**	**r_S**	**p-value**	**r_S**	**p-value**	**r_S**	**p-value**	**r_S**	**p-value**
ΔC_T EGFR	0.120	n.s.	-0.359	0.011	-0.451	0.001	-0.417	0.009	-0.376	0.007
ΔC_T HER2	0.129	n.s.	-0.276	n.s.	-0.590	<0.001	-0.150	n.s.	-0.355	0.012
ΔC_T HER3	0.039	n.s.	-0.230	n.s.	-0.495	<0.001	0.054	n.s.	-0.186	n.s.
ΔC_T HER4	0.347	n.s.	-0.022	n.s.	-0.162	n.s.	-0.370	n.s.	0.020	n.s.

n.s. = not significant

3.2.3.4 Implications of the expression of EGFR ligands for tumor growth and chemosensitivity

First, the expression levels measured for the EGFR receptors and ligands were correlated to the TDT or the RTV measurements for the control group during the characterization experiment. Neither the protein- nor the mRNA expression of any of the ligands correlated with the TDT or RTV of the untreated PDX models. This means, that neither the

expression of the EGFR receptors, nor their ligands, have influence on the individual growth of the PDX.

Table 18: Correlation analysis between the expression of ligands of EGFR and sensitivity of the models towards cytostatic therapies

mRNA expression	5-FU [opt T/C-value]		Irinotecan [opt T/C-value]		Oxaliplatin [opt T/C-value]	
	r_S	p-value	r_S	p-value	r_S	p-value
ΔC_T AREG	0.064	n.s.	0.037	n.s.	-0.082	n.s.
ΔC_T EREG	0.033	n.s.	0.107	n.s.	-0.123	n.s.
ΔC_T BTC	0.040	n.s.	-0.103	n.s.	-0.301	n.s.
ΔC_T EGF	0.015	n.s.	-0.252	n.s.	-0.120	n.s.
ΔC_T TGFα	-0.242	n.s.	-0.378	0.008	-0.164	n.s.
protein expression	**5-FU [opt T/C-value]**		**Irinotecan [opt T/C-value]**		**Oxaliplatin [opt T/C-value]**	
	r_S	p-value	r_S	p-value	r_S	p-value
AREG	0.011	n.s.	-0.196	n.s.	-0.072	n.s.
EREG	-0.125	n.s.	0.053	n.s.	0.219	n.s.
BTC	-0.078	n.s.	0.286	0.048	0.191	n.s.
EGF	0.046	n.s.	0.383	0.019	0.036	n.s.
TGFα	0.055	n.s.	0.515	<0.001	0.189	n.s.

n.s. = not significant

As shown in *Table 18,* almost no significant correlations could be found between the optT/C-values for the three cytostatic drugs used in the characterization experiments. Only in the case of irinotecan a significant, inverse correlation to the expression values for TGFα-mRNA ($r_S = -0.378$, $p < 0.001$) was found. This points to a higher mRNA amount in models with higher optT/C-values, hence resistant to irinotecan. Also the protein amount of BTC, EGF and TGFα significantly correlated with the sensitivity values for irinotecan, showing a higher protein amount of these molecules in the resistant models.

When the expression of the molecules was compared to the sensitivity panel for the targeted agents, much more significant correlations could be found (*Table 19*). The values describing the sensitivity towards bevacizumab significantly correlated with the expression values for TGFα at mRNA and protein level. Also in this case, a higher amount of TGFα protein could be measured in PDX resistant to bevacizumab. The expression of EREG (mRNA level) and AREG (protein level) inversely correlated with the T/C-values, pointing to a lower expression of these molecules in the bevacizumab resistant models.

Nevertheless, with coefficients of $r_S = 0.230$ and $r_S = -0.340$ these relationships were rather week.

Table 19: Correlation analysis between the expression of ligands of EGFR and sensitivity of the models towards targeted therapies

mRNA expression	Cetuximab [opt T/C-value]		Erlotinib [opt T/C-value]		Bevacizumab [opt T/C-value]	
	r_S	p-value	r_S	p-value	r_S	p-value
ΔC_T AREG	0.306	0.032	0.172	n.s.	0.230	n.s.
ΔC_T EREG	0.417	0.003	0.151	n.s.	0.290	0.044
ΔC_T BTC	0.074	n.s.	0.034	n.s.	-0.035	n.s.
ΔC_T EGF	-0.075	n.s.	-0.085	n.s.	-0.144	n.s.
ΔC_T TGFα	-0.295	0.040	-0.123	n.s.	-0.327	0.022
protein expression	**Cetuximab [opt T/C-value]**		**Erlotinib [opt T/C-value]**		**Bevacizumab [opt T/C-value]**	
	r_S	p-value	r_S	p-value	r_S	p-value
AREG	-0.437	0.002	-0.200	n.s.	-0.340	0.017
EREG	-0.347	0.015	-0.118	n.s.	-0.226	n.s.
BTC	0.088	n.s.	0.262	n.s.	0.032	n.s.
EGF	0.264	n.s.	0.093	n.s.	0.177	n.s.
TGFα	0.418	0.003	0.332	0.020	0.417	0.003

n.s. = not significant

As expected, the expression of the EGFR ligands showed only borderline or no correlations to the sensitivity towards cytostatic drugs. Unexpectedly, moderate, but significant correlations were observed between the sensitivity towards bevacizumab and the expression of the ligands, especially TGFα, which was also the only ligand that showed correlations to the sensitivity towards cytostatics. The ligands do not seem to interact with the sensitivity to erlotinib (which binds at the intracellular domain of EGFR). By contrast, clear, although moderate correlation pattern was found to cetuximab, which binds at the extracellular domain of EGFR, possibly in this way interacting with the ligands of EGFR. The results clearly depict the different mechanisms of action of both EGFR inhibitors.

3.2.3.5 Implications of the expression of EGF receptors for tumor growth and chemosensitivity

Neither the protein- nor the mRNA expression of any of the HER receptors correlated with the TDT or RTV of the untreated PDX models, suggesting that the expression of the HER receptor does not confer a PDX the capacity to grow faster *in vivo*. Although expected, the

mRNA expression level of the EGFR receptors did not correlate with the optT/C-values for the EGFR inhibitors or any of the substances used to characterize the models.

Table 20: Correlation analysis between the expression of the EGFR receptor family members and the sensitivity of the models towards EGFR-inhibiting therapies.

	opt T/C Cetuximab		opt T/C Erlotinib	
	r_S	p-value	r_S	p-value
EGFR (protein)	0.179	n.s.	0.149	n.s.
ΔC_T EGFR	-0.226	n.s.	-0.203	n.s.
ΔC_T HER2	-0.170	n.s.	-0.034	n.s.
ΔC_T HER3	-0.058	n.s.	0.065	n.s.
ΔC_T HER4	-0.184	n.s.	-0.088	n.s.

n.s. = not significant

The expression of the EGF receptor family in the PDX models appeared to be differential and elucidated HER1 (EGFR) and HER3 as the two receptors more highly expressed in the 49 PDX. The strong correlations between the receptors themselves, as well as in the expression between the receptors and the ligands AREG, EREG and BTC, reflect the dynamics of the EGFR pathway. No correlations were obtained between the receptor expression and sensitivity to cytostatic, nor targeted drugs. This means, that the expression of HER1 – HER4 had no influence on the growth rate or sensitivity of the PDX.

3.2.3.6 Status of KRAS and other effectors downstream of EGFR as biomarker for the response to EGFR inhibitors

The mutational status of KRAS has been recognized as a biomarker for resistance towards cetuximab treatment in patients with CRC. The influence of the KRAS mutational status on the sensitivity to cetuximab in the PDX models is analyzed in *Figure 20*. The PDX are arranged from left to right from the highest to the lowest optT/C-values. The ratio between PDX carrying mutated and wildtype KRAS was rather balanced (55% PDX with a mutation). Notably, if a cut off is set at optT/C = 25% (the models on this side of the graph also were staged as SD or PR according to the modified RECIST criteria), only two of the 16 sensitive models (13%) have an activating KRAS mutation. From the remaining 33 PDX, 26 (78%) carry an activating KRAS mutation. According to these results, KRAS is predictive for resistance to cetuximab in the set of 49 PDX.

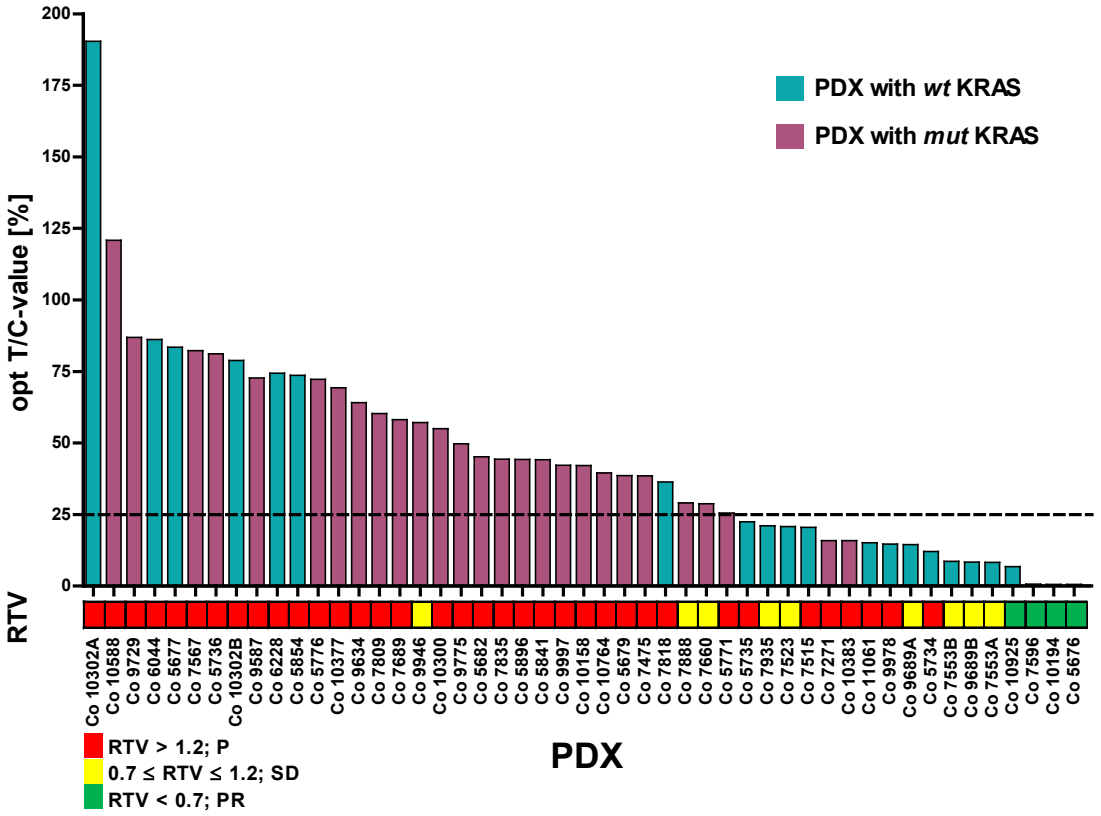

Figure 20: The 49 PDX models are grouped according to their optT/C-value for cetuximab. The bar below represents the RTV values. The colors of the bars were chosen according the mutational status of KRAS.

Similar analysis were done for BRAF and PIK3CA. The optT/C-values for cetuximab and erlotinib were not significantly different between PDX with a mutated or a wildtype PIK3CA. This was also the case for BRAF. From five PDX with a BRAF mutation, only the three carrying the V600E mutation (Co5854, Co10302A and Co10302B) were resistant to cetuximab. In this case the mutation V600E of BRAF could be also predictive for resistance to cetuximab. Nevertheless, PDX models which were triple wildtype for BRAF, KRAS and PIK3CA had significantly lower optT/C-values towards cetuximab and erlotinib than PDX models in which one or more of these genes were mutated ($p = 0.001$ and $p = 0.010$, respectively).

To further explore the role of KRAS and its influence on the sensitivity to EGFR inhibitors, the optT/C-values for cetuximab and erlotinib were compared between PDX models carrying the wildtype *KRAS* gene or a mutated one. The results of this comparison are summarized in *Figures 21* and *22*. For both EGFR inhibitors, the PDX models with a mutated copy of *KRAS* had significantly higher optT/C-values.

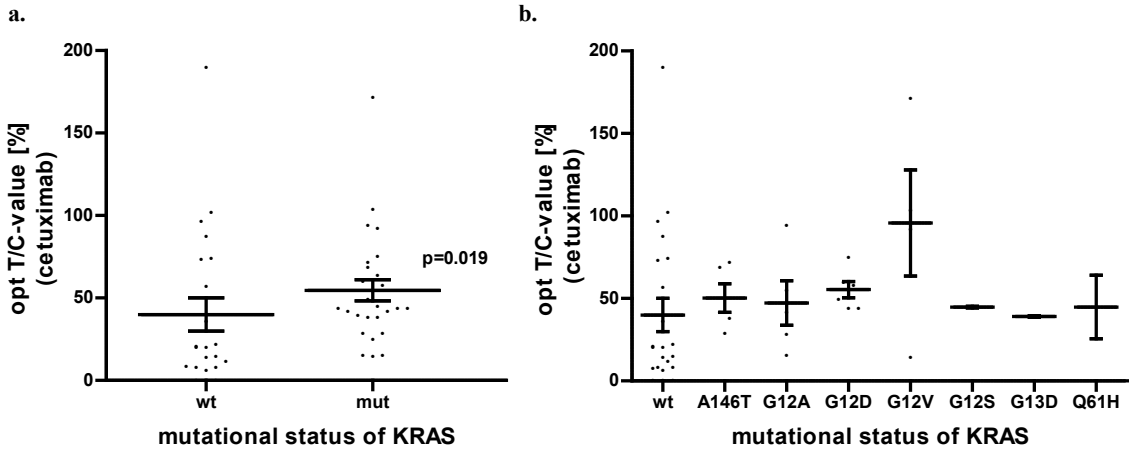

Figure 21: Comparison of the sensitivity to cetuximab (optT/C-values) between PDX with wildtype or mutated KRAS. **a.** Comparison between models with a mutated or wildtype KRAS; **b.** The different base exchanges were taken into account.

To further analyze, if the different aminoacid exchanges caused by the mutations had a differential influence on the sensitivity towards EGFR inhibitors, the different mutation variations were also compared. For both inhibitors, none of the specific mutations could show a predictive value for itself. There were also no significant differences in the T/C-values between the different mutations. The small sample number could also have been disadvantageous for the analysis, the biggest group was the one carrying the mutation G12V (6 PDX), all other groups had less subjects. The predictive role of a KRAS activating mutation has been recognized as a marker for cetuximab sensitivity. Clearly, the mutational status of KRAS is also predictive of the erlotinib sensitivity.

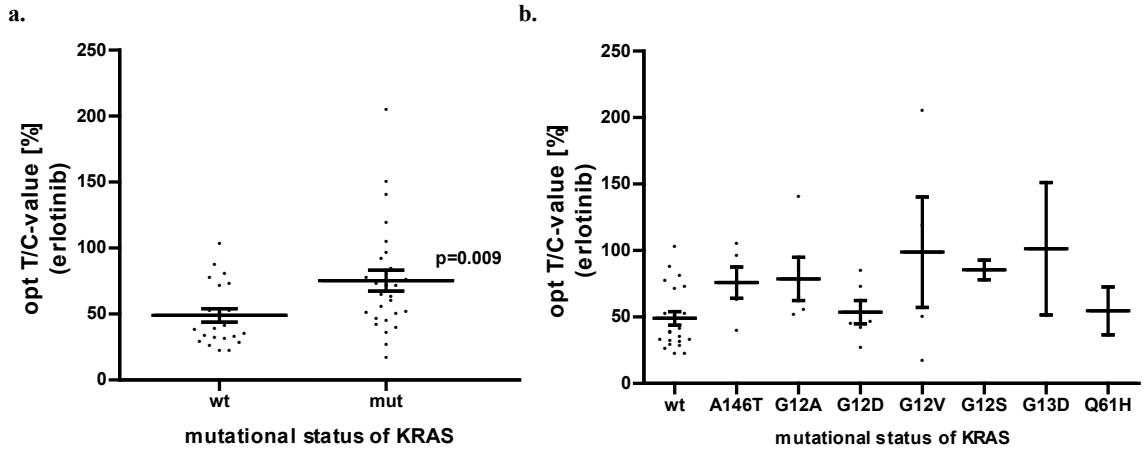

Figure 22: Comparison of the sensitivity to erlotinib (optT/C-values) between PDX with wildtype or mutated KRAS. **a.** Comparison between models with a mutated or wildtype KRAS; **b.** The different base exchanges were taken into account.

3.2.3.7 Analysis of gene copy number of key players of the EGFR pathway

Genetic aberrations can alter the sequence of a gene (mutations or SNPs), but also the gene's copy number, in this way also altering its expression. The gene copy number (GCN) of molecules downstream of EGFR, known to be relevant for the sensitivity towards cetuximab and other EGFR inhibitors, was also determined in the PDX models. For this a real-time PCR based approach was used. The genes scrutinized were EGFR, BRAF, KRAS, NRAS and c-MET. The results obtained can be found in *Annex V*. Even though c-MET is not a downstream effector of EGFR, it was taken into account for this measurement, since several reports already implicated its expression and GCN as markers for cetuximab sensitivity. Representatively, the GCN of EGFR and KRAS has been summarized in *Figure 23,* the values for all 49 PDX can be found in *Annex V*.

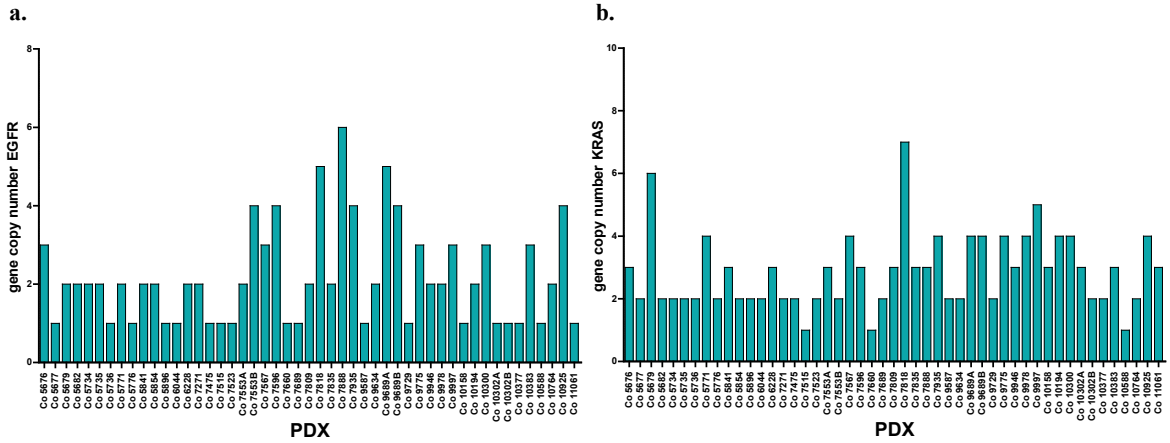

Figure 23: Gene copy number (GCN) of molecules involved in the EGFR pathway, determined by a real-time PCR-based approach. **a.** Gene copy number of EGFR in the set of 49 colorectal PDX models. **b.** Gene copy number of KRAS in the set of 49 colorectal PDX models.

Correlation analysis of the GCN of the molecules involved in the EGFR pathway

As well as for the other molecular analysis, the GCN were analyzed with the Spearman regression method in order to elucidate if the GCNs of the analyzed genes correlate with each other. *Table 21* summarized the obtained r_S and their respective p-values. As shown in *Table 21* all GCN correlate with each other, showing r_S-values above 0.5 in all cases and all p-values were lower than 0.001. The highest coefficients were found between EGFR and BRAF (r_S = 0.922) and EGFR and c-MET (r_S = 0.790), suggesting, that the copy number of these genes correlate positively.

Table 21: Correlation analysis of the gene copy numbers (GCN) of the key players of the EGFR network. This table summarizes the Spearman coefficients (r_s) and their corresponding p-values.

GCN	BRAF		EGFR		KRAS		MET		NRAS	
	r_S	p-value	r_S	p-value	r_S	p-value	r_S	p-value	r_S	p-value
BRAF	-	-	0.922	<0.001	0.599	<0.001	0.739	<0.001	0.670	<0.001
EGFR	0.922	<0.001	-	-	0.673	<0.001	0.790	<0.001	0.692	<0.001
KRAS	0.599	<0.001	0.673	<0.001	-	-	0.708	<0.001	0.552	<0.001
MET	0.739	<0.001	0.790	<0.001	0.708	<0.001	-	-	0.702	<0.001
NRAS	0.670	<0.001	0.692	<0.001	0.552	<0.001	0.702	<0.001	-	-

3.2.3.8 Correlation of GCN of the molecules involved in the EGFR pathway and the expression of the EGFR ligands and receptors

The expression of the EGFR ligands, as well as the EGFR receptor family, was determined in the set of 49 PDX. In order to see if the expression of these molecules correlates with the GCN of molecules downstream (BRAF, KRAS, and NRAS) linear correlation coefficients between the expression of the ligands and receptors and the GCN of genes downstream of EGFR are connected.

No significant correlations were found between the GCN of the selected molecules and the gene expression of the members of the EGFR receptor family (HER1, HER2, HER3 and HER4), nor their ligands. No significant correlations were detected neither at mRNA nor at protein level. Although expected, the GCN for EGFR did not correlate with its expression at protein or mRNA level.

3.2.3.9 Correlation of GCN of the molecules involved in the EGFR pathway and sensitivity towards EGFR inhibitors

No significant correlations were found between the GCN of the molecules, and the TDT and RTV values of the untreated PDX, thus, the amplification of the genes determined had no influence on the growth rate of a PDX.

The GCN of the molecules (EGFR, BRAF, KRAS, c-MET and NRAS) were also correlated to the optT/C-values for the cytostatics and targeted drugs. In the case of 5-FU, irinotecan, oxaliplatin and bevacizumab, no significant correlation coefficients were found. The analysis revealed statistically significant correlations, when the GCN-values of EGFR, BRAF, KRAS c-MET and NRAS were compared to the sensitivity towards EGFR inhibitors. The GCNs of all measured molecules correlated with the sensitivity towards

both inhibitors. The strongest correlations for cetuximab, as well as erlotinib, were to the GCN of EGFR and BRAF. Only the GCN of NRAS did not correlate to the optT/C-value for erlotinib, and correlated rather slightly to the sensitivity panel of cetuximab. The r_S for the EGFR inhibitors and the GCN of the molecules are shown in *Table 22*.

Table 22: Correlation analysis of the gene copy numbers (GCN) of the key players of the EGFR network and the sensitivity of the PDX towards cetuximab and erlotinib. This table summarizes the spearman coefficients (r_s) and their corresponding p-values.

GCN	opt T/C (Cetuximab)		opt T/C (Erlotinib)	
	r_S	p-value	r_S	p-value
BRAF	-0.533	<0.001	-0.498	<0.001
EGFR	-0.511	<0.001	-0.401	0.004
KRAS	-0.322	0.024	-0.325	0.023
MET	-0.423	0.002	-0.332	0.020
NRAS	-0.357	0.012	-0.266	n.s.

n.s. = not significant

Since the correlation coefficients are negative, higher optT/C-values are associated to a lower GCN. This could mean, that a higher GCN of the above mentioned molecules could be a marker for sensitivity to EGFR inhibition (see *Figure 24*) in the 49 PDX models. Models with a high copy number of molecules downstream of EGFR were more sensitive to its inhibition, possibly reflecting that models where the pathway was highly active from the beginning were sensitive to the inhibition of it. The difference in correlation coefficients between the GCN of EGFR, BRAF, KRAS, c-MET and NRAS and cytostatics and bevacizumab, compared to the correlation coefficients to the response to EGFR inhibitors, reflect that there is a specific interaction between the molecules that participate in the EGFR signaling cascade and cetuximab or erlotinib.

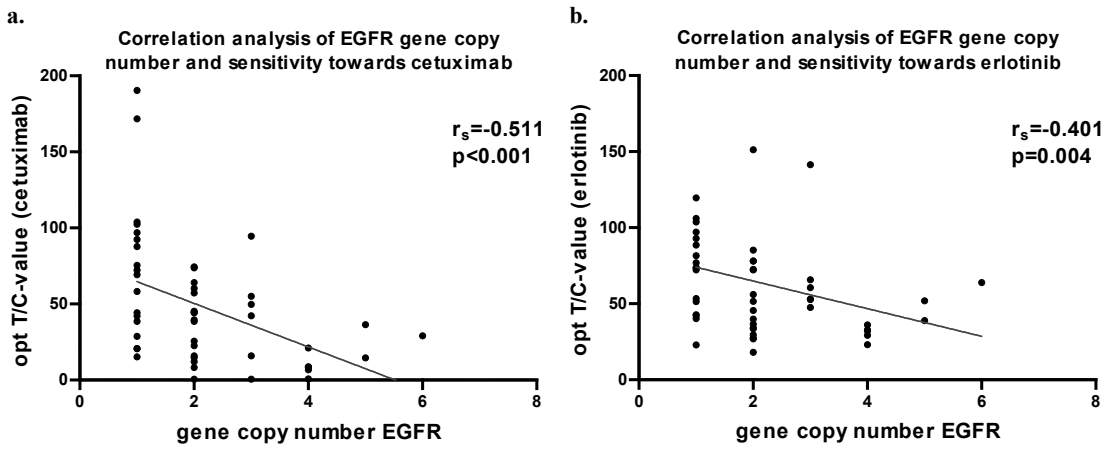

Figure 24: Correlation analysis between the gene copy number of EGFR and the sensitivity towards two EGFR targeting drugs, cetuximab **(a.)** and erlotinib **(b.)**. A non-parametric correlation analysis was carried out, Spearman r (r_S) was calculated.

3.3 Cetuximab resistant PDX sub-lines

One of the aims the this study was to elucidate the mechanics of the EGFR pathway and the sensitivity towards EGFR inhibitors in the 49 PDX models. A cetuximab resistant counterpart to a cetuximab sensitive model (Co7596) was established by continuous treatment of the mentioned PDX with cetuximab during 10 passages *in vivo*. Additionally, a PDX model which was not established with this group of 49 PDX, Co10718, was also chronically treated with cetuximab for 10 passages and became resistant.

3.3.1 Co7596_cetux PDX model

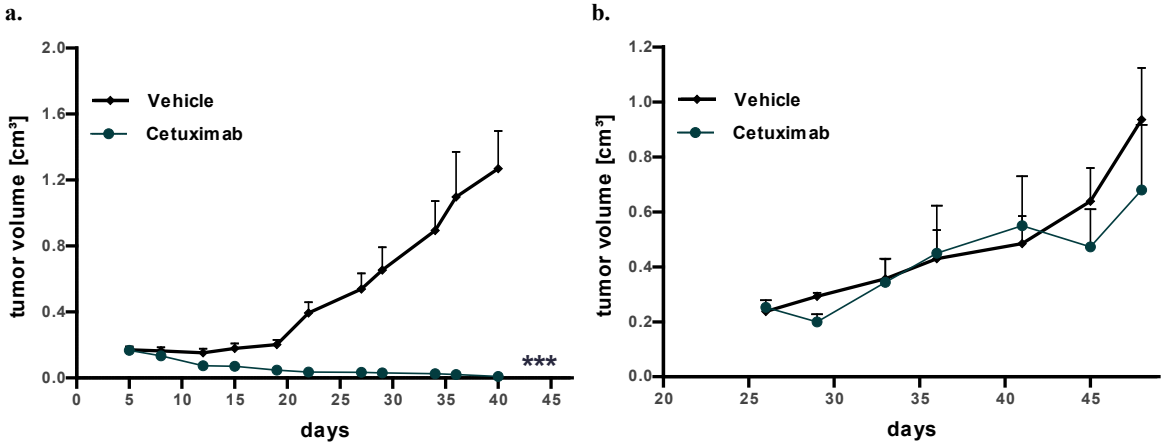

Figure 25: The PDX model Co7596 was initially sensitive towards cetuximab **(a.)**. After continuous treatment with cetuximab the PDX model was resistant **(b.)**.

As shown in *Figure 25*, the sensitivity to cetuximab of the PDX model Co7596 decreased drastically after the 10 passages of being continuously treated with it. The optT/C-value for this model, obtained on day 40, was 0.7% for the original PDX. The optT/C-value for the Co7596_cetux sub-line on day 45 was 74%. It is important to note, that the treatment schedule used in the original PDX was Q7Dx2 (*Figure 25.a*), while in the right graph the Co7596_cetux model was treated weekly until the end of the experiment.

3.3.2 Co10718_cetux PDX model

Similar results were obtained for the initially sensitive PDX Co10718 model. Initially, an optT/C-value of 23% was reached with the cetuximab treatment. The optT/C-value after serial cetuximab treatment in passage 10 was 46% on day 25 (see *Figure 26*). This PDX was initially not as sensitive towards cetuximab as Co7596, the difference in sensitivity towards cetuximab reached after 10 passages was also lower than by Co7596_cetux.

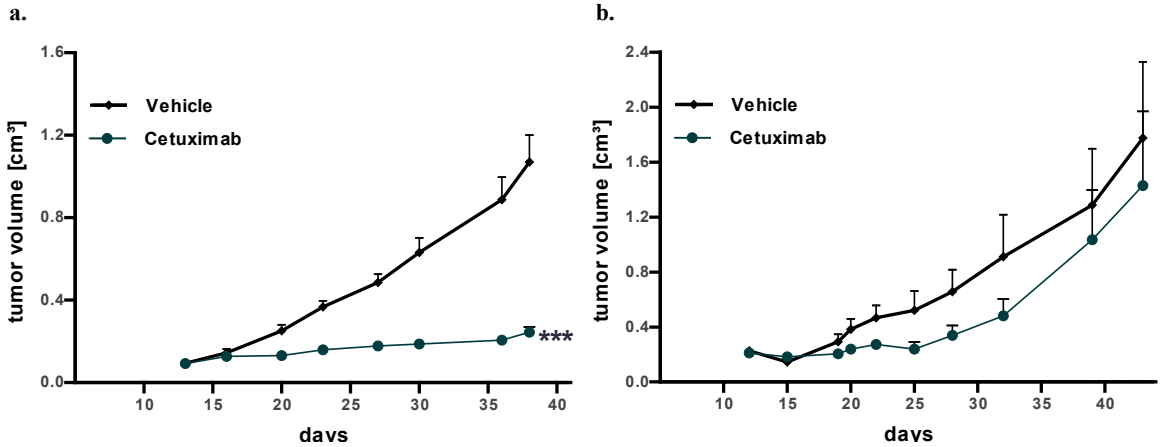

Figure 26: The PDX model Co10718 was initially sensitive towards cetuximab (**a.**). After continuous treatment with cetuximab the PDX model was resistant (**b.**).

Together with their sensitive counterparts, these cetuximab resistant PDX are an excellent tool to investigate acquired resistance mechanisms towards cetuximab and other EGFR targeting antibodies. They can also be used to test alternative drugs in order to overcome acquired resistance to cetuximab.

3.3.3 Comparison of the genetic profile between original PDX and cetuximab resistant sub-lines

With the aim to determine if the mutational profile of the PDX would change due to the treatment, tissue from the cetuximab resistant sub-lines was also subjected to sequencing with the Illumina TruSeq® Amplicon – Cancer Panel. The results obtained for the cetuximab resistant sub-lines are compared to the results obtained for the original PDX in *Table 23*. Genes for which mutations were detected (or expected after studying current literature) are summarized in the *Table 23*. The rest of genes targeted with the Illumina TruSeq® Amplicon – Cancer Panel were wildtype in all samples.

Table 23: The genetic profile of the original PDX and its cetuximab resistant counterparts were analyzed using the Illumina TruSeq® Amplicon – Cancer Panel. The results obtained for all genes in which mutations were detected and/or expected were summarized in this table.

PDX	Mutated gene *(mutated allele frequency [%], AA mutation)*						
	APC	BRAF	EGFR	KRAS	RET	SMAD4	TP53
Co 7596	99, R876X				99, Y791F		99, R243W
Co7596_cetux	99, R876X				99, Y791F		99, R282W
Co 10718	95, insertion 1554			67, G12S		72, Y353N	94, insertion 132
Co 10718_cetux	95, insertion 1554			93, G12S		55, Y353N	94, insertion 132

The genetic profile of Co7596 remained unchanged through 10 passages during which the PDX were subjected to treatment with cetuximab. In the case of Co10718, the ratio of DNA containing a mutation changed after the desensitization process. The mutated allele frequency for the KRAS G12S was elevated from 67% to 93%, and the frequency of the mutation Y353N in SMAD4 changed from 72% to 55%. The alternate allele frequency for both genes changed by 26% and 17%, respectively. These numbers point towards an emergence of a more homogeneous tumor cell population from a mixed cell population, since the numbers of the resistant sub-line resemble to those obtained for homogeneous populations of cells carrying an homozygote (KRAS) or heterozygous (SMAD4) mutation.

3.3.4 Expression of EGFR ligands in cetuximab resistant PDX sub-lines

As the expression of EGFR ligands correlated with the sensitivity to cetuximab in the 49 PDX models, the expression of these molecules was also analyzed in the cetuximab resistant PDX sub-lines and compared to their original counterparts. To ensure that the changes found were not a consequence of sequential passaging, samples from untreated PDX Co7596 and Co10718, that were passaged in parallel to the treated cetuximab resistant sub-lines, were used (n = 5).

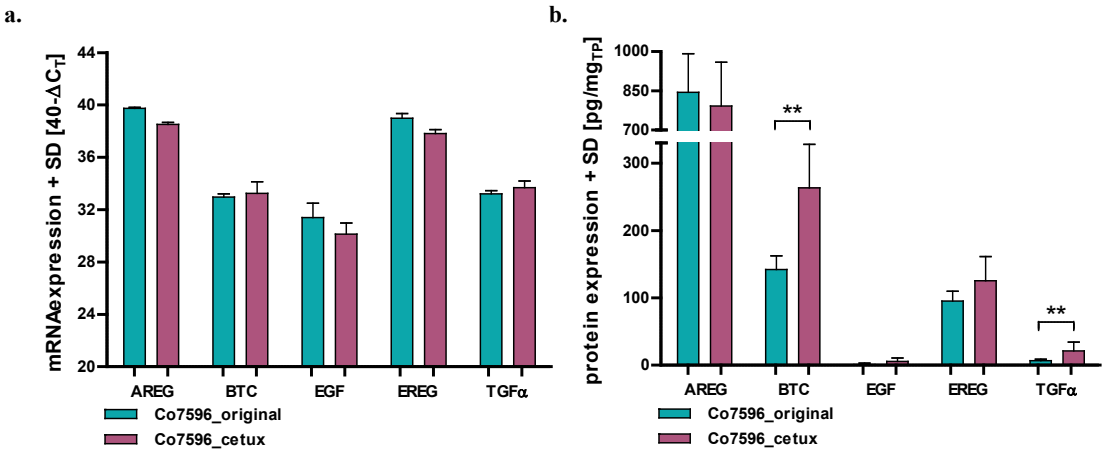

Figure 27: Comparison of the expression of EGFR ligands between Co7596 and its cetuximab resistant counterpart Co7596_cetux. **a.** mRNA expression; **b.** Protein expression.
** significantly different from original PDX, $p < 0.01$

Figure 27 depicts the mRNA and protein expression of EGFR ligands in Co7596 and Co7596_cetux (the cetuximab resistant counterpart to Co7596). The ΔC_T-values were again subtracted from the number of cycles used for the real-time RT-PCR (40 cycles) to maintain proportion on the graph. No statistically significant changes in the expression

level of mRNA of the molecules selected (AREG, EREG, BTC, EGF and TGFα) for this examination were detected. At protein level, the expression of BTC and TGFα were significantly elevated in the cetuximab resistant sub-line. The concentration of BTC in the PDX tissue was almost 2-fold in the sub-lines (from 141.95 ± 20.50 pg/mg_{TP} to 263.36 ± 64.4850 pg/mg_{TP}) and the concentration for TGFα showed 4-fold increase from 6.86 ± 1.98 pg/mg_{TP} to 21.14 ± 13.20 pg/mg_{TP}). The concentrations of TGFα were very low in all samples, also when compared to the concentrations of the remaining ligands. It should be questioned, if this concentration is able to induce changes in the signal transduction in the PDX or is a side effect of another change induced by the cetuximab treatment.

Table 24: Comparison of the expression levels of Co7596 and its cetuximab resistant counterpart Co7596_cetux. The mRNA expression was determined using real-time RT-PCR and the protein amount in the PDX tissue was measured with ELISA. Both PDX models were passaged the same amount of times.
**significantly different from original PDX, p<0.01

	mRNA expression [ΔC_T]				
	AREG	**BTC**	**EGF**	**EREG**	**TGFα**
Co 7596	0.27±0.08	7.04±0.25	8.61±1.09	1.02±0.37	6.80±0.24
Co 7596_cetux	1.47±0.14	6.75±0.89	9.88±1.85	2.19±0.30	6.31±0.51
	protein expression [pg/mg_{TP}]				
	AREG	**BTC**	**EGF**	**EREG**	**TGFα**
Co 7596	844.74±147.01	141.95±20.50	0.90±2.01	95.27±14.42	6.86±1.98
Co 7596_cetux	791.84±167.463	263.36±64.48**	5.64±4.90	125.58±35.80**	21.14±13.19

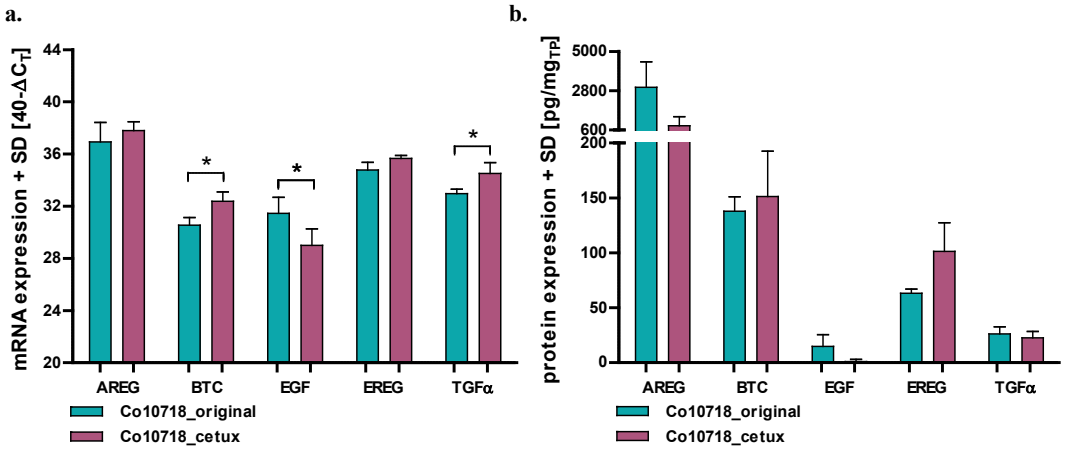

Figure 28: Comparison of the expression of EGFR ligands between Co10718 and its cetuximab resistant counterpart Co10718_cetux. **a.** mRNA expression; **b.** Protein expression.
* significantly different from original PDX, p < 0.05

Figure 28 depicts the mRNA and protein expression of EGFR ligands in Co10718 and Co10718_cetux (the cetuximab resistant counterpart to Co10178). A statistically significant difference in ΔC_T-values between the original and resistant PDX were detected for the genes BTC, EGF and TGFα. The expression levels of BTC and TGFα were

elevated (lower ΔC_T-values are a sign of a higher amount of the molecule mRNA in the sample) and the level of EGF mRNA was lowered. The difference in expression on mRNA level could not be corroborated on protein leve (the values are summarized in *Table 25*).
In both cetuximab resistant PDX sub-lines an elevated expression of BTC and TGFα was detected, at protein level in the case of Co7596, and mRNA-level in Co10718.

Table 25: Comparison of the expression levels of Co10718 and its cetuximab resistant counterpart Co10718_cetux. The mRNA expression was determined using real-time RT-PCR and the protein amount in the PDX tissue was measured with ELISA. Both PDX models were passaged the same amount of times.
*significantly different from original PDX, $p < 0.05$

	mRNA expression [ΔC_T]				
	AREG	**BTC**	**EGF**	**EREG**	**TGFα**
Co 10718	3.06±1.49	9.46±0.59	8.56±1.25	5.23±0.57	7.03±0.34
Co 10718_cetux	2.21±0.69	7.62±0.71*	10.99±1.27*	4.33±0.23	5.49±0.83*
	protein expression [pg/mg$_{TP}$]				
	AREG	**BTC**	**EGF**	**EREG**	**TGFα**
Co 10718	2995.58±2455.82	137.89±22.92	14.80±18.72	63.13±8.74	26.20±11.02
Co 10718_cetux	841.23±499.50	151.29±41.13	0.93±2.09	101.31±26.09	22.60±5.86

3.3.5 Expression of EGFR family members in cetuximab resistant PDX sub-lines

Figure 29 summarizes the comparison of the original and cetuximab resistant PDX models concerning the expression of the four receptors that build the EGFR receptor family.

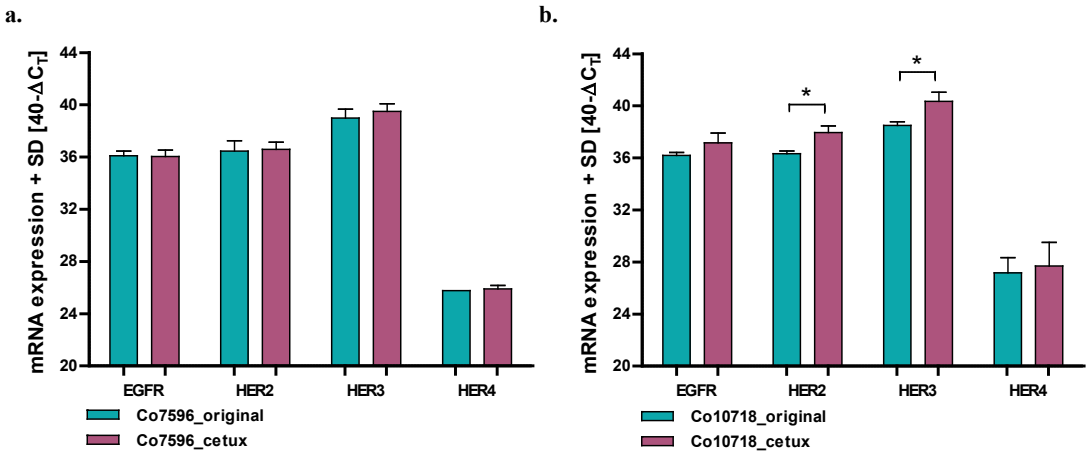

Figure 29: Comparison of the expression of mRNA of EGFR receptor family members between two PDX models chronically treated with cetuximab and its original counterparts. **a.** Co7596 and Co7596_cetux; **b.** Co10718 and Co10718_cetux.
*significantly different from original PDX, $p < 0.05$

No statistically significant changes in the expression level of mRNA of the HER receptors were detected in the tissue of the Co7596 derived models (*Figure 29*). In the case of Co10718 a statistically significant increase ($p < 0.05$) of HER2 and HER3 mRNA and decrease of EGFR protein was detected in the cetuximab resistant sub-line (see *Table 26*).

Table 26: Comparison of the expression levels of HER1, HER2, HER3 and HER4 in the PDX Co7596 and Co10718 and its cetuximab resistant counterparts Co7596_cetux and Co10718_cetux. The mRNA expression was determined using real-time RT-PCR and the protein amount for EGFR in the PDX tissue was measured with ELISA. The PDX models were passaged the same amount of times.
*significantly different from original PDX, $p < 0.05$

	mRNA expression [ΔC_T]				Protein expression [ng/mg_{TP}]
	EGFR	**HER2**	**HER3**	**HER4**	**EGFR**
Co 7596	3.90±0.37	3.54±0.79	1.01±0.67	14.24±0.00	2.27±0.54
Co 7596_cetux	3.97±0.50	3.40±0.55	0.50±0.58	14.09±0.26	2.78±0.60
	mRNA expression [ΔC_T]				**Protein expression [ng/mg_{TP}]**
	EGFR	**HER2**	**HER3**	**HER4**	**EGFR**
Co 10718	3.80±0.39	3.67±0.35	1.50±0.47	12.84±1.66	6.69±3.35
Co 10718_cetux	2.84±0.76	2.06±0.52*	-0.34±0.70*	12.31±1.82	1.65±0.39*

3.3.6 GCN of key players of EGFR pathway in cetuximab resistant PDX sub-lines

The CGN of BRAF, EGFR, KRAS, NRAS and c-MET significantly correlated with the optT/C-values of the 49 PDX models. In order to analyze if this relationship also plays a role in acquired resistance to cetuximab, samples of the original PDX and its cetuximab resistant counterparts, were examined regarding the GCN of the mentioned genes. No statistical differences could be detected in none of the two PDX models (see *Figure 30*).

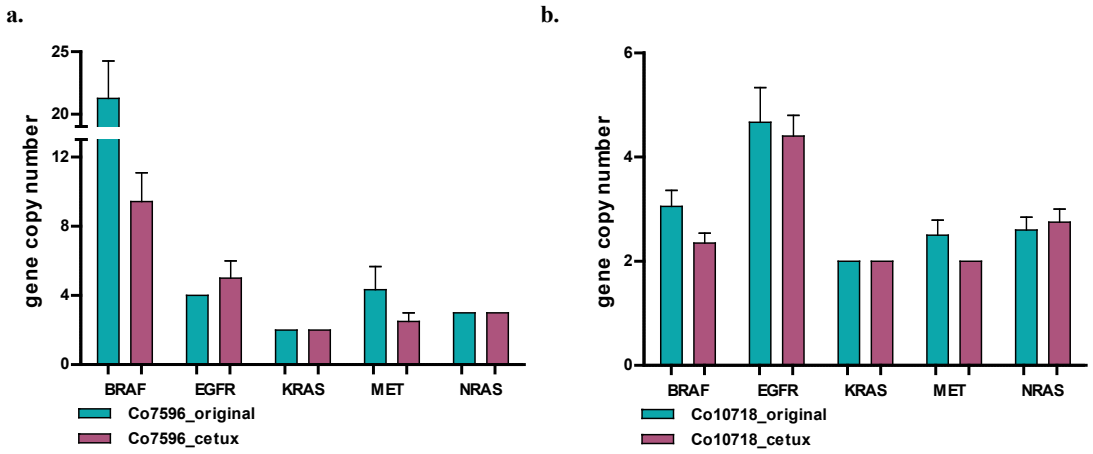

Figure 30: Comparison of the gene copy number of key players of the EGFR pathway between two PDX models chronically treated with cetuximab and its original counterparts passaged for the same number of times. **a.** Co7596 and Co7596_cetux; **b.** Co10718 and Co10718_cetux.

Table 27 summarizes the GCNs of the CRC PDX models and the cetuximab resistant sub-lines thereof. A decrease of BRAF GCN from 21.25 to 9.42 was observed in Co7596_cetux. It did not reach significance, though.

Table 27: Comparison of the GCN of BRAF, EGFR, KRAS,MET and NRAS in the PDX Co7596 and Co10718 and its cetuximab resistant counterparts Co7596_cetux and Co10718_cetux. The GCN was determined using a real-time PCR based assay (n = 5). The PDX models were passaged the same amount of times.

	Gene copy number				
	BRAF	**EGFR**	**KRAS**	**MET**	**NRAS**
Co 7596	21.25±4.24	4.00±0.00	2.00±0.00	4.33±2.31	3.00±0.00
Co 7596_cetux	9.42±2.90	5.00±1.41	2.00±0.00	2.50±0.71	3.00±0.00
	Gene copy number				
	BRAF	**EGFR**	**KRAS**	**MET**	**NRAS**
Co 10718	3.05±0.69	4.67±1.15	2.00±0.00	2.50±0.58	2.60±0.55
Co 10718_cetux	2.35±0.42	4.40±0.89	2.00±0.00	2.00±0.00	2.75±0.50

The measurements carried out for these two resistant models show that upon blockade of the EGFR pathway, the PDX react in a different way, changing the expression of molecules that take part of or interact with the EGFR pathway. In both cases an increased production of BTC was detected in the resistant PDX and in PDX Co10718, the receptors HER2 and HER3 were upregulated upon blockade of HER1 or EGFR.

Summary of results

For this study 87 surgical samples from CRC patients were subcutaneously transplanted to immunodeficient mice. The tumor entities were evenly distributed between colon and rectum, primary tumor and metastasis; lung and liver metastases. At a tumor size of TV ≥ 0.5cm³ the PDX were serially transplanted into further mice (passaging). When three subsequent passages were successful, a PDX model was regarded as stably passageable. Different methods were used to corroborate the similarity between patient tumor tissue and its corresponding PDX:

1. human nuclei staining of PDX tissue,
2. comparison of HE staining of tissue from several PDX passages and patient tissue,
3. expression of EpCAM, p53 and EGFR in the PDX tissue.

The genetic profiles of selected patient samples and its corresponding PDX were compared to insure similarity between the patient tumor and the corresponding PDX model. The growth characteristics and TDT of the PDX models were assessed. The origin of the tissue (derivation site, primary vs. metastasis) did not correlate to the growth rate of the PDX, but a faster growth was encountered in PDX models with a mutation in PIK3CA (TDT = 7.1 d vs. TDT = 10.5 d; p = 0.019). Every PDX model showed a different and individual mutational profile and ratios were calculated for each mutated gene. Different PDX derived from tissue of the same patient showed largely similar mutational profiles.

The models were also characterized regarding their sensitivity towards cytotoxic and targeted drugs. When a statistically significant ($p \leq 0.05$) optT/C-value ≤ 50% was taken as sensitivity read-out, response rates between 37% and 46% were obtained for bevacizumab, 5-FU and oxaliplatin. For targeted drug treatments, 63% and 67% responder rates were obtained for erlotinib and cetuximab, respectively. Overall, the best response rate was obtained with irinotecan treatment (92%).

In order to elucidate, if the molecular signaling pathway dynamics are maintained in the CRC PDX models, the 49 established PDX were extensively characterized at the molecular level. Key factors that take part in or that influence the EGFR pathway were analyzed and correlated towards the sensitivity panels of the EGFR inhibitors. Activating mutations in KRAS and BRAF were predictive of resistance to cetuximab and erlotinib. PDX models with widtype KRAS, BRAF and PIK3CA were significantly more sensitive towards EGFR targeting drugs ($p = 0.001$ and $p = 0.010$ for cetuximab and erlotinib, respectively).

Significant r_S were encountered between the expression panels of EGFR ligands and receptors, corroborating the existence of an autocrine loop between them. Significant r_S were also found between the expression of EGFR ligands and the sensitivity panel of cetuximab, in contrast to erlotinib, reflecting the fact, that the substances bind different domains of the EGFR. Furthermore, the GCN of BRAF, EGFR, KRAS, NRAS and c-MET correlated positively and significantly with sensitivity towards both EGFR inhibitors.

In order to further study the dynamics cetuximab resistance, two cetuximab resistant PDX models were established by continuous treatment of the PDX with cetuximab during subsequent passages. An increase in the expression of the EGFR ligands BTC and TGFα was observed in both resistant models. An increase in HER2 and HER3 expression, coupled to a decrease in expression of EGFR, was found in one of them, showing that a PDX setting could be used to elucidate resistance mechanisms to cetuximab *in vivo*.

4. Discussion

Cancer is a highly heterogeneous disease characterized by multiple genetic aberrations in extensively interconnected and redundant signaling cascades. The inherent complexity of the disease severely affects drug discovery leading to cancer therapies having the highest drug attrition rates among all other therapeutic areas. Novel targeted therapies have been developed, but preclinical biomarker oriented studies are needed to stratify responsive patients. Identifying correct targets using appropriate preclinical models is critical to prevent further treatment failures. Although there are various *in vivo* systems used to study cancer, mouse models represent the most widely used system. The ease of genetic manipulation, short gestation period and low maintenance cost are some of the advantages associated with the use of murine systems [188]. A set of 49 CRC PDX was established in this work and vastly characterized. Further, experiments were designed to explore the dynamics of the EGFR network in the PDX cohort in order to prove their functionality as preclinical tools for testing of novel substances or biomarker search.

4.1 Standarization of the PDX models

Choice of mouse strain and implantation site

Growth of human tumors in mouse models has been problematic for many reasons. Commonly used immunodeficient mouse strains carrying the *Prkdc*^{scid} mutation or deficient in the recombination activating genes 1 or 2 (*Rag1*^{null} or *Rag2*^{null}) were used with success for analyzing the growth of distinct subsets of purified or enriched CRC cells *in vivo*, but showed to be less reliable when used for intact tumor fragments [189–191, 167, 166]. These mouse strains have moderate natural killer (NK) cell activity and other innate immune function that impede primary human tumor engraftment [168]. Severely immunodeficient NOD-*scid* and NOD-*Rag1*^{null} strains carrying the *IL2rg*^{null} mutation (NSG and NRG) support the growth of many types of human primary tumors and the NSG mouse strain has recently been identified as an ideal model for growth of primary human tumor samples by several groups and showed high capacity to engraft tumor cells, as well as cells from the immune system or even tumor adjacent stroma cells [166, 168, 192–194]. In a study by Maykel *et al.*, that compared PDX growth for CRC tumor fragments in NOD-*scid*, NSG and NRG mice, higher engraftment rates were obtained in NSG and NRG. Besides, a higher variability in the tumor size of engrafted tumors and graft-versus-host

reactivity was observed in the NOD-*scid* mice [168]. Due to these advantages, the NSG mouse strain was chosen for first implantation of the tissue. After an initial engraftment in NSG mice, the PDX were transferred onto the less immunocompromised NMRI*:nu/nu* mice. This step had to be undertaken in order to make the sensitivity characterization, since NMRI*:nu/nu* show a better tolerance towards therapy and are easier to handle and examine due to the lack of fur. In most cases, tumors could be successfully passaged from NSG to NMRI*:nu/nu* mice, so the engraftment rate was not compromised by the change of strain. HE staining of the PDX formed exclusively in NSG (4 cases) revealed that the tissue lacked the histology characteristic to CRC and the gland structure observed in patient samples and other PDX was lost. These samples were classified as malignant lymphomas by the pathologist and were not further investigated within this study.

The original patient tissue architecture is also maintained in PDX when tumor fragments are implanted into the renal capsule of mice, and orthotopic implantation additionally yielded PDX that produced the proteases needed for extravasation and were able to metastasize in distant organs [168, 195, 196]. Nevertheless, the s.c. model was chosen because of its easy manipulation and higher reproducibility of results. Tumor fragments could be directly implanted into the subcutis of the mice, while a dissociation of tumor tissue would have been required for orthotopic implantation. Besides, the s.c. tumors could be easily examined and the TV could be measured by caliper and followed over time. A chemosensitivity testing with PDX growing orthotopically or in the renal capsule would involve more complicated examination methods (e.g. X-ray analysis of the animals or transfecting the cells with GFP or luciferase before implantation). Using these methods would make a comprehensive drug screening as presented in this work much more complicated and laborious, requiring a higher number of animals and a longer experimentation period. With the perspective of making this model available for individual therapy prediction and translational studies, processing times must be kept as short as possible. The s.c. PDX models are more capable to address this issue, nevertheless, orthotopic PDX models can be complementary to address other aspects of CRC or test metastasis inhibiting substances.

For melanoma, the level of immunosuppression in recipient mice is a key determinant of engraftment [197]. In BC tissue, however, NSG and *scid*-beige mice showed similar take rates [176]. In our set of samples, all PDX initially engrafted in NSG could be successfully transferred in NMRI*:nu/nu*, suggesting, both strains are equally suited for CRC PDX

generation. Nevertheless it has to be taken into account, that the initial propagation in NSG facilitated the availability of vital tissue for secondary engraftment, probably contributing to the take rate in NMRI*:nu/nu*.

4.1.1 Histology and analogy to original patient samples

Stroma and histology

There are constraints about the acquisition, utilization and distribution of patient tumor tissues [131], besides they are limited in the amount available for any individual tumor and contain varying (and often unknown) amounts of non-malignant cells, as can be seen on *Figure 4.a*. While original patient samples present highly variable ratios of tumor cells, PDX tissue contains clearly pronounced tumor areas. Added to the capacity of propagating the tumor tissue by passaging, this makes PDX models a well suited alternative for nucleic acid or protein analyzes which require a larger amount of tissue as can be obtained from the clinic. Moreover, PDX tissue and even patient tissue can be cryopreserved [198], giving the possibility to further expanding the tissue amount or working with low passages of the established PDX in future studies.

In order to serve as a valid model of human CRC tumor growth, the architecture of the original tumor must be maintained within recipient mice with regard to such features as retention of gland structure and location and distribution of stroma. All 49 established PDX displayed the characteristic adenocarcinoma architecture showing glandular morphology with well-defined epithelial and stromal components (see *Figure 4*). Human nuclei staining confirmed the observation made by the pathologist at HE staining examination, the human CRC tumor cells reconstructed the structures observed in patients. However, human stroma cells were replaced by murine stroma cells. PDX tumors maintained similar composition and quantity of stroma relative to tumor cells through several passages as seen on *Figure 6*. The Ki-67 and PCNA staining show that the CRC tumor cells actively proliferated *in vivo*, while stroma compartment murine cells were rather mitotically inactive. This observation has also been made by others, and similar results were obtained using staining for PCNA in CRC PDX [168].

The complete absence of human nuclei staining in the stromal compartment of the PDX shows that human stroma cells were lost and the stromal compartment was repopulated by murine cells. No data could be collected about the progression of this process, except, that

it was initiated in the P0. In a study by Maykel *et al.*, the human cell fraction in the stroma of PDX tissue declined to ca. 50 % of the original amount two weeks after transplantation, and further to ca. 25 % by four weeks. No identifiable human cells were detected in the stroma of secondary and tertiary hosts, although the size and composition of the tumor stroma remained consistent [168]. Even though there has been controversy over how long and to what extent the human-derived microvasculature and immune cells are maintained in PDX [193, 199], in the vast majority of studies, as well as this set of PDX, only murine stroma cells were detected in fully developed PDX. The PDX were normally harvested when they reached a volume of 1-2 cm^3, which took a mean time of 49.4 d. This period is long enough to complete the replacement of most of the human stroma by murine fibroblasts, consistent with a study in seven CRC PDX, where this was demonstrated using allelotyping analysis [172].

As shown in *Figure 4.4*, the staining pattern for EpCAM further verified the adenocarcinoma phenotype of the PDX. Positive staining for EpCAM was observed in all 49 PDX, and the staining marked the same cells as human nuclei staining. EpCAM is a transmembrane glycoprotein originally discovered as a colon carcinoma-associated antigen and is found on the cell surface of some normal and most neoplastic epithelial cells [200, 201]. It localizes at the basolateral membrane in normal polarized epithelia, but in carcinoma this expression pattern changes to an intense uniform membranous overexpression that is frequently associated with cytoplasmic staining [202]. EpCAM IHC of PDX samples showed a predominantly membrane bound staining pattern and the molecule was detected in moderate (e.g. Co9978) or strong (e.g. Co10194) intensity. Staining for EpCAM was used by our group for the quality control of NSCLC PDX due to its ubiquitous expression in epithelial derived cancers [173]. Others also used IHC staining for CEA or Cytokeratin 20 (CK20) for the identification of CRC PDX tissue, obtaining similar results and staining patterns [203, 174]. The expression of EpCAM in the tumor areas of the PDX tissue further confirmed the maintenance of the tumor characteristics *in vivo*. These findings were supported by the positive staining for human p53 and EGFR, nevertheless EpCAM was best suited for an initial analysis of engraftment since it showed a more homogeneous and detectable expression level in all PDX.

In contrast, cell line derived xenografts show little resemblance to the original tumor regardless of site of implantation. They generally show a more homogeneous, undifferentiated histology, probably indicative of the *in vitro* selection [131, 204].

Xenografts generated from such cell lines do not show adenocarcinoma histology as can be observed in PDX tissue (see *Figure 4* and *5*). Several other research groups as well as us demonstrated that implanting histologically intact tumor tissue more accurately represents the clinical features of tumors when compared with injecting tumor cell suspensions [174].

4.1.2 Stability of histology and genetic profile of the PDX models in serial passages

One of the major criticisms of cell lines is their inherent instability, especially on long term culture. The more divisions cells undergo, the greater is the likelihood of accumulating mutations. Because cell lines have short doubling times, they undergo more divisions, over a period of time, than do tumor cells in a patient. Most CRC cell lines cultured *in vitro* have doubling times of app. 24 h or less [205]. The mean TDT value for the 49 PDX was 10 d. Thus, cells growing in a PDX undergo much less divisions in the same period as tumor cells cultivated *in vitro*, making them less susceptible to genetic drift.
CRC cell lines grown as s.c. xenografts display half as short TDTs than the PDX in several studies (TDT was 4.1 - 5.3 d for the cell lines L174T, HCT15 and HT-29) [206–208]. Thus, CRC PDX display a more comparable growth rate to an original CRC tumor than cells cultivated *in vitro* or xenografts derived from established cell lines.

Samples from several passages from three PDX (Co9587, Co9775 and Co10925) were sequenced using the TruSeq® Amplicon – Cancer Panel and their mutational profiles were stable along the passages. PDX samples from three different passages (between P0 - P14), harvested at different time points and stored at -80°C, were used for the expression analysis of the four EGFR receptors (HER1 - HER4) and their ligands. Samples from the same PDX displayed similar expression values for all molecules analyzed and standard deviations were moderate (*Figures 12*, *14-19*), resulting in a well differentiated expression pattern of the 49 PDX. This finding corroborates the maintenance of biochemical characteristics and the conservation of a differential expression profile between the PDX through the passaging process.
The monoclonal nature and the absence of tumor stroma are biological factors that limit the direct comparison of data obtained with cell lines *in vitro* to *in vivo* tumors. There are also technical factors, like cross-contamination and culture adaptation, that limit this comparison [205]. Preclinical models failing to accurately predict activity of drugs in the appropriate clinical histology in the NCI program and other studies might be a

consequence of using cell lines *in vitro*, subjected to clonal selection for years, as the source of material for starting xenografts. For example, mutation of p53 or silencing of the gene encoding the DNA repair protein MGMT occurs relatively frequently in *in vitro* culture [209, 210]. Taking p53 as an example; 53% of all PDX displayed a mutation in this gene (see *Table 9*), in accordance with the incidence of 50% in CRC patients [34]. This shows that there is no positive selection for p53 mutated tumors during the engraftment process. While no mutations were found in Co 9587 and Co 10925, the PDX Co 9775 had a stably detectable homozygous mutation in p53 in tissue from all four passages analyzed and the corresponding patient tumor tissue. The increase in mutated DNA in the PDX in comparison to the patient tissue sample can be explained by the higher ratio of tumor cells in the PDX tissue and also by the fact that the stroma DNA is of murine origin and not recognized by the human specific sequencing assay. Analyses of copy number alterations (CNAs) and exome sequencing data in PDX also show extraordinary concordance between patient and PDX paired samples, also with a trend towards higher frequency of genomic alterations in the PDX, likely as a result of increased human tumor DNA purity in the PDX tissue [211]. Similarly to our findings, CRC PDX retained the major mutations of the primary tumor in all four cases examined in a recent study [203].

As these sequencing results demonstrate, the presence of pronounced fractions of stromal cells in the original patient samples may make interpretation of results obtained in the mutational profiling misleading. Interestingly, PC PDX models have been used to enrich the tumor DNA content for the PC genome sequencing project [212]. Contamination with non-malignant cells may mask the presence of mutations, and makes detection of gene deletions exceedingly difficult [131]. Presence of human non-malignant cells in CRC patient tissue was shown in some cases to impair detection of LOH, which can be circumvented by use of PDX tissue for the analysis [172]. The availability of high quality DNA and RNA from PDX tissue was greatly helpful for all molecular analyzes as an additional source of tumor material. The absence of human stromal cells has advantages and disadvantages. A pure human tumor cell population is analyzed when methods are adapted to consider murine background, greatly improving characterization of tumor cells. On the other hand, no information can be obtained about the stromal and inflammatory cells present in the original tumor, which can often play a crucial role in tumor formation, growth, angiogenesis, and sensitivity towards treatment.

Mutation profiling showed no major variations in the status of the principal genes mutated in CRC, indicating that the fundamental genetic elements driving tumor growth in the patients were maintained in PDX. For all mutations found, the ratios for the alternate variant frequency stayed stable along the passages, demonstrating, that no accumulation or negative selection of clones carrying a mutation took place during the passaging process.
One of the suggested pitfalls of using PDX cohorts to evaluate treatment options, is that there seems to be a selection of certain histology subtypes, like it has been reported for BC and NSCLC [170]. Since all CRC samples obtained in this study belonged to the adenoma histology, no selection regarding histology subtype could be elucidated. Besides, the high engraftment rate of 56 % rules out strong engraftment bias.

4.1.3 Proliferation and engraftment rate of the PDX models

An engraftment rate similar to other CRC PDX panels was obtained (56%) [213, 214, 161, 162]. In our group of 49 PDX, the sample derivation site was equally distributed between primary tumors (53%) and metastases (47%). The even distribution suggests, that tissue samples from metastases and primary tumors had comparable capacity to form PDX when implanted s.c. to immunodeficient mice, but information about the patient characteristics lacks for the non-engrafted tumor samples. Alternatively, the TDTs and RTVs of the PDX generated from the two different tissue sources were compared, in order to verify if the capacity to generate a xenograft varies between samples from primary tumor tissue or metastasis, yielding a negative result. There was also no difference between the RTV and TDT of PDX derived from primary tumors of patients which did not show metastases and the ones that had distant metastases at the time point of sampling (M0 vs. M1). PDX derived from tissue from tumors in G2 and G3 stages were also compared regarding their TDT, which did not yield statistically significant differences. Similar results were obtained by Burgenske *et al.* in a group of 16 CRC PDX. Nevertheless, head to head comparison of s.c. implantation from primary tumors and metastasis from uveal melanoma from the same patient yielded a higher engraftment rate for the metastases and in a study that included 116 tumor samples from different entities, metastatic tumors had a higher engraftment rate than primary tumors [215][216]. For CRC PDX, advanced stage and moderate to poor differentiation also positively correlated with engraftment in other studies [213]. A reason that these correlations were not observed in the established PDX panel can also be that the growth ratio as PDX does not reflect the potential for initial engraftment *in vivo*.

Although CRC PDX showed a high engraftment rate in this and other studies compared to other tissues (rates as low as 25% for NSCLC [173] or 10% for PC [217] have been reported), it is still desirable to improve the take rates for CRC PDX. The option of dissociating the tumor tissue and expanding it *in vivo* prior to implantation yielded a success rate of only 70% in establishing primary cultures, which often showed either a portion only or none of the mutations of the original CRC tumor, pointing to a considerable selection while culturing tumor cells *in vitro* and which lead to a formation of tumors *in vivo* in only 20% of cases [203]. This corroborates that the direct implantation of intact tumor tissue is still the method of choice for the generation of PDX.

4.1.4 General characteristics of the patients

Among the 49 PDX models established, a higher rate (61%) was derived from male patients, while the derivation sites were evenly distributed between colon and rectum as primary site. The ratio was also balanced between PDX derived from samples from primary tumor and metastases, also evenly distributed between liver and lung, and one lymph node metastasis is represented in the established set of PDX. Ten (20%) of the engrafted samples led to establish tumor pairs derived from the same patient. These five pairs can be a valuable tool to address metastasis related analysis in CRC, as well as resistance development or tumor heterogeneity focused studies. From the 70 CRC *in vitro* cell lines mostly used for preclinical studies, there are only 4 pairs known to be derived from the same patient, and one pair derived from a primary tumor and subsequent lymph node metastasis (SW480/SW620) [218]. Our five PDX pairs contribute substantially to the choice of models available for preclinical CRC research to date. Similar studies also demonstrated to have the advantage of harboring tumor pairs amongst the freshly established PDX sets [174]. Mutation differences between paired cell lines were detected, but they did not affect the CRC related genes APC, TP53, SMAD4, PIK3CA, KRAS and BRAF in 88% of the cases [218]. Similarly, the compared 5 PDX pairs displayed the same mutational profile, except for Co10302, from which only Co10302A had an heterozygous mutation of APC. When taking into account all the 48 genes analyzed, a heterozygous mutation of GNA11 was detected only in Co7553A, absent in Co7553B, and a heterozygous mutation in Erbb4 was detected in Co10300, derived from the metastasis of the same patient as Co9997. These results underline the heterogeneity of CRC and the importance of using comprehensively characterized models for cancer research.

4.2 Characterization of the PDX models

4.2.1 Mutational profiling

The gene most frequently mutated in the PDX was APC (67%). This was in accordance with the clinically reported incidence of this mutation in CRC patients (70 - 80%) [219]. All base exchanges and deletions detected in the PDX were mutations that lead to a truncated and functionally inactive protein, commonly found in patients. Somatic APC mutations are frequently found in the CRC mutation cluster region (MCR), between codons 1250 and 1450, the protein region where ß-catenin binding and degradation takes place. Most of the mutations detected were deletions, or base exchanges in this region (e.g. Co5679, Co5771, etc), and the mutation R876X, detected in Co7596 and Co10194, is also a truncating mutation, common in CRC [220]. APC mutations are the key genetic event in CRC carcinogenesis and lead to a deregulated WNT signaling, altering apoptosis [36].

Mutations in p53 (or *TP53* gene) were also found in 53% of the established PDX; five PDX carried a base substitution at R248*, four PDX at R175* and three at R273*. All these mutations are within the DNA binding domain of p53, a known hotspot, where 95% of all *TP53* mutations in cancer are found [221]. The p53 protein is a regulator of cell-cycle arrest and cell death and is mutated in about 50% of all CRC, this mutation is often part of the transition of a late adenoma to an invasive carcinoma [34].

55% of the established CRC PDX models carried an activating mutation in KRAS, while the ratio found in patients is ca. 40% [107, 108]. This finding suggests that an activating KRAS mutation confers a tumor the enhanced ability to engraft as a PDX, even though the TDTs were not higher in the PDX with a KRAS mutation than in the PDX with wildtype KRAS. In contrast, PDX carrying an activating mutation of PIK3CA (16%) were found to have significantly shorter TDTs than models carrying a wildtype copy of the gene (7.1 d vs. 10.5 d, $p = 0.019$). In a similar study carried out with NSCLC specimens, tumors with an activating KRAS mutation showed a higher engraftment rate [222]. Both these findings are in line with the reported prognostic value of these mutations in CRC patients [45, 46, 106], which indicate that tumors with a biologically more aggressive phenotype and higher risk of recurrence in association with worse prognosis, are more likely to engraft.

Also the incidence of BRAF mutated tumors in the PDX set reflected the reported incidence for CRC (ca. 10%) [219]. As well as in CRC patients [223, 224], KRAS and BRAF mutations were mutually exclusive in the PDX set. This suggests that an activating

mutation in only one of these genes is sufficient to promote tumorigenesis and BRAF seems to be mutated at a similar phase of tumorigenesis as KRAS [219, 225]. The high incidence of KRAS mutations in CRC and in this set of PDX reflects the fact that KRAS mutations are a relatively early event in the adenoma-carcinoma progression sequence; although they occur after the APC mutations. This assumption was also supported by the fact that KRAS and BRAF mutations match in paired primary tumors and their metastasis [226], as well as in all five tumor pairs derived from the same patient in this set of 49 PDX.

In conclusion, the mutations detected in the PDX overlapped with common mutations found in patients, making these models well suited for sensitivity testing. Other groups that established large CRC PDX cohorts also confirmed that the frequency of mutations in CRC relevant genes closely mirrors the frequency in human samples [161, 162].

4.2.2 Sensitivity towards conventional cytostatics and targeted drugs

4.2.2.1 Sensitivity towards standard of care cytostatic agents

In general, the models display a differential pattern of response to the agents tested. Some of the models had a high responsiveness towards all three agents tested (e.g., Co5735, Co10925 and Co11061) while others were resistant (e.g., Co10588 and Co9587), in this way probably indicating for more invasive and malignant tumors. Even if a few tumors seem sensitive or resistant to chemotherapy in general, the set of PDX reflects the heterogeneity of CRC and different mechanisms of action of the drugs. Nevertheless, the optT/C-values for the three cytostatic drugs all significantly and inversely correlated with the RTV of the untreated tumors, thus demonstrating, that cytostatic drugs act in a largely ubiquitous manner and affect mainly fast dividing cells. The response to the three drugs was largely concordant in all five tumor pairs derived from the same patient, further confirming the reproducibility and specificity of the results (*Table 11*).

5-FU

When an optT/C value of 50% was set as cut off for sensitivity, 21/49 PDX models (44%) were classified as sensitive to the drug and using the modified RECIST criteria to evaluate the response, a responder rate of 6% was obtained. The doses used for the cytostatic agents corresponded to the Maximum Tolerated Doses (MTD) in NMRI*:nu/nu* mice, previously

elicited by this research group. In this case, the dose administered to the mice was lower than the equivalent for humans. Treatment with 5-FU reduces tumor size by 50% or more in 10 - 15% of patients with advanced CRC (Objective-Response Rate or ORR) [56, 227].

Irinotecan

Irinotecan reached the highest response rate among all cytostatics (92%), when using a 50% optT/C value as a cut-off for sensitivity and 50% of the PDX showed a SD or PR. This differs from the clinical ORR. Phase II trials demonstrated that irinotecan monotherapy results in ORRs of 16 - 27%, with SD occurring in a further 40 - 60% of patients and response rates in 5-FU-pretreated and chemotherapy-naive patients were similar, suggesting lack of cross-resistance. In contrast, the four PDX resistant to irinotecan (Co9587, Co97829, Co9946 and Co10588) were as well resistant to 5-FU and oxaliplatin. The dose used in this study (15 mg/kg, equivalent to 45 mg/m²) is comparable to the dose used in clinical studies. Nevertheless, after bolus administration of irinotecan to patients, only 5% of the drug is converted to its active metabolite SN-38, in contrast to 50% measured in mice [228]. Certain compounds, such as camptothecins, show a better tumor response in mice due to differences in protein binding or metabolism [229]. In the case of irinotecan, the expression of the enzyme carboxylesterase is responsible for the increased metabolization of the compound in comparison to humans.

Oxaliplatin

The lowest response rate amongst the three used cytostatic agents was achieved with oxaliplatin (37% responder) and 8% of the models showed an RTV below 1.2, independenty of patient characteristics. When used as a single agent, oxaliplatin achieved a 10% ORR in CRC patients refractory to 5-FU and ORRs of 20 - 24% were achieved in two different studies that tested oxaliplatin as first-line monotherapy [60, 230, 231].
Similar response rates were obtained with 5-FU and oxaliplatin, as well as in the clinic, while irinotecan showed to be more active in NMRI*:nu/nu* mice than in humans.

4.2.2.2 Sensitivity towards targeted agents

Bevacizumab and cetuximab achieved very similar and high response rates in the 49 PDX (67% and 63%, respectively) and erlotinib had a lower response rate (41%). The optT/C values for cetuximab and erlotinib strongly correlated to each other, but also correlated

moderately to bevacizumab. In contrast to the cytostatic agents, the optT/C values for the EGFR-inhibitors did not correlate to the TDT or RTV of the PDX. The sensitivity values for bevacizumab correlated negatively and significantly with the RTV values, indicating that faster growing PDX were less sensitive to bevacizumab.

Bevacizumab

Bevacizumab reached the highest response ratio among the targeted agents tested (67%). The addition of bevacizumab to the FOLFOX or IFL regimen increased the ORR from 35% to 45% for CRC patients [232]. The response rate was also in this case higher in the PDX models; even though the dose used was similar to the one in humans (5 mg/kg).
Tumor xenografts are largely used in preclinical anti-angiogenic assays, since it is impossible to measure vascularization in a 2D cell culture system. The assessment of sensitivity to anti-angiogenic therapies in a xenograft system is controversial, since human stroma and endothelial cells are replaced by murine cells. Nevertheless, a differential sensitivity profile was obtained for the 49 PDX to the human specific bevacizumab, proven not to cross-react with murine VEGF-A [233], thus demonstrating that the sensitivity was tumor specific. A study using 150 PDX from different histologies demonstrated, that the relative amount of murine endothelial cells remains stable, independently of the density of the stroma, while the expression of the human pro-angiogenic molecules varied within the PDX and rather correlated with the tumor type [234]. VEGFs are not only expressed on endothelial cells, but can also be expressed on tumor cells, which play a role in resistance to therapies, mainly by secreting pro-angiogenic factors and undergoing vascular mimicry (the ability of tumor cells to form functional vessel like networks and cancer stem cell differentiation into tumor cells [235]). A study in CRC PDX models assessed the response to two angiogenesis inhibitors (aflibercept and bevacizumab) and concluded, that the tumor growth is driven more by the VEGF-A produced by the malignant, rather than the stromal cells, and confirmed that CRC tumor cells express high levels of angiogenic factors [236], which makes PDX an appropriate tool to test anti-angiogenic therapies.

Cetuximab

A response rate of 63% was obtained for cetuximab in the PDX panel, higher to the 10 - 15% response rate observed in unstratified CRC patients [237]. When using the modified RECIST criteria, 4/49 (8%) of PDX reached a PR, and SD was observed in further 9 PDX

(18%). Similar results were obtained when using the recommended cetuximab doses (250 mg/m² to 400 mg/m²) in CRC patients; PR was reached in 8% of the cases and SD in 46 - 54% and was higher when superior, although not recommended, doses were used [237].

Erlotinib

The EGFR TKI erlotinib showed a decreased activity in the PDX panel compared to cetuximab. 4/49 PDX (8%) displayed a SD upon erlotinib treatment. Erlotinib has an ORR of 10% in NSCLC patients and is not approved by the FDA for the treatment of CRC [80]. In a phase II study of erlotinib in CRC patients, SD was observed in 12/31 patients [83]. The optT/C-values obtained for this TKI correlated strongly with those for cetuximab, thus underlining the similar mechanism of action of both drugs. From the 20/49 PDX models with an optT/C < 50%, 18 showed a similar or lower T/C-value to cetuximab and only two of them (Co5854 and Co9587), were resistant to it. These results demonstrate that erlotinib shows some activity in CRC and could be used as an EGFR-I in certain cetuximab-resistant patients. The PDX setting is appropriate to identify non-standard treatments for particular tumors, thus being an excellent tool for personalized medicine.
In contrast to the cytostatic agents, the optT/C values for the EGFR-I did not correlate with the RTV. This can be explained by the fact, that cytostatics usually target dividing cells, while EGFR-I act in a targeted manner. It also underlines the value of PDX as a predictive tool for solid tumors, in contrast to cell line derived xenografts, which showed to be predictive only for fast growing malignancies rather than for solid tumors [150].

In summary, the sensitivity characterization of the PDX panel demonstrated, that it is difficult to predict the efficacy of a drug if only an evaluation of the optT/C value or RECIST criteria is used. The choice of endpoints is a critical variable when translating a PDX response to the clinic. The evaluation of sensitivity using the optT/C value showed higher response rates as in the clinical setting. The results obtained with the more stringent modified RECIST criteria mirrored the clinical situation more closely. The response evaluation criteria in solid tumors used in clinical trials require at least 50% shrinkage to be considered an objective response (OR). A growth inhibition of 50% classifies a PDX as responder, but tumors are treated at an early time point after engraftment (ca. 0.1 cm³), in contrast to patients, where already advanced tumors formed at treatment start and cannot be treated as effectively, e.g. as result of lack of drug delivery to the tumor tissue due to

necrotic areas or abnormal vascularization. On the other hand, the head to head comparison to an untreated control group will identify tumors that in spite of not being completely eradicated by the treatment, still show a transient growth delay, which can be used to identify new treatment possibilities and explore mechanisms of resistance. Moreover, the PDX model offers the possibility of testing several agents in one tissue sample, thus eliciting the most effective treatment for the particular tumor. The response panel established can also be used as a reference when evaluating the sensitivity of a single tumor to a particular agent. Further, the way a substance is administered (dose, route, scheduling) and formulated is a critical variable when translating preclinical results into the clinic. The MTD of most drugs that could be given to mice is usually 4 - 5 times higher than in humans and *in vivo* studies must be designed in a way that no severe drug-induced toxicity will be experienced by the animals [238]. Unfortunately, these are variables that will commonly influence the treatment course of a patient and hence also the response to the drug. Especially the irinotecan sensitivity panel shows, that PDX studies should be designed with dose levels that mimic biological exposure in patient populations in order to increase the correlation between preclinical and clinical results.

The results obtained depict the need for analogous, standard protocols, ideally reaching a protocol designed and approved by an authority for generating and evaluating PDX models with comparable standards in the different research groups to reliably correlate results obtained from different independent studies.

4.2.3 Characterization of the dynamics of the EGFR-pathway in the PDX models with focus on EGFR inhibition

The EGFR and its ligands have been correlated to CRC and other cancers. The expression of these molecules has been linked to a more aggressive disease or a poor prognosis in several cancers, including CRC, NSCLC and PC, among others [239, 240]**.** This group of molecules was chosen to be studied in the CRC PDX with the aim to find out, how closely the dynamics of the signaling pathway in PDX recapitulate the situation in patients.

4.2.3.1 Expression of ligands of EGFR

The expression of the ligands of EGFR was measured in PDX tissue from different passages at mRNA and protein level. The protein concentrations showed high correlation coefficients with the ΔC_T-values in all cases except TGFα, which means that a high mRNA

amount in the tissue leads to a high protein concentration. In the case of TGFα a rather modest r_S of 0.45 suggests the possibility of post-transcriptional regulation of expression. TGFα is likely to be modulated post-transcriptionally, since its disproportionately large 3'UTR region contains multiple putative microRNA seed sequences [241].

The highest and most differential expression (at mRNA and protein level) was found for AREG, closely followed by EREG, indicating that the expression of these molecules could be biologically relevant. The lowest expression was measured for EGF and TGFα. BTC showed mRNA values similar to those of TGFα and EGF, but a protein expression similar to that from EREG. These results are in accordance with a study that assessed the expression of EGFR ligands in 144 samples of CRC and observed, that AREG and EREG expression was higher than the expression of EGF, TGFα and HB-EGF [242].

Correlation coefficients were calculated for all analyzed ligands at mRNA and protein level. At mRNA level, significant r_S were found between all ligands analyzed, except TGFα and EREG. The highest r_S were found between AREG, EREG and BTC (r_S between 0.580 and 0.824 at mRNA level), indicating a tight correlation of expression of these three genes. These genes have been mapped to chromosome 4 in humans and localized in close proximity to each other [243], which suggests a possible common regulation of expression. An analysis of 144 CRC tumors also determined that AREG and EREG are tightly co-expressed, and it was further confirmed, that this correlation is maintained in primary tumors as well as liver metastases [242, 244, 245]. This work shows, that the link between AREG and EREG already made by others extends to BTC. The expression of AREG and EREG has also been correlated to the increased likelihood of liver metastasis [246, 247], and this phenomenon could also involve BTC, since CRC tumors that tend to express high levels of AREG and EREG, also would express high levels of BTC as these results show. The expression of EGFR ligands can be upregulated upon activation of the receptor by the ligand itself (auto-induction), as well as by other members of the EGFR ligand family [243], which is in wide agreement with the results obtained.

4.2.3.2 Expression of EGFR and the HER receptor family

EGFR is overexpressed in many different cancer types, including 60 - 80% of CRC [248, 249]. Also in other cancer types, like oral squamous cell carcinoma, expression of HER1 - HER4 were higher in tumor cells compared to adjacent normal tissue [239].

EGFR mRNA and protein could be detected in all PDX models by IF, real-time RT-PCR and ELISA. Since IF did not detect differential expression levels, ELISA was chosen to quantify EGFR protein in the PDX tissue, and a dynamic expression range was obtained by this method. The protein concentration of EGFR was considerably higher than the concentration of the ligands. There was no significant correlation between the mRNA and protein expression, which means that a high amount of mRNA does not necessarily lead to a high amount of protein, and post-translational regulation of expression takes place.
The mRNA expression of HER2 - HER4 was assessed in the 49 PDX models. While high expression, comparable to EGFR, was detected for HER2 and HER3, a much lower expression of HER4 was measured and no HER4 mRNA was detected in 16/49 PDX. While comparable expression of HER2 - HER4 was found in CRC patient tumors using IHC, lower mRNA levels of HER4 compared to HER2 and HER3 were found in CRC cell lines [248, 250–252], a finding also made in this set of PDX. The expression of all HERs significantly correlated with each other. Several studies showed co-expression of the ErbB receptors in CRC, and this co-expression increased with tumor progression [251, 252].

4.2.3.3 Correlation analysis of the expression of HER receptors and ligands

Correlation coefficients were calculated using the ΔC_T-values for receptor-ligand pairs. The expression levels of TGFα and BTC yielded high, significant r_S with all four receptors, while AREG correlated to HER1-HER3. Surprisingly, the expression of EREG did not correlate to the expression of any of the receptors at mRNA level, this in spite of the strong correlation of expression between AREG and EREG. Controversially, in oral squamous carcinoma, EREG, and not AREG, correlated with the expression of HER2, HER3 and HER4 [239]. The obtained results confirm the redundant and intricate nature of the EGFR signaling system, even though different ligands have different receptor binding properties, and also a presence of an autostimulatory loop in cancer cells [253].

4.2.3.4 Implications of the expression of EGFR ligands for tumor growth and chemosensitivity

No significant correlations were obtained between the optT/C-values for 5-FU and oxaliplatin and the analyzed EGFR ligands. The PDX response to irinotecan correlated strongly to the expression of TGFα, as well as the expression of EGF protein (*Table 18*). The PDX expressing higher levels of these molecules tend to be resistant to irinotecan.

Since irinotecan sensitivity was found to be overpredictive in PDX models and strongly and negatively correlated with the RTV of untreated tumors, and TGFα and EGF are epithelial mitogens, this is not a targeted phenomenon, but rather a ubiquitous finding, that the expression of these growth factors protects the CRC cells from irinotecan.

Concerning bevacizumab, the expression of AREG mRNA and EREG protein showed moderate r_S to sensitivity (r_S-values of 0.29 and 0.34, respectively). No patient studies that addressed the expression of EGFR ligands and sensitivity to angiogenesis inhibitors were found to date. The low r_S-values suggest that the identified relationship is not robust. TGFα, on the other hand, correlated modesltly to the optT/C-values at protein and mRNA level, PDX with a higher TGFα expression were resistant to bevacizumab. It is possible, that the mitogenic action of TGFα protects the PDX from bevacizumab induced growth inhibition. TGFα is not only an epithelial-specific autocrine mitogen, but it also acts in a paracrine manner; derivatives of KM12C CRC cells, expressing 10-fold higher levels of TGFα than parental cells, were able to recruit VEGF-producing macrophages and resulted in highly vascularized and metastatic tumors *in vivo* [254].

AREG and EREG correlated robustly to the optT/C values for cetuximab. PDX with a higher expression of these two molecules tended to show a great tumor growth inhibition upon treatment with the antibody. This relationship is well documented in CRC patients. Khambata-Ford *et al.* firstly reported that AREG and EREG tumor mRNA levels represent promising predictors of benefit with anti-EGFR antibodies [255]. This relationship was also confirmed in a series of irinotecan-refractory patients [256]. Also, an increase of serum level of AREG, EREG and EGF after cetuximab therapy was found, and plasma concentrations correlated with response to cetuximab monotherapy [257]. This depicts the cancer hallmark of oncogene addiction; hence, PDX tumors with a growth dependence on a certain pathway will be inhibited by the inhibition of it. Interestingly, these correlations were not observed for erlotinib, underlining the different mechanisms of action of the two drugs. Since cetuximab binds to the extracellular domain of EGFR, it competes with the ligands for the binding site. Erlotinib binds to the intracellular TK domain, thus not interacting with the ligands. TGFα behaved inversely, and its expression showed to be predictive of resistance towards cetuximab, but not erlotinib. In a study including 62 CRC patients treated with cetuximab monotherapy, AREG and EREG were elevated in sensitive tumors and TGFα behaved inversely [237]. Also, compared to AREG, tumor EREG mRNA was a stronger predictor of cetuximab benefit, which is also in accordance with the

results obtained for the 49 PDX, AREG and EREG are not identical. AREG only binds to EGFR and EREG binds to EGFR and HER4 and leads to a prolonged state of EGFR activation [245, 255]. In contrast to KRAS, a "smooth" relationship between the ligand expression and sensitivity to cetuximab was elucidated, which does not allow a clear cut-off value to distinguish sensitive from resistant tumors, a problem already pointed out by studies in CRC patients [245, 256]. A score system using four of the EGFR ligands was proposed to predict sensitivity towards anti-EGFR antibodies [258]. CRC PDX cohorts are suitable to further explore this proposal, since the obtained results show the robust recapitulation of the EGFR-driven pathway in this set of 49 PDX.

4.2.3.5 Implications of the expression of EGF receptors for tumor growth and chemosensitivity

No significant r_S were found between the expression of HER1 - HER4 and therapy outcome, nor RTV or TDT. The lack of correlation with the growth rate of the PDX was surprising, since the expression of these four receptors was demonstrated to be relevant for cancer development and aggressiveness [119]. Nevertheless, the complexity of the ErbB signaling network (as well as cancer) has to be taken into account; factors like phosphorylation status of the molecules, their mutational status, cellular localization as well as intracellular trafficking can influence their activity and its consequences on tumor growth. No previous reports about correlation of HER1 - HER4 to chemotherapy outcome were found, while several studies examined the influence of EGFR on the response to EGFR-I, finding no significant link between both. Furthermore, cetuximab activity was even reported in tumors with no EGFR expression [95, 259]. There was no correlation between the degree of EGFR expression and response to cetuximab, but the EGFR GCN seems to be predictive of cetuximab response [95, 99–101, 259, 260].

4.2.3.6 Status of KRAS and other effectors downstream of EGFR as biomarker for the response to EGFR inhibitors

The optT/C values of PDX resistant and sensitive to the EGFR inhibitors were compared, and for both inhibitors, the optT/C values were significantly higher for KRAS mutated tumors. KRAS is a downstream effector in the EGFR signaling cascade, and an activating mutation of this molecule leads to a strong mitogenic signaling independent of EGFR activation. The role of KRAS activating mutations, mainly in codons 12 and 13, but also

61 and 143, in resistance to cetuximab has been confirmed by several clinical and PDX studies. The FDA additionally approved the first KRAS companion diagnostic test, the *Therascreen*® *KRAS* RGQ PCR diagnostic kit for prescreening of CRC patients [46, 106–109]. Even though the optT/C from KRAS mutated and wildtype PDX were significantly different, not all PDX with an activating KRAS mutation were resistant to cetuximab (e.g. Co7271), showing there are exceptions to this statistical relationship.

The link between KRAS activating mutations and resistance to erlotinib has also been demonstrated for NSCLC and PC, but not CRC, since erlotinib is not approved for CRC treatment [261]. The results obtained in this set of PDX show that even if erlotinib can represent an alternative EGFR inhibitor for some tumors (e.g. Co5854 and Co9587), it is not a treatment alternative for tumors with an activating KRAS mutation.

4.2.4 Analysis of gene copy number of key players of the EGFR pathway

The amplification of the oncogenes or deletion of tumor suppressor genes could play a decisive role in the development of CRC or drug resistance. The GCNs of BRAF, EGFR, KRAS, NRAS and c-MET were analyzed in the PDX models and correlated to proliferation and drug response. PDX tissue only was used for these analyzes, since there was not enough patient tissue available. A study by Cho *et al.* demonstrated, that the patterns of DNA amplification were maintained in the CRC PDX using comparative genomic hybridization (aCGH) microarrays [174]. Thus, we consider the PDX samples representative of the patient tissue regarding GCN.

An amplification of the EGFR gene was detected in 14/49 PDX models, and no gene deletions were found. GCN greater than 4 were detected in 3 models (Co7818, Co7888 and Co9689A). For KRAS, 3/49 PDX had more than 4 copies of the gene. BRAF amplifications were detected in 9/49 PDX and Co7596 had a notably high number of BRAF copies when compared to the rest of the PDX. c-MET amplifications were detected in 36/49 PDX and Co7818 carried the most gene copies. The lowest GCNs were detected for NRAS. The high incidence of gene amplifications measured by a real-time PCR based method in comparison to studies using FISH can be attributed to the exponential nature of template amplification during the PCR (only 10% or 0.67% of CRC patients carry an EGFR or KRAS amplification, respectively, as assessed by FISH) [114].

Some studies report that EGFR gene amplification (determined by *in situ* hybridization methods, using a cut off value of 5 gene copies) is uncommon in CRC, but in recent

studies, modest increases in copy number (three- to fivefold) are present in up to 50% of cases [100, 262, 263]. This is in accordance with the GCN numbers obtained in this set of 49 PDX. However, increased EGFR gene dosage does not always mean increased EGFR protein expression; only 14% of tumors that stained positively for EGFR protein were associated with EGFR gene amplification in a study by Shia *el al.* [262].

Correlation analysis of the GCN of the molecules involved in the EGFR pathway

Notably, the GCNs of all molecules analyzed correlated with each other. Since all these genes have been linked to a more aggressive tumor phenotype, as well as resistance to cetuximab, and are part of the same signaling network, this relationship could be indicative of tumors with a certain pathway addiction. Nevertheless, c-MET, that drives a different pathway than the rest of the molecules, also correlated with all of them. Although it can be that the strong correlation just points out poliploid cells, the c-MET and EGFR receptors have been shown to be able to cross-activate each other, and both pathways play a pivotal role in CRC, which would explain these results [264–266].

Correlation of GCN of the molecules involved in the EGFR pathway and sensitivity towards EGFR inhibitors

The GCN of all molecules analyzed correlated to the outcome of treatment of the PDX with EGFR-I. Only the GCN for NRAS and the optT/C values for erlotinib showed no correlation. The r_S were negative in all cases, meaning that a high GCNs of the analyzed genes is indicative of sensitivity towards EGFR inhibition. These genes seem to be specifically involved in response to EGFR-inhibitors, since no significant correlations between GCNs of the analyzed genes and any of the other treatments were found.
Amplification of EGFR has been associated with sensitivity to cetuximab by several studies, which is in accordance with the results at hand [99, 100, 267, 268]. The three PDX, that displayed EGFR GCN > 4, were all sensitive to cetuximab. KRAS gene amplification in CRC patients has been associated with acquired resistance to cetuximab, since this aberration was shown to emerge in cell lines and patients that were initially sensitive to cetuximab and became refractory after treatment [113, 269, 270]. Also amplifications of c-MET have been associated with cetuximab resistance in NSCLC and CRC [117, 271, 272]. Several papers suggest an interaction between HGF/MET and EGFR signaling pathways. The c-MET activation results in EGFR activation, which contributes

to HGF-induced cell proliferation; e.g. in NSCLC, amplification of c-MET causes gefitinib resistance by driving HER3-dependent PI3K activation [272, 273]. BRAF amplifications are not documented with regard to EGFR-I sensitivity, but were associated with resistance to MEK inhibitors [274]. All of this is contradictory to the gathered results. The analysis seems to identify PDX addicted to the EGFR pathway. Nevertheless, gene amplification can occur as a response to therapy. In order to further elucidate this, GCNs of the molecules were compared between cetuximab-sensitive PDX and their resistant sub-lines.

4.3 Cetuximab resistant sub-lines

Cetuximab resistant counterparts of two cetuximab PDX sensitive models were generated by chronic treatment with cetuximab and their resistance was confirmed *in vivo*. The genetic profile, expression and GCN of molecules documented to be involved in resistance to EGFR-inhibition were analyzed in original PDX and cetuximab-resistant counterparts.

4.3.1 Comparison of the genetic profile between original PDX and cetuximab resistant sub-lines

While no differences in the genetic profiles of Co7596 and Co7596_cetux were detected, an increase of KRAS mutated DNA (67% to 93%) and a decrease of SMAD4 mutated DNA (72% to 55%) were detected in Co10718_cetux. KRAS amplification and emergence of KRAS mutations have been demonstrated to take place in CRC patients with acquired cetuximab resistance. Deletions or inactivating mutations of SMAD are associated with late stage CRC and can make tumor cells resistant to TGFß mediated growth control [275, 276]. This would point out, that cells with a more aggressive phenotype were selected by the treatment. Nevertheless, a heterogeneous population was observed in the initially sensitive xenograft (P2). This represents a rather uncommon phenomenon in the 49 PDX. Whenever possible, PDX with passage numbers lower than five are used for characterization experiments. Since the tumor was passaged 10 times in order to obtain the resistant clones, a selection of the more aggressive population could have happened.

4.3.2 Expression of EGFR ligands in cetuximab resistant PDX sub-lines

Significant increases in BTC and TGFα were found in both resistant sub-lines at protein (Co7596) and mRNA (Co10718) level. Also, a decrease in EGF mRNA was found in Co10718_cetux. Even though not robust, an increased ligand production was observed in

both models, indicating that ligand production can be a general mechanism of resistance to EGRF blockade. A chemotherapy induced ligand shedding by activation of ADAM17 has already been documented in CRC [277], but this phenomenon can also be a response to targeted therapy as demonstrated by these results.

4.3.3 Expression of EGFR family members in cetuximab resistant PDX sub-lines

Only Co10718 showed changes in mRNA expression of the HER receptors. The mRNA levels of HER2 and HER3 were elevated in the cetuximab resistant sub-line, while protein level of EGFR was decreased. The upregulation of the HER2 and HER3 receptors or their increased activation as response to EGFR inhibition has been reported in preclinical models and cancer patients [162, 278, 279]. In these studies, increased GCN of the molecules, as well as their activation status, was determinant for resistance to EGFR-I. This data demonstrates that an upregulation of transcription plays a crucial role in Co10718_cetux. This contributes to the notion that redundant signaling of the EGFR pathway and the ability of a tumor cell to utilize alternative receptors to activate downstream mitogenic cascades (HER reprogramming) play a crucial role in resistance to cetuximab and other inhibitors. The lack of mRNA upregulation in Co7596 does not necessarily mean, that no HER reprogramming took place, since overactivation of a pathway can be detected by means of increased GCN, phosphorylation status or protein expression, among others. This increased expression of HER2 and HER3 can open novel treatments to inhibitors that target HER2 and/or HER3, like afatinib, trastuzumab, lapatinib, sapitinib, etc. Ideally, a panel of resistant CRC PDX should be characterized with alternative inhibitors, which could guide choice of therapy in cetuximab refractory patients, e.g. chronic treatment of BC cell lines with herceptin sensitized them to cetuximab, since the EGFR pathway was upregulated as response to HER2 blockade [280].

4.3.4 GCN of key players of EGFR pathway in cetuximab resistant PDX sub-lines

No statistically significant GCN variations were detected between the original models and their resistant counterparts. Acquired resistance to cetuximab has been associated with amplifications of KRAS, c-MET and HER2. Nevertheless, these events are very rare in CRC. KRAS amplifications were detected in 0.67% of patients and c-MET was only amplified in 2/192 CRC PDX [114, 117]. Thus, the statistical possibility of finding these changes in a set of 2 PDX was very low. The results obtained by analysis of the two

generated resistant sub-lines confirm the notion, that mechanisms of acquired and intrinsic resistance to EGFR inhibitors greatly overlap [113].

In conclusion, here we present two *in vivo* models of acquired cetuximab resistance. These models provide the possibility of examining relevant mechanisms of acquired cetuximab-resistance on molecular level, and they further may be used to test targeting of these tumors with agents that would circumvent or restore sensitivity towards the drug. Efforts to generate preclinical models of cetuximab-resistance from xenograft tumors have been limited to date. A CRC model of acquired cetuximab resistance was generated, but known to have an activating KRAS mutation [281]. Others reported a model of cetuximab resistance, but were unable to propagate it [282]. Further models of cetuximab resistance were established for renal and head-and-neck carcinomas and could be used to test alternative therapies for cetuximab-refractory tumors [278, 283]. All these preclinical models were generated from cell lines, and had the advantage that the desensitization process happened *in vivo*, compared to cell lines that received chronic treatment *in vitro* and were then transplanted. Nevertheless, the growth of established cell lines like GEO, or A431, is usually stimulated by highly pronounced mitogenic pathways, lacking the heterogeneity inherent to cancer. In this study we generated cetuximab-resistant PDX directly from patient tissue, and confirmed that the resistance is robust in the PDX.
Performing characterization of patient tumors at the molecular level will only elucidate the tumor characteristics at one time point, limiting the understanding of mechanisms of tumor development and chemoresistance. However, the use of PDX, where the tumor tissue can be harvested at different time points, can help understanding of the molecular changes driving resistance to drug therapy. Tumor profiling (genome, transcriptome, proteome or metabolome) at different time points, with different treatments, can determine possible changes in the molecular drivers and signaling pathways of the original tumor as response to drug treatment and in this way elucidate resistance mechanisms.

In summary, a set of CRC PDX was established and extensively characterized. The genetic and sensitivity profile of the PDX reflects the heterogeneity of CRC. The correlation analysis of molecules envolved in the EGFR pathway among each other, as well as targeted therapy addressing this pathway, reflected the dynamics of the EGFR pathway in the PDX models, confirming their validity as a tool for preclinical cancer research.

5. Outlook

This set of 49 PDX models was established and comprehensively characterized, corroborating its utility for screening of anticancer substances. In addition, the two established cetuximab resistant models reflect the dynamics of CRC resistance to EGFR blockade. The CRC PDX set can be used for screening of novel substances, especially second-generation therapeutics and compare their efficacy to the existing panels of known ones in a head-to-head comparison. Also, the existing genetic and expression data can be combined with sensitivity profiles of known and novel therapeutics in biomarker oriented xenopatient trials, since they were confirmed to reflect known resistance mechanisms. The cetuximab resistant sublines can be further characterized in order to elucidate alternative therapies for CRC PDX tumors with acquired resistance. Sub-lines with resistance to other therapeutics should be generated. Elucidation of alternative signaling pathways active in the CRC PDX with the aim to identify potential pharmacological interventions can be addressed with this set of PDX.

Observations made during the characterization of the PDX could be addressed in detail in following studies. For example, the characteristics of CRC PDX with an activating KRAS mutation that showed strong sensitivity to cetuximab should be further addressed and compared to CRC PDX with a KRAS mutation that are inherently resistant. This can aid the elucidation of new subsets of patients that can profit from this targeted therapy and alternative signaling pathways active in these PDX in order to identify new potential pharmacological interventions.

Coupling the obtained PDX data with retrospective patient's outcome data would aid to validate this method of therapy guidance. Finally, the PDX models can be combined with the humanized mice technology in order to amplify the use of this set of PDX models for the screening of cancer immunotherapeutic drugs.

6. Bibliography

1. SEARO | World Cancer Report 2014.
2. What Is Cancer? - National Cancer Institute. http://www.cancer.gov/cancertopics/cancerlibrary/what-is-cancer.
3. Bertram JS (2000) The molecular biology of cancer. Mol Aspects Med 21:167–223.
4. Stratton MR, Campbell PJ, Futreal PA (2009) The cancer genome. Nature 458:719–724.
5. Tomasetti C, Vogelstein B (2015) Cancer etiology. Variation in cancer risk among tissues can be explained by the number of stem cell divisions. Science 347:78–81.
6. Hanahan D, Weinberg RA (2000) The hallmarks of cancer. Cell 100:57–70.
7. Hanahan D, Weinberg RA (2011) Hallmarks of cancer: the next generation. Cell 144:646–674.
8. Medema RH, Bos JL (1993) The role of p21ras in receptor tyrosine kinase signaling. Crit Rev Oncog 4:615–661.
9. Di Fiore PP, Pierce JH, Kraus MH, et al. (1987) erbB-2 is a potent oncogene when overexpressed in NIH/3T3 cells. Science 237:178–182.
10. Cheng N, Chytil A, Shyr Y, et al. (2008) Transforming growth factor-beta signaling-deficient fibroblasts enhance hepatocyte growth factor signaling in mammary carcinoma cells to promote scattering and invasion. Mol Cancer Res 6:1521–1533.
11. Fynan TM, Reiss M (1993) Resistance to inhibition of cell growth by transforming growth factor-beta and its role in oncogenesis. Crit Rev Oncog 4:493–540.
12. Markowitz S, Wang J, Myeroff L, et al. (1995) Inactivation of the type II TGF-beta receptor in colon cancer cells with microsatellite instability. Science 268:1336–1338.
13. Schutte M, Hruban RH, Hedrick L, et al. (1996) DPC4 gene in various tumor types. Cancer Res 56:2527–2530.
14. Kinzler KW, Vogelstein B (1996) Lessons from hereditary colorectal cancer. Cell 87:159–170.
15. Harris CC (1996) p53 tumor suppressor gene: from the basic research laboratory to the clinic--an abridged historical perspective. Carcinogenesis 17:1187–1198.
16. Junttila MR, Evan GI (2009) p53--a Jack of all trades but master of none. Nat Rev Cancer 9:821–829.
17. Blasco MA (2005) Telomeres and human disease: ageing, cancer and beyond. Nat Rev Genet 6:611–622.
18. Hanahan D, Folkman J (1996) Patterns and emerging mechanisms of the angiogenic switch during tumorigenesis. Cell 86:353–364.
19. Ferrara N (2010) Pathways mediating VEGF-independent tumor angiogenesis. Cytokine Growth Factor Rev 21:21–26.
20. Baeriswyl V, Christofori G (2009) The angiogenic switch in carcinogenesis. Semin Cancer Biol 19:329–337.

21. Cavallaro U, Christofori G (2004) Cell adhesion and signalling by cadherins and Ig-CAMs in cancer. Nat Rev Cancer 4:118–132.

22. Ferlay J, Soerjomataram I, Dikshit R, et al. (2015) Cancer incidence and mortality worldwide: Sources, methods and major patterns in GLOBOCAN 2012. Int J Cancer 136:E359–86.

23. Ferlay J, Parkin DM, Steliarova-Foucher E (2010) Estimates of cancer incidence and mortality in Europe in 2008. Eur J Cancer 46:765–781.

24. Brenner H, Bouvier AM, Foschi R, et al. (2012) Progress in colorectal cancer survival in Europe from the late 1980s to the early 21st century: the EUROCARE study. Int J Cancer 131:1649–1658.

25. Ferlay J, Steliarova-Foucher E, Lortet-Tieulent J, et al. (2013) Cancer incidence and mortality patterns in Europe: estimates for 40 countries in 2012. Eur J Cancer 49:1374–1403.

26. Van Schaeybroeck, S.; Lawler M.; Johnston B et al. (2014) Colorectal cancer. In: Abeloff's Clin. Oncol., 5th ed. Elsevier, Philadelphia, pp 1278–1335

27. Sobin LH, Gospodarowicz MK, Mary K, et al. Cancer IU against (2009) TNM classification of malignant tumours, 7th ed. Wiley-Blackwell, New York

28. Compton CC, Greene FL (2004) The Staging of Colorectal Cancer: 2004 and Beyond. CA Cancer J Clin 54:295–308.

29. Bruckner HW, Pitrelli J MM (2010) Carcinoma of the colon and rectum. In: Bosman FT, Carneiro F, Hruban RH T, ND (eds) WHO Classif. Tumours Dig. Syst. IARC Press, Lyon, pp 138–139

30. Compton CC (2007) Optimal pathologic staging: defining stage II disease. Clin Cancer Res 13:6862s–70s.

31. DeSantis CE, Lin CC, Mariotto AB, et al. Cancer treatment and survivorship statistics, 2014. CA Cancer J Clin 64:252–71.

32. Gunderson LL, Sargent DJ, Tepper JE, et al. (2004) Impact of T and N stage and treatment on survival and relapse in adjuvant rectal cancer: a pooled analysis. J Clin Oncol 22:1785–1796.

33. Vogelstein B, Fearon ER, Kern SE, et al. (1989) Allelotype of colorectal carcinomas. Science 244:207–211.

34. Pritchard CC, Grady WM (2011) Colorectal cancer molecular biology moves into clinical practice. Gut 60:116–129.

35. Markowitz SD, Bertagnolli MM (2009) Molecular origins of cancer: Molecular basis of colorectal cancer. N Engl J Med 361:2449–2460.

36. Caldwell CM, Kaplan KB (2009) The role of APC in mitosis and in chromosome instability. Adv Exp Med Biol 656:51–64.

37. Sieber OM, Tomlinson IP, Lamlum H (2000) The adenomatous polyposis coli (APC) tumour suppressor--genetics, function and disease. Mol Med Today 6:462–469.

38. Goldstein NS (2006) Serrated pathway and APC (conventional)-type colorectal polyps: molecular-morphologic correlations, genetic pathways, and implications for

classification. Am J Clin Pathol 125:146–153.

39. Noffsinger AE (2009) Serrated polyps and colorectal cancer: new pathway to malignancy. Annu Rev Pathol 4:343–364.

40. Rex DK, Ahnen DJ, Baron JA, et al. (2012) Serrated lesions of the colorectum: review and recommendations from an expert panel. Am J Gastroenterol 107:1315–29; quiz 1314, 1330.

41. Moon B-S, Jeong W-J, Park J, et al. (2014) Role of oncogenic K-Ras in cancer stem cell activation by aberrant Wnt/beta-catenin signaling. J Natl Cancer Inst 106:djt373.

42. Fearon ER, Vogelstein B (1990) A genetic model for colorectal tumorigenesis. Cell 61:759–767.

43. Liao X, Lochhead P, Nishihara R, et al. (2012) Aspirin use, tumor PIK3CA mutation, and colorectal-cancer survival. N Engl J Med 367:1596–1606.

44. Frattini M, Saletti P, Romagnani E, et al. (2007) PTEN loss of expression predicts cetuximab efficacy in metastatic colorectal cancer patients. Br J Cancer 97:1139–1145.

45. Barault L, Veyrie N, Jooste V, et al. (2008) Mutations in the RAS-MAPK, PI(3)K (phosphatidylinositol-3-OH kinase) signaling network correlate with poor survival in a population-based series of colon cancers. Int J Cancer 122:2255–2259.

46. Benvenuti S, Sartore-Bianchi A, Di Nicolantonio F, et al. (2007) Oncogenic activation of the RAS/RAF signaling pathway impairs the response of metastatic colorectal cancers to anti-epidermal growth factor receptor antibody therapies. Cancer Res 67:2643–2648.

47. Frattini M, Signoroni S, Pilotti S, et al. (2005) Phosphatase protein homologue to tensin expression and phosphatidylinositol-3 phosphate kinase mutations in colorectal cancer. Cancer Res 65:11227.

48. Velho S, Oliveira C, Ferreira A, et al. (2005) The prevalence of PIK3CA mutations in gastric and colon cancer. Eur J Cancer 41:1649–1654.

49. Perrone F, Lampis A, Orsenigo M, et al. (2009) PI3KCA/PTEN deregulation contributes to impaired responses to cetuximab in metastatic colorectal cancer patients. Ann Oncol 20:84–90.

50. Chalhoub N, Baker SJ (2009) PTEN and the PI3-kinase pathway in cancer. Annu Rev Pathol 4:127–150.

51. Laurent-Puig P, Cayre A, Manceau G, et al. (2009) Analysis of PTEN, BRAF, and EGFR status in determining benefit from cetuximab therapy in wild-type KRAS metastatic colon cancer. J Clin Oncol 27:5924–5930.

52. Siegel R, DeSantis C, Virgo K, et al. Cancer treatment and survivorship statistics, 2012. CA Cancer J Clin 62:220–41.

53. Lyman GH (2009) Impact of chemotherapy dose intensity on cancer patient outcomes. J Natl Compr Canc Netw 7:99–108.

54. Simmonds PC (2000) Palliative chemotherapy for advanced colorectal cancer: systematic review and meta-analysis. Colorectal Cancer Collaborative Group. BMJ

321:531–535.

55. Wohlhueter RM, McIvor RS, Plagemann PG (1980) Facilitated transport of uracil and 5-fluorouracil, and permeation of orotic acid into cultured mammalian cells. J Cell Physiol 104:309–319.

56. Longley DB, Harkin DP, Johnston PG (2003) 5-fluorouracil: mechanisms of action and clinical strategies. Nat Rev Cancer 3:330–338.

57. Sargent DJ, Goldberg RM, Jacobson SD, et al. (2001) A pooled analysis of adjuvant chemotherapy for resected colon cancer in elderly patients. N Engl J Med 345:1091–1097.

58. Figueredo A, Charette ML, Maroun J, et al. (2004) Adjuvant therapy for stage II colon cancer: a systematic review from the Cancer Care Ontario Program in evidence-based care's gastrointestinal cancer disease site group. J Clin Oncol 22:3395–3407.

59. Douillard JY, Cunningham D, Roth AD, et al. (2000) Irinotecan combined with fluorouracil compared with fluorouracil alone as first-line treatment for metastatic colorectal cancer: a multicentre randomised trial. Lancet 355:1041–1047.

60. Giacchetti S, Perpoint B, Zidani R, et al. (2000) Phase III multicenter randomized trial of oxaliplatin added to chronomodulated fluorouracil-leucovorin as first-line treatment of metastatic colorectal cancer. J Clin Oncol 18:136–147.

61. Koukourakis G V, Kouloulias V, Koukourakis MJ, et al. (2008) Efficacy of the oral fluorouracil pro-drug capecitabine in cancer treatment: a review. Molecules 13:1897–1922.

62. Kawato Y, Aonuma M, Hirota Y, et al. (1991) Intracellular roles of SN-38, a metabolite of the camptothecin derivative CPT-11, in the antitumor effect of CPT-11. Cancer Res 51:4187–4191.

63. Hsiang YH, Lihou MG, Liu LF (1989) Arrest of replication forks by drug-stabilized topoisomerase I-DNA cleavable complexes as a mechanism of cell killing by camptothecin. Cancer Res 49:5077–5082.

64. Saltz LB, Cox J V, Blanke C, et al. (2000) Irinotecan plus fluorouracil and leucovorin for metastatic colorectal cancer. Irinotecan Study Group. N Engl J Med 343:905–914.

65. Hind D, Tappenden P, Tumur I, et al. (2008) The use of irinotecan, oxaliplatin and raltitrexed for the treatment of advanced colorectal cancer: systematic review and economic evaluation. Health Technol Assess 12:iii–ix, xi–162.

66. Woynarowski JM, Faivre S, Herzig MC, et al. (2000) Oxaliplatin-induced damage of cellular DNA. Mol Pharmacol 58:920–927.

67. Raymond E, Faivre S, Chaney S, et al. (2002) Cellular and Molecular Pharmacology of Oxaliplatin. Mol Cancer Ther 1:227–235.

68. Raymond E, Lawrence R, Izbicka E, et al. (1998) Activity of oxaliplatin against human tumor colony-forming units. Clin Cancer Res 4:1021–1029.

69. Simpson D, Dunn C, Curran M, et al. (2003) Oxaliplatin: a review of its use in combination therapy for advanced metastatic colorectal cancer. Drugs 63:2127–2156.

70. Ellis LM, Takahashi Y, Liu W, et al. (2000) Vascular endothelial growth factor in human colon cancer: biology and therapeutic implications. Oncologist 5 Suppl 1:11–15.

71. Jain RK (1994) Barriers to drug delivery in solid tumors. Sci Am 271:58–65.

72. Ferrara N, Davis-Smyth T (1997) The biology of vascular endothelial growth factor. Endocr Rev 18:4–25.

73. Willett CG, Boucher Y, di Tomaso E, et al. (2004) Direct evidence that the VEGF-specific antibody bevacizumab has antivascular effects in human rectal cancer. Nat Med 10:145–147.

74. Hurwitz H, Fehrenbacher L, Novotny W, et al. (2004) Bevacizumab plus irinotecan, fluorouracil, and leucovorin for metastatic colorectal cancer. N Engl J Med 350:2335–2342.

75. Kabbinavar F (2003) Phase II, Randomized Trial Comparing Bevacizumab Plus Fluorouracil (FU)/Leucovorin (LV) With FU/LV Alone in Patients With Metastatic Colorectal Cancer. J Clin Oncol 21:60–65.

76. Giantonio BJ, Catalano PJ, Meropol NJ, et al. (2007) Bevacizumab in combination with oxaliplatin, fluorouracil, and leucovorin (FOLFOX4) for previously treated metastatic colorectal cancer: results from the Eastern Cooperative Oncology Group Study E3200. J Clin Oncol 25:1539–44.

77. Moyer JD, Barbacci EG, Iwata KK, et al. (1997) Induction of apoptosis and cell cycle arrest by CP-358,774, an inhibitor of epidermal growth factor receptor tyrosine kinase. Cancer Res 57:4838–4848.

78. Wood ER, Truesdale AT, McDonald OB, et al. (2004) A unique structure for epidermal growth factor receptor bound to GW572016 (Lapatinib): relationships among protein conformation, inhibitor off-rate, and receptor activity in tumor cells. Cancer Res 64:6652–6659.

79. Pollack VA, Savage DM, Baker DA, et al. (1999) Inhibition of epidermal growth factor receptor-associated tyrosine phosphorylation in human carcinomas with CP-358,774: dynamics of receptor inhibition in situ and antitumor effects in athymic mice. J Pharmacol Exp Ther 291:739–748.

80. Shepherd FA, Rodrigues Pereira J, Ciuleanu T, et al. (2005) Erlotinib in previously treated non-small-cell lung cancer. N Engl J Med 353:123–132.

81. Rosell R, Carcereny E, Gervais R, et al. (2012) Erlotinib versus standard chemotherapy as first-line treatment for European patients with advanced EGFR mutation-positive non-small-cell lung cancer (EURTAC): a multicentre, open-label, randomised phase 3 trial. Lancet Oncol 13:239–246.

82. Zhou C, Wu Y-L, Chen G, et al. (2011) Erlotinib versus chemotherapy as first-line treatment for patients with advanced EGFR mutation-positive non-small-cell lung cancer (OPTIMAL, CTONG-0802): a multicentre, open-label, randomised, phase 3 study. Lancet Oncol 12:735–742.

83. Townsley CA, Major P, Siu LL, et al. (2006) Phase II study of erlotinib (OSI-774) in patients with metastatic colorectal cancer. Br J Cancer 94:1136–1143.

84. Goldstein NI, Prewett M, Zuklys K, et al. (1995) Biological efficacy of a chimeric

antibody to the epidermal growth factor receptor in a human tumor xenograft model. Clin Cancer Res 1:1311–1318.

85. KÖHLER G, MILSTEIN C (1975) Continuous cultures of fused cells secreting antibody of predefined specificity. Nature 256:495–497.

86. Vaswani SK, Hamilton RG (1998) Humanized antibodies as potential therapeutic drugs. Ann Allergy Asthma Immunol 81:105–106,119.

87. Liu B, Fang M, Lu Y, et al. (2001) Fibroblast growth factor and insulin-like growth factor differentially modulate the apoptosis and G1 arrest induced by anti-epidermal growth factor receptor monoclonal antibody. Oncogene 20:1913–22.

88. Wu X, Fan Z, Masui H, et al. (1995) Apoptosis induced by an anti-epidermal growth factor receptor monoclonal antibody in a human colorectal carcinoma cell line and its delay by insulin. J Clin Invest 95:1897–905.

89. Perrotte P, Matsumoto T, Inoue K, et al. (1999) Anti-epidermal growth factor receptor antibody C225 inhibits angiogenesis in human transitional cell carcinoma growing orthotopically in nude mice. Clin Cancer Res 5:257–265.

90. Huang SM, Harari PM (2000) Modulation of radiation response after epidermal growth factor receptor blockade in squamous cell carcinomas: inhibition of damage repair, cell cycle kinetics, and tumor angiogenesis. Clin Cancer Res 6:2166–2174.

91. Kawaguchi Y, Kono K, Mimura K, et al. (2007) Cetuximab induce antibody-dependent cellular cytotoxicity against EGFR-expressing esophageal squamous cell carcinoma. Int J Cancer 120:781–7.

92. Meyers MB, Yu P, Mendelsohn J (1993) Crosstalk between epidermal growth factor receptor and P-glycoprotein in actinomycin D-resistant Chinese hamster lung cells. Biochem Pharmacol 46:1841–1848.

93. Naruse I, Ohmori T, Ao Y, et al. (2002) Antitumor activity of the selective epidermal growth factor receptor-tyrosine kinase inhibitor (EGFR-TKI) Iressa (ZD1839) in an EGFR-expressing multidrug-resistant cell line in vitro and in vivo. Int J Cancer 98:310–315.

94. Sclabas GM, Fujioka S, Schmidt C, et al. (2003) Restoring apoptosis in pancreatic cancer cells by targeting the nuclear factor-kappaB signaling pathway with the anti-epidermal growth factor antibody IMC-C225. J Gastrointest Surg 7:37–43; discussion 43.

95. Chung KY, Shia J, Kemeny NE, et al. (2005) Cetuximab shows activity in colorectal cancer patients with tumors that do not express the epidermal growth factor receptor by immunohistochemistry. J Clin Oncol 23:1803–1810.

96. Sequist L V, Bell DW, Lynch TJ, et al. (2007) Molecular predictors of response to epidermal growth factor receptor antagonists in non-small-cell lung cancer. J Clin Oncol 25:587–595.

97. Tsuchihashi Z, Khambata-Ford S, Hanna N, et al. (2005) Responsiveness to cetuximab without mutations in EGFR. N Engl J Med 353:208–209.

98. Jiang Z, Li C, Li F, et al. (2013) EGFR gene copy number as a prognostic marker in colorectal cancer patients treated with cetuximab or panitumumab: a systematic review and meta analysis. PLoS One 8:e56205.

99. Moroni M, Veronese S, Benvenuti S, et al. (2005) Gene copy number for epidermal growth factor receptor (EGFR) and clinical response to antiEGFR treatment in colorectal cancer: a cohort study. Lancet Oncol 6:279–286.

100. Cappuzzo F, Finocchiaro G, Rossi E, et al. (2008) EGFR FISH assay predicts for response to cetuximab in chemotherapy refractory colorectal cancer patients. Ann Oncol 19:717–723.

101. Personeni N, Fieuws S, Piessevaux H, et al. (2008) Clinical usefulness of EGFR gene copy number as a predictive marker in colorectal cancer patients treated with cetuximab: a fluorescent in situ hybridization study. Clin Cancer Res 14:5869–5876.

102. Sartore-Bianchi A, Moroni M, Veronese S, et al. (2007) Epidermal growth factor receptor gene copy number and clinical outcome of metastatic colorectal cancer treated with panitumumab. J Clin Oncol 25:3238–3245.

103. Saltz LB, Meropol NJ, Loehrer PJS, et al. (2004) Phase II trial of cetuximab in patients with refractory colorectal cancer that expresses the epidermal growth factor receptor. J Clin Oncol 22:1201–1208.

104. Cunningham D, Humblet Y, Siena S, et al. (2004) Cetuximab monotherapy and cetuximab plus irinotecan in irinotecan-refractory metastatic colorectal cancer. N Engl J Med 351:337–345.

105. Russo A, Bazan V, Agnese V, et al. (2005) Prognostic and predictive factors in colorectal cancer: Kirsten Ras in CRC (RASCAL) and TP53CRC collaborative studies. Ann Oncol 16 Suppl 4:iv44–49.

106. De Roock W, Piessevaux H, De Schutter J, et al. (2008) KRAS wild-type state predicts survival and is associated to early radiological response in metastatic colorectal cancer treated with cetuximab. Ann Oncol 19:508–515.

107. Di Fiore F, Blanchard F, Charbonnier F, et al. (2007) Clinical relevance of KRAS mutation detection in metastatic colorectal cancer treated by Cetuximab plus chemotherapy. Br J Cancer 96:1166–1169.

108. Lievre A, Bachet J-B, Boige V, et al. (2008) KRAS mutations as an independent prognostic factor in patients with advanced colorectal cancer treated with cetuximab. J Clin Oncol 26:374–379.

109. Lievre A, Bachet J-B, Le Corre D, et al. (2006) KRAS mutation status is predictive of response to cetuximab therapy in colorectal cancer. Cancer Res 66:3992–3995.

110. McCubrey JA, Steelman LS, Abrams SL, et al. (2006) Roles of the RAF/MEK/ERK and PI3K/PTEN/AKT pathways in malignant transformation and drug resistance. Adv Enzyme Regul 46:249–279.

111. Sood A, McClain D, Maitra R, et al. (2012) PTEN gene expression and mutations in the PIK3CA gene as predictors of clinical benefit to anti-epidermal growth factor receptor antibody therapy in patients with KRAS wild-type metastatic colorectal cancer. Clin Colorectal Cancer 11:143–150.

112. Misale S, Yaeger R, Hobor S, et al. (2012) Emergence of KRAS mutations and acquired resistance to anti-EGFR therapy in colorectal cancer. Nature 486:532–536.

113. Misale S, Arena S, Lamba S, et al. (2014) Blockade of EGFR and MEK intercepts heterogeneous mechanisms of acquired resistance to anti-EGFR therapies in

colorectal cancer. Sci Transl Med 6:224ra26.

114. Valtorta E, Misale S, Sartore-Bianchi A, et al. (2013) KRAS gene amplification in colorectal cancer and impact on response to EGFR-targeted therapy. Int J Cancer 133:1259–65.

115. Khambata-Ford S, Garrett CR, Meropol NJ, et al. (2007) Expression of epiregulin and amphiregulin and K-ras mutation status predict disease control in metastatic colorectal cancer patients treated with cetuximab. J Clin Oncol 25:3230–3237.

116. Jacobs B, De Roock W, Piessevaux H, et al. (2009) Amphiregulin and epiregulin mRNA expression in primary tumors predicts outcome in metastatic colorectal cancer treated with cetuximab. J Clin Oncol 27:5068–5074.

117. Bardelli A, Corso S, Bertotti A, et al. (2013) Amplification of the MET receptor drives resistance to anti-EGFR therapies in colorectal cancer. Cancer Discov 3:658–673.

118. Carpenter G, Cohen S (1979) Epidermal growth factor. Annu Rev Biochem 48:193–216.

119. Linggi B, Carpenter G (2006) ErbB receptors: new insights on mechanisms and biology. Trends Cell Biol 16:649–656.

120. Hynes NE, Lane HA (2005) ERBB receptors and cancer: the complexity of targeted inhibitors. Nat Rev Cancer 5:341–354.

121. Yarden Y, Sliwkowski MX (2001) Untangling the ErbB signalling network. Nat Rev Mol Cell Biol 2:127–137.

122. Sanderson MP, Dempsey PJ, Dunbar AJ (2006) Control of ErbB signaling through metalloprotease mediated ectodomain shedding of EGF-like factors. Growth Factors 24:121–136.

123. Shoemaker RH (2006) The NCI60 human tumour cell line anticancer drug screen. Nat Rev Cancer 6:813–823.

124. Monks A, Scudiero DA, Johnson GS, et al. (1997) The NCI anti-cancer drug screen: a smart screen to identify effectors of novel targets. Anticancer Drug Des 12:533–541.

125. Mosmann T (1983) Rapid colorimetric assay for cellular growth and survival: application to proliferation and cytotoxicity assays. J Immunol Methods 65:55–63.

126. Skehan P, Storeng R, Scudiero D, et al. (1990) New colorimetric cytotoxicity assay for anticancer-drug screening. J Natl Cancer Inst 82:1107–1112.

127. Hongo T, Yajima S, Sakurai M, et al. (1997) In vitro drug sensitivity testing can predict induction failure and early relapse of childhood acute lymphoblastic leukemia. Blood 89:2959–2965.

128. HogenEsch H, Nikitin AY (2012) Challenges in pre-clinical testing of anti-cancer drugs in cell culture and in animal models. J Control Release 164:183–6.

129. Houshdaran S, Hawley S, Palmer C, et al. (2010) DNA methylation profiles of ovarian epithelial carcinoma tumors and cell lines. PLoS One 5:e9359.

130. Hennessey PT, Ochs MF, Mydlarz WW, et al. (2011) Promoter methylation in head and neck squamous cell carcinoma cell lines is significantly different than

methylation in primary tumors and xenografts. PLoS One 6:e20584.

131. Gazdar AF, Gao B, Minna JD (2010) Lung cancer cell lines: Useless artifacts or invaluable tools for medical science? Lung Cancer 68:309–18.

132. Ruggeri BA, Camp F, Miknyoczki S (2014) Animal models of disease: pre-clinical animal models of cancer and their applications and utility in drug discovery. Biochem Pharmacol 87:150–61.

133. Voskoglou-Nomikos T, Pater JL, Seymour L (2003) Clinical predictive value of the in vitro cell line, human xenograft, and mouse allograft preclinical cancer models. Clin Cancer Res 9:4227–39.

134. Johnson JI, Decker S, Zaharevitz D, et al. (2001) Relationships between drug activity in NCI preclinical in vitro and in vivo models and early clinical trials. Br J Cancer 84:1424–1431.

135. Nyga A, Cheema U, Loizidou M (2011) 3D tumour models: novel in vitro approaches to cancer studies. J Cell Commun Signal 5:239–248.

136. Amatangelo MD, Bassi DE, Klein-Szanto AJP, Cukierman E (2005) Stroma-derived three-dimensional matrices are necessary and sufficient to promote desmoplastic differentiation of normal fibroblasts. Am J Pathol 167:475–488.

137. Ghajar CM, Bissell MJ (2010) Tumor engineering: the other face of tissue engineering. Tissue Eng Part A 16:2153–6.

138. Sutherland RM (1988) Cell and environment interactions in tumor microregions: the multicell spheroid model. Science 240:177–184.

139. Kunz-Schughart LA, Kreutz M, Knuechel R (1998) Multicellular spheroids: a three-dimensional in vitro culture system to study tumour biology. Int J Exp Pathol 79:1–23.

140. Weiswald L-B, Richon S, Validire P, et al. (2009) Newly characterised ex vivo colospheres as a three-dimensional colon cancer cell model of tumour aggressiveness. Br J Cancer 101:473–82.

141. Burger AM (2004) Preclinical Screening for New Anticancer Agents. In: McLeod WDFHL (ed) Handb. Anticancer Pharmacokinet. Pharmacodyn. Humana Press Inc., Totowa, NJ, pp 29–45

142. Suggitt M, Bibby MC (2005) 50 years of preclinical anticancer drug screening: empirical to target-driven approaches. Clin Cancer Res 11:971–981.

143. Shultz LD, Ishikawa F, Greiner DL (2007) Humanized mice in translational biomedical research. Nat Rev Immunol 7:118–130.

144. Rygaard J, Povlsen CO (1969) Heterotransplantation of a human malignant tumour to “Nude” mice. Acta Pathol Microbiol Scand 77:758–760.

145. Bosma GC, Custer RP, Bosma MJ (1983) A severe combined immunodeficiency mutation in the mouse. Nature 301:527–530.

146. Ji H, Li D, Chen L, et al. (2006) The impact of human EGFR kinase domain mutations on lung tumorigenesis and in vivo sensitivity to EGFR-targeted therapies. Cancer Cell 9:485–95.

147. Yang H, Higgins B, Kolinsky K, et al. (2012) Antitumor activity of BRAF inhibitor

vemurafenib in preclinical models of BRAF-mutant colorectal cancer. Cancer Res 72:779–89.

148. Prahallad A, Sun C, Huang S, et al. (2012) Unresponsiveness of colon cancer to BRAF(V600E) inhibition through feedback activation of EGFR. Nature 483:100–3.

149. Kerbel RS (2003) Human tumor xenografts as predictive preclinical models for anticancer drug activity in humans: better than commonly perceived-but they can be improved. Cancer Biol Ther 2:S134–9.

150. Talmadge JE, Singh RK, Fidler IJ, et al. (2007) Murine models to evaluate novel and conventional therapeutic strategies for cancer. Am J Pathol 170:793–804.

151. Pittet MJ, Weissleder R (2011) Intravital imaging. Cell 147:983–991.

152. Wilmanns C, Fan D, O'Brian CA, et al. (1992) Orthotopic and ectopic organ environments differentially influence the sensitivity of murine colon carcinoma cells to doxorubicin and 5-fluorouracil. Int J Cancer 52:98–104.

153. Vesely MD, Kershaw MH, Schreiber RD, et al. (2011) Natural innate and adaptive immunity to cancer. Annu Rev Immunol 29:235–271.

154. Apetoh L, Ghiringhelli F, Tesniere A, et al. (2007) Toll-like receptor 4-dependent contribution of the immune system to anticancer chemotherapy and radiotherapy. Nat Med 13:1050–1059.

155. Legrand N, Weijer K, Spits H (2006) Experimental models to study development and function of the human immune system in vivo. J Immunol 176:2053–2058.

156. Tentler JJ, Tan AC, Weekes CD, et al. (2012) Patient-derived tumour xenografts as models for oncology drug development. Nat Rev Clin Oncol 9:338–50.

157. Fiebig HH, Neumann HA, Henss H, et al. (1985) Development of three human small cell lung cancer models in nude mice. Recent Results Cancer Res 97:77–86.

158. Houghton JA, Houghton PJ, Green AA (1982) Chemotherapy of childhood rhabdomyosarcomas growing as xenografts in immune-deprived mice. Cancer Res 42:535–9.

159. Berger DP, Fiebig HH, Winterhalter BR, et al. (1990) Preclinical phase II study of ifosfamide in human tumour xenografts in vivo. Cancer Chemother Pharmacol 26 Suppl:S7–11.

160. Morton CL, Houghton PJ (2007) Establishment of human tumor xenografts in immunodeficient mice. Nat Protoc 2:247–50.

161. Julien S, Merino-Trigo A, Lacroix L, et al. (2012) Characterization of a large panel of patient-derived tumor xenografts representing the clinical heterogeneity of human colorectal cancer. Clin Cancer Res 18:5314–28.

162. Bertotti A, Migliardi G, Galimi F, et al. (2011) A molecularly annotated platform of patient-derived xenografts ("xenopatients") identifies HER2 as an effective therapeutic target in cetuximab-resistant colorectal cancer. Cancer Discov 1:508–23.

163. Fichtner I, Rolff J, Soong R, et al. (2008) Establishment of patient-derived non-small cell lung cancer xenografts as models for the identification of predictive biomarkers. Clin Cancer Res 14:6456–68.

164. DeRose YS, Wang G, Lin Y-C, et al. (2011) Tumor grafts derived from women with

breast cancer authentically reflect tumor pathology, growth, metastasis and disease outcomes. Nat Med 17:1514–20.

165. Fichtner I, Slisow W, Gill J, et al. (2004) Anticancer drug response and expression of molecular markers in early-passage xenotransplanted colon carcinomas. Eur J Cancer 40:298–307.

166. Priolo C, Agostini M, Vena N, et al. (2010) Establishment and genomic characterization of mouse xenografts of human primary prostate tumors. Am J Pathol 176:1901–13.

167. Kubota T, Yamaguchi H, Watanabe M, et al. (1993) Growth of human tumor xenografts in nude mice and mice with severe combined immunodeficiency (SCID). Surg Today 23:375–7.

168. Maykel J, Liu JH, Li H, et al. (2014) NOD-scidIl2rg (tm1Wjl) and NOD-Rag1 (null) Il2rg (tm1Wjl) : a model for stromal cell-tumor cell interaction for human colon cancer. Dig Dis Sci 59:1169–79.

169. Zhao X, Liu Z, Yu L, et al. (2012) Global gene expression profiling confirms the molecular fidelity of primary tumor-based orthotopic xenograft mouse models of medulloblastoma. Neuro Oncol 14:574–83.

170. Siolas D, Hannon GJ (2013) Patient-derived tumor xenografts: transforming clinical samples into mouse models. Cancer Res 73:5315–9.

171. Fiebig HH, Maier A, Burger AM (2004) Clonogenic assay with established human tumour xenografts: correlation of in vitro to in vivo activity as a basis for anticancer drug discovery. Eur J Cancer 40:802–820.

172. Guenot D, Guérin E, Aguillon-Romain S, et al. (2006) Primary tumour genetic alterations and intra-tumoral heterogeneity are maintained in xenografts of human colon cancers showing chromosome instability. J Pathol 208:643–52.

173. Merk J, Rolff J, Becker M, et al. (2009) Patient-derived xenografts of non-small-cell lung cancer: a pre-clinical model to evaluate adjuvant chemotherapy? Eur J Cardiothorac Surg 36:454–9.

174. Cho YB, Hong HK, Choi Y-L, et al. (2014) Colorectal cancer patient-derived xenografted tumors maintain characteristic features of the original tumors. J Surg Res 187:502–9.

175. Hidalgo M, Bruckheimer E, Rajeshkumar N V, et al. (2011) A pilot clinical study of treatment guided by personalized tumorgrafts in patients with advanced cancer. Mol Cancer Ther 10:1311–6.

176. Zhang X, Claerhout S, Prat A, et al. (2013) A renewable tissue resource of phenotypically stable, biologically and ethnically diverse, patient-derived human breast cancer xenograft models. Cancer Res 73:4885–97.

177. Marangoni E, Vincent-Salomon A, Auger N, et al. (2007) A new model of patient tumor-derived breast cancer xenografts for preclinical assays. Clin Cancer Res 13:3989–98.

178. Topp MD, Hartley L, Cook M, et al. (2014) Molecular correlates of platinum response in human high-grade serous ovarian cancer patient-derived xenografts. Mol Oncol 8:656–68.

179. Krumbach R, Schüler J, Hofmann M, et al. (2011) Primary resistance to cetuximab in a panel of patient-derived tumour xenograft models: activation of MET as one mechanism for drug resistance. Eur J Cancer 47:1231–43.

180. Ducker GS, Atreya CE, Simko JP, et al. (2014) Incomplete inhibition of phosphorylation of 4E-BP1 as a mechanism of primary resistance to ATP-competitive mTOR inhibitors. Oncogene 33:1590–600.

181. Tentler JJ, Nallapareddy S, Tan AC, et al. (2010) Identification of predictive markers of response to the MEK1/2 inhibitor selumetinib (AZD6244) in K-ras-mutated colorectal cancer. Mol Cancer Ther 9:3351–62.

182. Walters DM, Lindberg JM, Adair SJ, et al. (2013) Inhibition of the growth of patient-derived pancreatic cancer xenografts with the MEK inhibitor trametinib is augmented by combined treatment with the epidermal growth factor receptor/HER2 inhibitor lapatinib. Neoplasia 15:143–55.

183. Zhu H, Zhou W, Hu J, et al. (2012) Suppressing the growth of rectal cancer xenografts derived from patient tumors by an adenovector expressing small hairpin RNA targeting Bcl-XL. J Gene Med 14:761–8.

184. Zhou W, Zhu H, Chen W, et al. (2011) Treatment of patient tumor-derived colon cancer xenografts by a TRAIL gene-armed oncolytic adenovirus. Cancer Gene Ther 18:336–45.

185. Therasse P, Arbuck SG, Eisenhauer EA, et al. (2000) New Guidelines to Evaluate the Response to Treatment. 92:205–16

186. Livak KJ, Schmittgen TD (2001) Analysis of relative gene expression data using real-time quantitative PCR and the 2(-Delta Delta C(T)) Method. Methods 25:402–8.

187. Troiani T, Martinelli E, Napolitano S, et al. (2013) Increased TGF- as a Mechanism of Acquired Resistance to the Anti-EGFR Inhibitor Cetuximab through EGFR-MET Interaction and Activation of MET Signaling in Colon Cancer Cells. Clin Cancer Res 19:6751–6765.

188. Cheon D-J, Orsulic S (2011) Mouse Models of Cancer.

189. Shmelkov S V, Butler JM, Hooper AT, et al. (2008) CD133 expression is not restricted to stem cells, and both CD133+ and CD133- metastatic colon cancer cells initiate tumors. J Clin Invest 118:2111–20.

190. O'Brien CA, Pollett A, Gallinger S, Dick JE (2007) A human colon cancer cell capable of initiating tumour growth in immunodeficient mice. Nature 445:106–10.

191. Ricci-Vitiani L, Lombardi DG, Pilozzi E, et al. (2007) Identification and expansion of human colon-cancer-initiating cells. Nature 445:111–5.

192. Shultz LD, Brehm MA, Garcia-Martinez JV, Greiner DL (2012) Humanized mice for immune system investigation: progress, promise and challenges. Nat Rev Immunol 12:786–98.

193. Simpson-Abelson MR, Sonnenberg GF, Takita H, et al. (2008) Long-term engraftment and expansion of tumor-derived memory T cells following the implantation of non-disrupted pieces of human lung tumor into NOD-scid IL2Rgamma(null) mice. J Immunol 180:7009–18.

194. Li M, Zhou M, Gong M, et al. (2012) A novel animal model for bone metastasis in human lung cancer. Oncol Lett 3:802–806.

195. Morikawa K, Walker SM, Nakajima M, et al. (1988) Influence of organ environment on the growth, selection, and metastasis of human colon carcinoma cells in nude mice. Cancer Res 48:6863–71.

196. Fidler IJ (1991) Orthotopic implantation of human colon carcinomas into nude mice provides a valuable model for the biology and therapy of metastasis. Cancer Metastasis Rev 10:229–43.

197. Quintana E, Shackleton M, Sabel MS, et al. (2008) Efficient tumour formation by single human melanoma cells. Nature 456:593–8.

198. Linnebacher M, Maletzki C, Ostwald C, et al. (2010) Cryopreservation of human colorectal carcinomas prior to xenografting. BMC Cancer 10:362.

199. Sanz L, Cuesta AM, Salas C, et al. (2009) Differential transplantability of human endothelial cells in colorectal cancer and renal cell carcinoma primary xenografts. Lab Invest 89:91–7.

200. Herlyn M, Steplewski Z, Herlyn D, Koprowski H (1979) Colorectal carcinoma-specific antigen: detection by means of monoclonal antibodies. Proc Natl Acad Sci U S A 76:1438–42.

201. Zhou FQ, Qi YM, Xu H, et al. (2015) Expression of EpCAM and Wnt/ β-catenin in human colon cancer. Genet Mol Res 14:4485–94.

202. Gosens MJEM, van Kempen LCL, van de Velde CJH, et al. (2007) Loss of membranous Ep-CAM in budding colorectal carcinoma cells. Mod Pathol 20:221–32.

203. Seol HS, Kang HJ, Kang H, et al. (2014) Development and characterization of a colon PDX model that reproduces drug responsiveness and the mutation profiles of its original tumor. Cancer Lett 345:56–64.

204. Mills J, Matos T, Charytonowicz E, et al. (2009) Characterization and comparison of the properties of sarcoma cell lines in vitro and in vivo. Hum Cell 22:85–93.

205. Ahmed D, Eide PW, Eilertsen IA, et al. (2013) Epigenetic and genetic features of 24 colon cancer cell lines. Oncogenesis 2:e71.

206. Graves SS, Dearstyne E, Lin Y, et al. (2003) Combination Therapy with Pretarget CC49 Radioimmunotherapy and Gemcitabine Prolongs Tumor Doubling Time in a Murine Xenograft Model of Colon Cancer More Effectively Than Either Monotherapy. Clin Cancer Res 9:3712–3721.

207. Hlatky L, Olesiak M, Hahnfeldt P (1996) Measurement of potential doubling time for human tumor xenografts using the cytokinesis-block method. Cancer Res 56:1660–3.

208. Radulovic S, Miller G, Schally A V. (1991) Inhibition of Growth of HT-29 Human Colon Cancer Xenografts in Nude Mice by Treatment with Bombesin/Gastrin Releasing Peptide Antagonist (RC-3095). Cancer Res 51:6006–6009.

209. Taylor AC, Shu L, Danks MK, et al. (2000) P53 mutation and MDM2 amplification frequency in pediatric rhabdomyosarcoma tumors and cell lines. Med Pediatr Oncol 35:96–103.

210. Harris LC, von Wronski MA, Venable CC, et al. (1996) Changes in O6-methylguanine-DNA methyltransferase expression during immortalization of cloned human fibroblasts. Carcinogenesis 17:219–24.

211. Hidalgo M, Amant F, Biankin A V., et al. (2014) Patient-Derived Xenograft Models: An Emerging Platform for Translational Cancer Research. Cancer Discov 4:998–1013.

212. Jones S, Zhang X, Parsons DW, et al. (2008) Core signaling pathways in human pancreatic cancers revealed by global genomic analyses. Science 321:1801–6.

213. Oh BY, Lee WY, Jung S, et al. (2015) Correlation between tumor engraftment in patient-derived xenograft models and clinical outcomes in colorectal cancer patients. Oncotarget

214. Burgenske DM, Monsma DJ, Dylewski D, et al. (2014) Establishment of genetically diverse patient-derived xenografts of colorectal cancer. Am J Cancer Res 4:824–37.

215. Némati F, Sastre-Garau X, Laurent C, et al. (2010) Establishment and characterization of a panel of human uveal melanoma xenografts derived from primary and/or metastatic tumors. Clin Cancer Res 16:2352–62.

216. Chijiwa T, Kawai K, Noguchi A, et al. (2015) Establishment of patient-derived cancer xenografts in immunodeficient NOG mice. Int J Oncol.

217. Russell PJ, Russell P, Rudduck C, et al. (2015) Establishing prostate cancer patient derived xenografts: lessons learned from older studies. Prostate 75:628–36.

218. Mouradov D, Sloggett C, Jorissen RN, et al. (2014) Colorectal Cancer Cell Lines Are Representative Models of the Main Molecular Subtypes of Primary Cancer. Cancer Res 74:3238–3247.

219. Fearon ER (2011) Molecular Genetics of Colorectal Cancer.

220. Mihalatos M, Apessos A, Papadopoulou E, et al. Genetic alterations of the APC gene in familial adenomatous polyposis patients of the hellenic group for the study of colorectal cancer. Anticancer Res 23:2191–3.

221. Muller PAJ, Vousden KH (2013) p53 mutations in cancer. Nat Cell Biol 15:2–8.

222. John T, Kohler D, Pintilie M, et al. (2011) The ability to form primary tumor xenografts is predictive of increased risk of disease recurrence in early-stage non-small cell lung cancer. Clin Cancer Res 17:134–41.

223. Di Nicolantonio F, Martini M, Molinari F, et al. (2008) Wild-type BRAF is required for response to panitumumab or cetuximab in metastatic colorectal cancer. J Clin Oncol 26:5705–12.

224. Van Cutsem E, Köhne C-H, Láng I, et al. (2011) Cetuximab plus irinotecan, fluorouracil, and leucovorin as first-line treatment for metastatic colorectal cancer: updated analysis of overall survival according to tumor KRAS and BRAF mutation status. J Clin Oncol 29:2011–9.

225. Rajagopalan H, Bardelli A, Lengauer C, et al. (2002) Tumorigenesis: RAF/RAS oncogenes and mismatch-repair status. Nature 418:934.

226. Artale S, Sartore-Bianchi A, Veronese SM, et al. (2008) Mutations of KRAS and BRAF in primary and matched metastatic sites of colorectal cancer. J Clin Oncol

26:4217–9.

227. Johnston PG, Kaye S (2001) Capecitabine: a novel agent for the treatment of solid tumors. Anticancer Drugs 12:639–46.

228. Morton CL, Iacono L, Hyatt JL, et al. (2005) Activation and antitumor activity of CPT-11 in plasma esterase-deficient mice. Cancer Chemother Pharmacol 56:629–36.

229. Mi Z, Burke TG (1994) Marked interspecies variations concerning the interactions of camptothecin with serum albumins: a frequency-domain fluorescence spectroscopic study. Biochemistry 33:12540–5.

230. Machover D, Diaz-Rubio E, de Gramont A, et al. (1996) Two consecutive phase II studies of oxaliplatin (L-OHP) for treatment of patients with advanced colorectal carcinoma who were resistant to previous treatment with fluoropyrimidines. Ann Oncol 7:95–8.

231. Becouarn Y, Rougier P (1998) Clinical efficacy of oxaliplatin monotherapy: phase II trials in advanced colorectal cancer. Semin Oncol 25:23–31.

232. Kopetz S, Hoff PM, Morris JS, et al. (2010) Phase II trial of infusional fluorouracil, irinotecan, and bevacizumab for metastatic colorectal cancer: efficacy and circulating angiogenic biomarkers associated with therapeutic resistance. J Clin Oncol 28:453–459.

233. Yu L, Wu X, Cheng Z, et al. (2008) Interaction between bevacizumab and murine VEGF-A: a reassessment. Invest Ophthalmol Vis Sci 49:522–7.

234. Bieche I, Vacher S, Vallerand D, et al. (2014) Vasculature analysis of patient derived tumor xenografts using species-specific PCR assays: evidence of tumor endothelial cells and atypical VEGFA-VEGFR1/2 signalings. BMC Cancer 14:178.

235. Lichtenberger BM, Tan PK, Niederleithner H, et al. (2010) Autocrine VEGF signaling synergizes with EGFR in tumor cells to promote epithelial cancer development. Cell 140:268–79.

236. Chiron M, Bagley RG, Pollard J, et al. (2014) Differential antitumor activity of aflibercept and bevacizumab in patient-derived xenograft models of colorectal cancer. Mol Cancer Ther 13:1636–44.

237. Tabernero J, Ciardiello F, Rivera F, et al. (2010) Cetuximab administered once every second week to patients with metastatic colorectal cancer: a two-part pharmacokinetic/pharmacodynamic phase I dose-escalation study. Ann Oncol 21:1537–45.

238. Troiani T, Schettino C, Martinelli E, et al. (2008) The use of xenograft models for the selection of cancer treatments with the EGFR as an example. Crit Rev Oncol Hematol 65:200–211.

239. Shigeishi H, Higashikawa K, Hiraoka M, et al. (2008) Expression of epiregulin, a novel epidermal growth factor ligand associated with prognosis in human oral squamous cell carcinomas. Oncol Rep 19:1557–64.

240. Zhang J, Iwanaga K, Choi KC, et al. (2008) Intratumoral epiregulin is a marker of advanced disease in non-small cell lung cancer patients and confers invasive properties on EGFR-mutant cells. Cancer Prev Res (Phila) 1:201–7.

241. Jin Y, Peng D, Shen Y, et al. (2013) MicroRNA-376c inhibits cell proliferation and invasion in osteosarcoma by targeting to transforming growth factor-alpha. DNA Cell Biol 32:302–9.

242. Baker JB, Dutta D, Watson D, et al. (2011) Tumour gene expression predicts response to cetuximab in patients with KRAS wild-type metastatic colorectal cancer. Br J Cancer 104:488–95.

243. Dahlhoff M, Wolf E, Schneider MR (2014) The ABC of BTC: structural properties and biological roles of betacellulin. Semin Cell Dev Biol 28:42–8.

244. Kuramochi H, Nakajima G, Kaneko Y, et al. (2012) Amphiregulin and Epiregulin mRNA expression in primary colorectal cancer and corresponding liver metastases. BMC Cancer 12:88.

245. Pentheroudakis G, Kotoula V, De Roock W, et al. (2013) Biomarkers of benefit from cetuximab-based therapy in metastatic colorectal cancer: interaction of EGFR ligand expression with RAS/RAF, PIK3CA genotypes. BMC Cancer 13:49.

246. Watanabe T, Kobunai T, Yamamoto Y, et al. (2010) Prediction of liver metastasis after colorectal cancer using reverse transcription-polymerase chain reaction analysis of 10 genes. Eur J Cancer 46:2119–26.

247. Yamada M, Ichikawa Y, Yamagishi S, et al. (2008) Amphiregulin is a promising prognostic marker for liver metastases of colorectal cancer. Clin Cancer Res 14:2351–6.

248. Porebska I, Harlozińska A, Bojarowski T Expression of the tyrosine kinase activity growth factor receptors (EGFR, ERB B2, ERB B3) in colorectal adenocarcinomas and adenomas. Tumour Biol 21:105–15.

249. Mayer A, Takimoto M, Fritz E, et al. (1993) The prognostic significance of proliferating cell nuclear antigen, epidermal growth factor receptor, and mdr gene expression in colorectal cancer. Cancer 71:2454–60.

250. Ebi M, Kataoka H, Shimura T, et al. (2011) The role of neuregulin4 and HER4 in gastrointestinal malignant lymphoma. Mol Med Rep 4:1151–1155.

251. Ljuslinder I, Malmer B, Isaksson-Mettävainio M, et al. (2009) ErbB 1-4 expression alterations in primary colorectal cancers and their corresponding metastases. Anticancer Res 29:1489–94.

252. Kountourakis P, Pavlakis K, Psyrri A, et al. (2006) Prognostic significance of HER3 and HER4 protein expression in colorectal adenocarcinomas. BMC Cancer 6:46.

253. Shelly M, Pinkas-Kramarski R, Guarino BC, et al. (1998) Epiregulin is a potent pan-ErbB ligand that preferentially activates heterodimeric receptor complexes. J Biol Chem 273:10496–505.

254. Sasaki T, Nakamura T, Rebhun RB, et al. (2008) Modification of the primary tumor microenvironment by transforming growth factor alpha-epidermal growth factor receptor signaling promotes metastasis in an orthotopic colon cancer model. Am J Pathol 173:205–16.

255. Khambata-Ford S, Garrett CR, Meropol NJ, et al. (2007) Expression of epiregulin and amphiregulin and K-ras mutation status predict disease control in metastatic colorectal cancer patients treated with cetuximab. J Clin Oncol 25:3230–7.

256. Jacobs B, De Roock W, Piessevaux H, et al. (2009) Amphiregulin and epiregulin mRNA expression in primary tumors predicts outcome in metastatic colorectal cancer treated with cetuximab. J Clin Oncol 27:5068–74.

257. Tabernero J, Cervantes A, Rivera F, et al. (2010) Pharmacogenomic and pharmacoproteomic studies of cetuximab in metastatic colorectal cancer: biomarker analysis of a phase I dose-escalation study. J Clin Oncol 28:1181–9.

258. Yoshida M, Shimura T, Sato M, et al. (2013) A novel predictive strategy by immunohistochemical analysis of four EGFR ligands in metastatic colorectal cancer treated with anti-EGFR antibodies. J Cancer Res Clin Oncol 139:367–78.

259. Cunningham D, Humblet Y, Siena S, et al. (2004) Cetuximab monotherapy and cetuximab plus irinotecan in irinotecan-refractory metastatic colorectal cancer. N Engl J Med 351:337–45.

260. Saltz LB, Meropol NJ, Loehrer PJ, et al. (2004) Phase II trial of cetuximab in patients with refractory colorectal cancer that expresses the epidermal growth factor receptor. J Clin Oncol 22:1201–8.

261. Zhu C-Q, da Cunha Santos G, Ding K, et al. (2008) Role of KRAS and EGFR as biomarkers of response to erlotinib in National Cancer Institute of Canada Clinical Trials Group Study BR.21. J Clin Oncol 26:4268–4275.

262. Shia J, Klimstra DS, Li AR, et al. (2005) Epidermal growth factor receptor expression and gene amplification in colorectal carcinoma: an immunohistochemical and chromogenic in situ hybridization study. Mod Pathol 18:1350–6.

263. Spindler K-LG, Lindebjerg J, Nielsen JN, et al. (2006) Epidermal growth factor receptor analyses in colorectal cancer: A comparison of methods. Int J Oncol 29:1159–1165.

264. Martínez-Palacián A, del Castillo G, Herrera B, et al. (2012) EGFR is dispensable for c-Met-mediated proliferation and survival activities in mouse adult liver oval cells. Cell Signal 24:505–13.

265. Dulak AM, Gubish CT, Stabile LP, et al. (2011) HGF-independent potentiation of EGFR action by c-Met. Oncogene 30:3625–35.

266. Puri N, Salgia R (2008) Synergism of EGFR and c-Met pathways, cross-talk and inhibition, in non-small cell lung cancer. J Carcinog 7:9.

267. Campanella C, Mottolese M, Cianciulli A, et al. (2010) Epidermal growth factor receptor gene copy number in 101 advanced colorectal cancer patients treated with chemotherapy plus cetuximab. J Transl Med 8:36.

268. Scartozzi M, Bearzi I, Mandolesi A, et al. (2009) Epidermal Growth Factor Receptor (EGFR) gene copy number (GCN) correlates with clinical activity of irinotecan-cetuximab in K-RAS wild-type colorectal cancer: a fluorescence in situ (FISH) and chromogenic in situ hybridization (CISH) analysis. BMC Cancer 9:303.

269. Misale S, Yaeger R, Hobor S, et al. (2012) Emergence of KRAS mutations and acquired resistance to anti-EGFR therapy in colorectal cancer. Nature 486:532–6.

270. Troiani T, Napolitano S, Vitagliano D, et al. (2014) Primary and acquired resistance of colorectal cancer cells to anti-EGFR antibodies converge on MEK/ERK pathway activation and can be overcome by combined MEK/EGFR inhibition. Clin Cancer

Res 20:3775–86.

271. Bean J, Brennan C, Shih J-Y, et al. (2007) MET amplification occurs with or without T790M mutations in EGFR mutant lung tumors with acquired resistance to gefitinib or erlotinib. Proc Natl Acad Sci U S A 104:20932–7.

272. Engelman JA, Zejnullahu K, Mitsudomi T, et al. (2007) MET amplification leads to gefitinib resistance in lung cancer by activating ERBB3 signaling. Science 316:1039–43.

273. Reznik TE, Sang Y, Ma Y, et al. (2008) Transcription-dependent epidermal growth factor receptor activation by hepatocyte growth factor. Mol Cancer Res 6:139–50.

274. Corcoran RB, Dias-Santagata D, Bergethon K, et al. (2010) BRAF gene amplification can promote acquired resistance to MEK inhibitors in cancer cells harboring the BRAF V600E mutation. Sci Signal 3:ra84.

275. de Caestecker MP (2000) Role of Transforming Growth Factor-beta Signaling in Cancer. J Natl Cancer Inst 92:1388–1402.

276. Fleming NI, Jorissen RN, Mouradov D, et al. (2013) SMAD2, SMAD3 and SMAD4 mutations in colorectal cancer. Cancer Res 73:725–35.

277. Van Schaeybroeck S, Kyula JN, Fenton A, et al. (2011) Oncogenic Kras promotes chemotherapy-induced growth factor shedding via ADAM17. Cancer Res 71:1071–80.

278. Quesnelle KM, Grandis JR (2011) Dual kinase inhibition of EGFR and HER2 overcomes resistance to cetuximab in a novel in vivo model of acquired cetuximab resistance. Clin Cancer Res 17:5935–44.

279. Yonesaka K, Zejnullahu K, Okamoto I, et al. (2011) Activation of ERBB2 signaling causes resistance to the EGFR-directed therapeutic antibody cetuximab. Sci Transl Med 3:99ra86.

280. Wheeler DL, Huang S, Kruser TJ, et al. (2008) Mechanisms of acquired resistance to cetuximab: role of HER (ErbB) family members. Oncogene 27:3944–56.

281. Ciardiello F, Bianco R, Caputo R, et al. (2004) Antitumor activity of ZD6474, a vascular endothelial growth factor receptor tyrosine kinase inhibitor, in human cancer cells with acquired resistance to antiepidermal growth factor receptor therapy. Clin Cancer Res 10:784–93.

282. Viloria-Petit A, Crombet T, Jothy S, et al. (2001) Acquired resistance to the antitumor effect of epidermal growth factor receptor-blocking antibodies in vivo: a role for altered tumor angiogenesis. Cancer Res 61:5090–101.

283. Quesnelle KM, Wheeler SE, Ratay MK, Grandis JR (2012) Preclinical modeling of EGFR inhibitor resistance in head and neck cancer. Cancer Biol Ther 13:935–45.

7. Annex

Annex I: 48 oncogenes, targeted in 212 amplicons by the Illumina TruSeq® Amplicon – Cancer Panel.

Oncogenes targeted by the Illumina TruSeq® Amplicon – Cancer Panel				
ABL1	EGFR	GNAS	MLH1	RET
AKT1	ERBB2	HNF1A	MPL	SMAD4
ALK	ERBB4	HRAS	NOTCH1	SMARCB1
APC	FBXW7	IDH1	NPM1	SMO
ATM	FGFR1	JAK2	NRAS	SRC
BRAF	FGFR2	JAK3	PDGFRA	STK11
CDH1	FGFR3	KDR	PIK3CA	TP53
CDKN2A	FLT3	KIT	PTEN	VHL
CSF1R	GNA11	KRAS	PTPN11	
CTNNB1	GNAQ	MET	RB1	

Annex II: Tumor doubling times (TDT) of the PDX models

PDX	TDT [days]
Co 5676	7.0 ± 1.0
Co 5677	5.6 ± 2.2
Co 5679	7.1 ± 0.6
Co 5682	16.8 ± 3.9
Co 5734	11.7 ± 1.9
Co 5735	6.9 ± 2.3
Co 5736	9.0 ± 1.8
Co 5771	17.5 ± 17.5
Co 5776	8.3 ± 2.0
Co 5841	8.1 ± 2.7
Co 5854	5.8 ± 1.7
Co 5896	7.3 ± 0.6
Co 6044	7.3 ± 1.8
Co 6228	8.6 ± 2.1
Co 7271[1]	6.5 ± 0.9
Co 7475	5.0 ± 1.1
Co 7515	11.4 ± 3.5
Co 7523	10.5 ± 4.2
Co 7553A[2]	9.4 ± 2.7
Co 7553B[2]	16.5 ± 5.6
Co 7567	13.4 ± 4.7
Co 7596	12.8 ± 3.0
Co 7660[1]	11.0 ± 0.6
Co 7689	13.0 ± 2.9
Co 7809	7.4 ± 2.9
Co 7818	7.1 ± 1.6
Co 7835	9.6 ± 2.3
Co 7888	14.8 ± 4.5
Co 7935	21.6 ± 7.7
Co 9587	6.6 ± 2.0
Co 9634	5.4 ± 1.0
Co 9689A[3]	9.8 ± 2.1
Co 9689B[3]	10.4 ± 1.6
Co 9729	37.7 ± 18.4
Co 9775	9.9 ± 1.4
Co 9946	11.4 ± 18.0
Co 9978	2.5 ± 0.2
Co 9997[4]	11.7 ± 3.5
Co 10158	9.1 ± 4.5
Co 10194	13.5 ± 4.7
Co 10300[4]	12.6 ± 2.0
Co10302A[5]	10.3 ± 3.3
Co10302B[5]	23.5 ± 16.4
Co 10377	3.6 ± 0.7
Co 10383	7.1 ± 0.7
Co 10588	6.7 ± 2.4
Co 10764	5.8 ± 0.9
Co 10925	19.5 ± 14.0
Co 11061	7.1 ± 2.6

[1 -5] PDX models were derived from the same patient; n.d. = not detected

Annex III.a: mRNA expression of EGFR ligands in the PDX models

The mRNA expression was measured using real-time RT-PCR (n = 3), and the C_T values were normalized with the C_T values for ß-actin.

PDX	ΔC_T AREG	ΔC_T EREG	ΔC_T BTC	ΔC_T EGF	ΔC_T TGFα
	Mean ± SD	*Mean ± SD*	*Mean ± SD*	*Mean ± SD*	*Mean ± SD*
Co 5676	5.79 ± 0.68	4.80 ± 0.48	11.34 ± 0.84	10.83 ± 1.08	7.77 ± 0.51
Co 5677	7.18 ± 0.69	7.26 ± 0.56	10.35 ± 1.07	9.67 ± 3.24	7.87 ± 2.98
Co 5679	5.84 ± 0.88	4.68 ± 0.86	10.39 ± 0.68	n.d.	6.59 ± 0.76
Co 5682	3.11 ± 2.43	1.61 ± 1.32	10.49 ± 1.31	9.70 ± 2.22	7.60 ± 0.82
Co 5734	4.31 ± 0.32	3.64 ± 0.58	11.45 ± 0.40	11.35 ± 0.80	8.01 ± 0.48
Co 5735	4.28 ± 0.29	4.63 ± 0.84	10.99 ± 0.45	n.d.	8.40 ± 0.67
Co 5736	6.22 ± 1.74	8.51 ± 2.53	11.49 ± 0.69	15.89 ± 3.69	6.88 ± 0.11
Co 5771	4.21 ± 0.51	4.35 ± 0.06	10.27 ± 0.06	15.84 ± 1.14	6.76 ± 0.33
Co 5776	7.82 ± 0.12	8.12 ± 0.98	13.28 ± 1.02	15.03 ± 2.59	7.79 ± 0.33
Co 5841	8.89 ± 0.75	9.39 ± 0.40	14.70 ± 0.49	12.33 ± 0.56	7.82 ± 0.55
Co 5854	7.12 ± 0.55	9.96 ± 0.46	14.39 ± 1.76	8.86 ± 0.71	7.22 ± 0.36
Co 5896	5.53 ± 1.20	5.93 ± 0.43	9.97 ± 0.85	14.41 ± 1.14	6.90 ± 0.65
Co 6044	8.71 ± 1.25	7.26 ± 0.42	13.51 ± 2.78	12.18 ± 0.36	7.78 ± 0.58
Co 6228	5.36 ± 0.32	4.43 ± 0.35	11.27 ± 1.53	16.41 ± 0.62	7.23 ± 0.25
Co 7271[1]	8.41 ± 1.33	7.57 ± 1.18	13.15 ± 1.08	n.d.	8.32 ± 0.36
Co 7475	3.28 ± 1.62	3.39 ± 0.94	9.15 ± 2.18	13.92 ± 2.89	8.57 ± 0.80
Co 7515	5.35 ± 1.06	3.37 ± 0.51	9.01 ± 1.51	8.86 ± 0.62	7.08 ± 0.37
Co 7523	6.47 ± 0.95	8.28 ± 0.48	13.20 ± 2.70	12.60 ± 0.58	9.50 ± 0.38
Co 7553A[2]	5.71 ± 0.60	5.20 ± 0.39	10.34 ± 2.12	16.23 ± -	8.63 ± 0.76
Co 7553B[2]	7.10 ± 4.39	4.52 ± 1.58	11.28 ± 1.65	16.54 ± -	8.03 ± 0.65
Co 7567	5.76 ± 0.25	6.37 ± 0.33	10.26 ± 2.06	10.53 ± 0.52	7.24 ± 0.32
Co 7596	2.95 ± 1.94	2.23 ± 1.06	9.16 ± 2.73	11.65 ± 1.12	8.55 ± 0.74
Co 7660[1]	7.45 ± 0.69	7.34 ± 0.38	11.04 ± 2.51	n.d.	7.50 ± 0.38
Co 7689	7.08 ± 0.43	8.31 ± 0.75	11.52 ± 0.86	18.57 ± 0.57	7.14 ± 1.17
Co 7809	5.87 ± 0.76	5.55 ± 0.61	15.04 ± 2.36	8.33 ± 1.57	9.78 ± 0.59
Co 7818	6.09 ± 1.29	4.45 ± 0.73	11.86 ± 0.17	15.91 ± 0.55	9.07 ± 0.44
Co 7835	5.15 ± 1.02	5.97 ± 0.40	9.63 ± 0.09	16.71 ± 1.38	7.43 ± 0.91
Co 7888	3.93 ± 0.79	3.78 ± 0.45	10.75 ± 0.29	n.d.	8.95 ± 0.67
Co 7935	6.25 ± 1.52	6.06 ± 0.64	11.83 ± 0.70	16.62 ± -	8.46 ± 1.10
Co 9587	2.92 ± 0.22	5.00 ± 0.17	6.66 ± 0.80	7.40 ± 0.73	5.03 ± 0.76
Co 9634	2.05 ± 1.74	2.56 ± 0.57	8.34 ± 0.18	6.35 ± 1.80	6.26 ± 0.27
Co 9689A[3]	0.45 ± 2.22	2.87 ± 0.50	9.28 ± 0.59	n.d.	6.56 ± 1.21
Co 9689B[3]	0.67 ± 0.80	2.13 ± 0.06	7.11 ± 0.04	12.43 ± -	5.91 ± 0.71
Co 9729	1.31 ± 0.30	2.93 ± 0.74	6.89 ± 0.49	9.17 ± -	5.45 ± 0.84
Co 9775	6.70 ± 1.26	9.72 ± 0.37	8.20 ± 0.62	n.d.	5.87 ± 0.97
Co 9946	4.57 ± 0.99	2.98 ± 0.45	8.17 ± 0.50	11.89 ± 2.69	6.71 ± 0.70
Co 9978	2.80 ± 0.49	3.42 ± 0.23	9.98 ± 0.69	13.79 ± 1.09	9.05 ± 1.22
Co 9997[4]	4.81 ± 0.36	4.34 ± 0.55	9.18 ± 0.68	6.97 ± 2.28	6.07 ± 1.45
Co 10158	3.95 ± 0.99	3.71 ± 0.61	8.83 ± 0.39	12.50 ± 3.51	6.62 ± 1.94
Co 10194	2.17 ± 0.50	3.20 ± 0.41	7.95 ± 0.73	9.14 ± 1.15	5.64 ± 0.69
Co 10300[4]	3.54 ± 0.53	5.80 ± 0.13	6.61 ± 0.06	7.36 ± 0.53	5.84 ± 0.38
Co10302A[5]	5.72 ± 0.13	7.80 ± 0.02	9.94 ± 0.25	n.d.	5.94 ± 1.40
Co10302B[5]	6.12 ± 0.94	8.34 ± 0.25	9.81 ± 0.53	12.89	6.21 ± 0.95
Co 10377	3.89 ± 0.97	4.56 ± 0.42	9.91 ± 0.30	n.d.	6.05 ± 0.70
Co 10383	2.57 ± 0.11	3.60 ± 0.11	7.97 ± 0.36	n.d.	7.64 ± 0.51
Co 10588	5.76 ± 0.03	4.01 ± 0.03	8.35 ± 0.47	11.34	6.35 ± 1.51
Co 10764	4.81 ± 0.34	8.09 ± 0.14	10.60 ± 0.41	n.d.	7.21 ± 0.08
Co 10925	1.80 ± 0.29	2.97 ± 0.57	6.49 ± 0.30	8.05	7.00 ± 0.85
Co 11061	2.47 ± 0.02	2.12 ± 0.52	7.05 ± 0.06	3.84	4.01

[1 -5] PDX models were derived from the same patient; n.d. = not detected

Annex III.b: Protein expression of EGFR ligands in the PDX models

The protein expression was measured using ELISA (n = 3).

PDX	AREG [pg/mg$_{TP}$] Mean ± SD	EREG [pg/mg$_{TP}$] Mean ± SD	BTC [pg/mg$_{TP}$] Mean ± SD	EGF [pg/mg$_{TP}$] Mean ± SD	TGFα [pg/mg$_{TP}$] Mean ± SD
Co 5676	2620.0 ± 387.33	112.81 ± 26.05	76.02 ± 4.67	30.72 ± 5.39	36.43 ± 13.17
Co 5677	548.9 ± 299.90	29.54 ± 22.21	84.65 ± 51.33	81.09 ± 6.07	32.67 ± 10.97
Co 5679	1258.6 ± 414.17	63.58 ± 27.78	101.79 ± 20.09	4.16 ± 3.80	60.01 ± 20.59
Co 5682	6525.1 ± 1177.17	154.29 ± 39.68	104.63 ± 71.80	30.12 ± 1.26	47.40 ± 29.62
Co 5734	2273.8 ± 303.41	74.75 ± 18.24	59.37 ± 6.76	9.67 ± 1.94	22.04 ± 8.18
Co 5735	5317.5 ± 2051.28	29.66 ± 10.49	101.24 ± 24.57	3.43 ± 3.15	14.81 ± 8.89
Co 5736	519.9 ± 96.93	27.31 ± 15.27	54.38 ± 9.43	6.10 ± 1.98	52.07 ± 32.07
Co 5771	1930.1 ± 564.00	31.32 ± 4.88	54.24 ± 15.72	3.05 ± 1.58	20.59 ± 5.92
Co 5776	844.7 ± 313.96	13.21 ± 0.08	34.57 ± 0.35	7.10 ± 3.93	34.15 ± 8.90
Co 5841	407.3 ± 89.54	24.82 ± 20.93	19.81 ± 2.10	12.36 ± 4.50	31.69 ± 3.82
Co 5854	622.9 ± 233.79	20.36 ± 2.27	30.60 ± 6.29	23.35 ± 5.53	24.49 ± 1.31
Co 5896	1335.2 ± 441.58	40.75 ± 11.52	145.61 ± 7.23	5.07 ± 4.63	41.96 ± 2.86
Co 6044	192.4 ± 76.62	21.30 ± 1.99	13.11 ± 6.61	6.50 ± 4.73	29.22 ± 7.71
Co 6228	1294.2 ± 70.46	77.45 ± 56.64	68.12 ± 64.70	1.96 ± 3.39	28.28 ± 4.95
Co 7271[1]	404.5 ± 208.99	26.80 ± 4.01	42.59 ± 19.23	4.61 ± 7.99	32.80 ± 11.71
Co 7475	1166.1 ± 935.47	82.21 ± 63.90	60.25 ± 30.90	6.67 ± 7.14	30.55 ± 15.60
Co 7515	633.5 ± 202.87	187.74 ± 75.95	68.85 ± 20.29	10.01 ± 3.35	39.24 ± 16.38
Co 7523	1201.4 ± 322.86	16.75 ± 4.16	37.40 ± 8.98	8.87 ± 8.63	32.57 ± 15.77
Co 7553A[2]	927.1 ± 320.19	35.01 ± 16.05	49.35 ± 12.03	4.47 ± 7.73	22.65 ± 10.44
Co 7553B[2]	481.6 ± 407.98	93.13 ± 7.65	18.12 ± 9.22	4.07 ± 7.04	12.73 ± 6.11
Co 7567	212.1 ± 121.89	43.82 ± 4.54	69.49 ± 72.54	11.67 ± 10.42	17.18 ± 9.64
Co 7596	2635.5 ± 1081.58	100.59 ± 34.73	46.56 ± 25.45	3.32 ± 5.75	8.81 ± 2.68
Co 7660[1]	196.1 ± 92.95	28.61 ± 10.23	54.50 ± 20.94	2.76 ± 4.78	17.36 ± 13.43
Co 7689	208.9 ± 88.66	12.87 ± 7.82	43.09 ± 18.06	2.09 ± 3.61	10.67 ± 7.33
Co 7809	1372.6 ± 247.35	59.13 ± 31.16	13.28 ± 12.03	32.10 ± 9.57	16.21 ± 7.91
Co 7818	1088.7 ± 33.50	58.29 ± 4.02	48.37 ± 9.21	6.26 ± 9.08	24.54 ± 11.81
Co 7835	1068.8 ± 581.44	19.34 ± 14.83	68.99 ± 37.27	5.12 ± 8.87	29.79 ± 10.90
Co 7888	2753.7 ± 2215.17	68.61 ± 45.80	48.48 ± 38.00	4.34 ± 7.51	20.12 ± 11.31
Co 7935	4142.9 ± 746.20	28.40 ± 14.26	65.21 ± 8.77	8.60 ± 3.13	34.38 ± 18.03
Co 9587	537.3 ± 95.80	146.5 ± 3.99	75.34 ± 3.01	9.92 ± 0.96	73.76 ± 4.89
Co 9634	1850.9 ± 93.74	61.95 ± 2.95	132.8 ± 25.21	77.4 ± 9.92	42.61 ± 2.22
Co 9689A[3]	2780.0 ± 215.16	80.13 ± 8.13	86.35 ± 12.15	n.d.	55.21 ± 9.20
Co 9689B[3]	1735.7 ± 345.70	63.66 ± 16.80	57.30 ± 19.14	n.d.	17.09 ± 0.51
Co 9729	1377.4 ± 325.77	54.49 ± 3.18	85.79 ± 42.97	16.26 ± 11.56	159.04 ± 42.11
Co 9775	414.4 ± 47.41	91.24 ± 14.03	78.41 ± 17.17	n.d.	47.99 ± 6.94
Co 9946	614.3 ± 17.10	72.92 ± 31.20	101.38 ± 21.04	8.63 ± 6.10	31.99 ± 2.10
Co 9978	1252.8 ± 240.59	62.11 ± 4.69	32.44 ± 8.00	n.d.	11.23 ± 1.02
Co 9997[4]	818.2 ± 1.55	75.99 ± 1.35	68.82 ± 2.23	19.41 ± 13.73	82.40 ± 18.51
Co 10158	1919.8 ± 1125.43	70.61 ± 7.66	112.59 ± 56.11	n.d.	53.01 ± 23.14
Co 10194	2123.5 ± 416.89	62.84 ± 0.21	62.64 ± 1.74	5.01 ± 3.54	25.26 ± 8.04
Co 10300[4]	275.3 ± 45.85	77.01 ± 3.39	62.52 ± 1.87	10.40 ± 7.35	18.66 ± 0.58
Co10302A[5]	486.8 ± 82.24	41.59 ± 164.74	69.35 ± 33.57	n.d.	86.10 ± 16.80
Co10302B[5]	613.8 ± 106.48	44.29 ± 2.13	53.83 ± 6.15	n.d.	46.27 ± 14.56
Co 10377	1952.5 ± 485.10	55.36 ± 8.81	73.04 ± 15.64	n.d.	29.61 ± 8.43
Co 10383	1395.1 ± 28.06	99.16 ± 9.64	123.52 ± 25.28	n.d.	13.13 ± 2.60
Co 10588	883.5 ± 153.76	53.53 ± 9.66	136.15 ± 40.72	n.d.	56.03 ± 9.92
Co 10764	1018.9 ± 268.94	44.22 ± 12.26	64.53 ± 14.06	n.d.	38.74 ± 0.93
Co 10925	845.4 ± 19.26	92.03 ± 10.01	109.80 ± 22.43	9.36 ± 9.80	20.56 ± 6.32
Co 11061	1565.7 ± 273.00	66.61 ± 6.13	109.83 ± 2.06	27.51 ± 8.28	19.60 ± 1.52

[1 -5] PDX models were derived from the same patient; n.d. = not detected

Annex IV: Expression of EGFR and the HER receptor family

The mRNA expression was measured with real-time RT-PCR and protein expression was measured with ELISA (n = 3).

PDX	ΔC_T EGFR *Mean ± SD*	ΔC_T HER2 *Mean ± SD*	ΔC_T HER3 *Mean ± SD*	ΔC_T HER4 *Mean ± SD*	EGFR [pg/mg$_{TP}$] *Mean ± SD*
Co 5676	5.81 ± 0.05	4.74 ± 0.05	3.76 ± 0.10	n.d.	4.80 ± 0.61
Co 5677	4.85 ± 0.81	3.53 ± 1.82	3.62 ± 1.70	14.23 ± 1.93	5.18 ± 1,71
Co 5679	4.74 ± 0.10	2.74 ± 0.60	1.86 ± 0.38	18.28	4.48 ± 0.75
Co 5682	4.79 ± 1.72	3.68 ± 1.36	3.18 ± 0.63	19.75 ± 0.84	2.33 ± 0,42
Co 5734	5.64 ± 0.30	4.26 ± 0.15	3.51 ± 0.26	n.d.	3.93 ± 2.14
Co 5735	5.58 ± 0.60	3.18 ± 0.34	1.14 ± 0.23	16.25	1.74 ± 0.95
Co 5736	5.24 ± 1.97	2.98 ± 1.30	3.24 ± 0.00	n.d.	2.21 ± 1.48
Co 5771	6.27 ± 0.10	4.16 ± 0.16	2.48 ± 0.14	16.63 ± 2.00	1.77 ± 1,83
Co 5776	6.29 ± 0.32	5.74 ± 0.27	3.78 ± 0.60	n.d.	3.79 ± 1.02
Co 5841	5.38 ± 0.08	3.83 ± 0.48	2.08 ± 0.48	12.82 ± 1.76	6.90 ± 2,03
Co 5854	5.37 ± 0.49	4.59 ± 0.50	3.41 ± 0.47	n.d.	4.34 ± 1.23
Co 5896	5.26 ± 0.65	1.88 ± 0.84	1.02 ± 0.95	n.d.	2.71 ± 0.62
Co 6044	5.54 ± 0.60	4.33 ± 0.32	2.91 ± 0.43	n.d.	3.21 ± 1.23
Co 6228	5.87 ± 0.37	3.95 ± 0.32	2.67 ± 0.25	n.d.	3.01 ± 2.35
Co 7271[1]	5.08 ± 0.41	4.54 ± 0.45	2.91 ± 0.32	14.59	11.48 ± 4.03
Co 7475	5.77 ± 0.94	4.75 ± 0.83	2.86 ± 0.89	n.d.	3.62 ± 3.16
Co 7515	5.20 ± 0.57	3.47 ± 0.08	3.60 ± 0.22	n.d.	2.20 ± 1.74
Co 7523	6.39 ± 0.15	4.55 ± 0.49	3.85 ± 0.65	n.d.	2.58 ± 0.31
Co 7553A[2]	5.93 ± 0.51	4.36 ± 0.46	2.85 ± 0.07	18.10 ± 0.54	3.11 ± 0,89
Co 7553B[2]	5.25 ± 0.42	3.52 ± 3.69	2.50 ± 0.51	16.45 ± 1.95	1.74 ± 1,00
Co 7567	5.35 ± 0.39	4.08 ± 0.10	2.69 ± 0.09	17.17 ± 0.91	2.52 ± 0,83
Co 7596	6.18 ± 0.34	4.72 ± 0.74	2.28 ± 0.64	18.00 ± 1.76	1.18 ± 0,09
Co 7660[1]	5.02 ± 0.42	4.41 ± 0.14	3.00 ± 0.04	14.79	2.89 ± 0.51
Co 7689	6.03 ± 0.33	4.75 ± 0.36	3.26 ± 0.16	n.d.	0.79 ± 0.02
Co 7809	4.62 ± 0.25	4.95 ± 0.46	4.30 ± 0.40	n.d.	11.47 ± 2.39
Co 7818	5.92 ± 0.41	4.65 ± 0.17	3.52 ± 0.39	n.d.	3.64 ± 0.70
Co 7835	6.35 ± 0.35	3.66 ± 0.14	2.23 ± 0.28	15.70 ± 1.02	1.19 ± 0,56
Co 7888	5.51 ± 0.19	5.55 ± 0.11	3.89 ± 0.38	n.d.	1.81 ± 1.05
Co 7935	6.07 ± 0.34	4.82 ± 0.48	3.13 ± 0.65	17.84 ± 3.25	2.70 ± 1,04
Co 9587	2.41 ± 0.56	2.23 ± 0.36	1.30 ± 0.78	n.d.	2.37 ± 0.50
Co 9634	2.43 ± 1.19	2.70 ± 0.28	0.24 ± 1.51	n.d.	2.86 ± 0.11
Co 9689A[3]	4.08 ± 0.62	3.63 ± 0.30	2.67 ± 0.68	15.10	2.27 ± 0.36
Co 9689B[3]	2.38 ± 0.80	1.22 ± 0.74	0.09 ± 0.48	12.81	2.07 ± 0.39
Co 9729	1.44 ± 0.70	1.67 ± 0.31	0.31 ± 0.32	10.45	2.52 ± 0.53
Co 9775	3.37 ± 0.44	0.50 ± 1.10	-1.05 ± 1.37	n.d.	4.59 ± 1.20
Co 9946	4.01 ± 0.64	2.68 ± 0.35	1.58 ± 0.22	13.57 ± 1.28	5.26 ± 0,41
Co 9978	5.15 ± 0.25	3.73 ± 0.52	1.57 ± 0.95	n.d.	2.79 ± 0.64
Co 9997[4]	3.74 ± 0.44	3.92 ± 0.33	0.44 ± 1.87	n.d.	4.14 ± 1.11
Co 10158	4.12 ± 0.50	3.48 ± 0.02	1.95 ± 0.42	13.76	3.43 ± 0.75
Co 10194	3.25 ± 0.56	2.37 ± 0.83	0.04 ± 0.09	14.82	3.73 ± 0.34
Co 10300[4]	2.61 ± 0.88	1.46 ± 0.51	-0.78 ± 0.64	11.89	4.94 ± 0.16
Co10302A[5]	1.89 ± 0.08	1.20 ± 0.09	-0.41 ± 1.30	n.d.	3.88 ± 0.29
Co10302B[5]	3.81 ± 0.84	2.73 ± 0.97	1.29 ± 1.08	n.d.	3.73 ± 0.37
Co 10377	3.81 ± 0.64	3.97 ± 0.73	2.02 ± 0.93	n.d.	1.77 ± 0.39
Co 10383	4.32 ± 0.30	3.59 ± 0.62	1.64 ± 0.24	12.35	1.30 ± 0.23
Co 10588	2.93 ± 1.63	1.59 ± 1.08	-0.65 ± 1.82	n.d.	3.03 ± 0.76
Co 10764	2.86 ± 0.93	3.54 ± 0.24	1.45 ± 0.18	n.d.	9.27 ± 3.36
Co 10925	1.78 ± 0.42	0.73 ± 0.50	-1.31 ± 0.37	12.72	3.40 ± 0.75
Co 11061	5.32 ± 0.38	3.27 ± 0.35	1.30 ± 2.28	n.d.	0.82 ± 0.28

[1 -5] PDX models were derived from the same patient; n.d. = not detected

Annex V: **Gene copy number of key molecules of the EGFR pathway**

GCN of the PDX was measured using a real-time PCR based approach.

PDX	Gene copy number				
	BRAF	EGFR	KRAS	MET	NRAS
Co 5676	2	3	3	6	3
Co 5677	1	1	2	2	1
Co 5679	2	2	6	5	3
Co 5682	2	2	2	2	0
Co 5734	2	2	2	4	2
Co 5735	2	2	2	4	3
Co 5736	1	1	2	3	2
Co 5771	2	2	4	5	2
Co 5776	1	1	2	2	1
Co 5841	2	2	3	6	2
Co 5854	2	2	2	4	2
Co 5896	1	1	2	3	2
Co 6044	1	1	2	3	2
Co 6228	1	2	3	4	3
Co 7271[1]	2	2	2	5	2
Co 7475	1	1	2	3	2
Co 7515	1	1	1	3	2
Co 7523	1	1	2	3	3
Co 7553A[2]	2	2	3	5	2
Co 7553B[2]	4	4	6	9	4
Co 7567	2	3	4	7	4
Co 7596	23	4	9	9	4
Co 7660[1]	1	1	1	0	0
Co 7689	1	1	2	2	1
Co 7809	1	2	3	3	1
Co 7818	6	5	7	9	7
Co 7835	2	2	3	4	3
Co 7888	3	6	3	6	3
Co 7935	3	4	4	5	3
Co 9587	1	1	2	1	1
Co 9634	2	2	2	3	3
Co 9689A[3]	3	5	4	6	3
Co 9689B[3]	3	4	4	5	3
Co 9729	1	1	2	2	2
Co 9775	4	3	4	6	3
Co 9946	2	2	3	3	1
Co 9978	2	2	4	4	3
Co 9997[4]	3	3	5	6	6
Co 10158	1	1	3	2	2
Co 10194	2	2	4	4	1
Co 10300[4]	2	3	4	5	3
Co10302A[5]	1	1	3	2	2
Co10302B[5]	1	1	2	2	1
Co 10377	1	1	2	2	1
Co 10383	2	3	3	5	3
Co 10588	1	1	1	1	0
Co 10764	2	2	2	3	2
Co 10925	2	4	4	4	2
Co 11061	1	1	3	2	2

[1 -5] PDX models were derived from the same patient

Abbreviations

18qLOH	loss of heterozygosity at chromosome 18q
5-FU	5-Fluorouracil
ADCC	antibody dependent cellular toxicity
AJCC	American Joint Committee on Cancer
APC	adenomatous polyposis coli
BC	breast cancer
BIW	twice a week
BWC	change of body weight
aCGH	comparative genomic hybridization
CEA	Carcinoembryonic antigen
CIN	chromosome instability pathway
CK20	cytokeratin 20
CR	complete remission
CRC	colorectal cancer
DTP	Developmental Therapeutics Program
DNA	desoxyribonucleic acid
ECM	extracellular matrix
EGFR	epidermal growth factor receptor
EGFR-I	EGFR inhibitors
ELISA	Enzyme Linked Immunosorbent Assay
EMT	epithelial-to-mesenchymal transition
FAP	familiar adenomatous polyposis
FDA	Food and Drug Administration
FFPE	formalin fixed, paraffin embedded
GIST	gastrointestinal stromal tumors
HGF	Hepatocyte Growth Factor
IHC	immunohistochemistry
i.p.	intraperitoneally
KRAS	Kirsten rat sarcoma-2 viral oncogene homolog
LOH	loss of heterozygosity
LV	leucovorin
mAb	monoclonal antibody
MAPK	mitogen-associated protein kinase
MCR	mutation cluster region
mCRC	metastatic colorectal cancer
MMR	mismatch repair
MSI	microsatellite instability
MTD	maximum tolerated dose
NCI	National Cancer Institute
NK	natural killer
n.a.	not analyzed
NOD	non-obese diabetic
n.s.	not significant
NSCLC	non-small cell lung cancer
OR	objective response
ORR	objective response rate
QoL	quality of life

optT/C	optimal treated to control value
PC	pancreatic carcinoma
PCNA	proliferating-cell-nuclear antigen
PD	progressive disease
PI3K	phosphatidylinositol 3-kinase
PIK3CA	phosphatidylinositol-4,5-bisphosphate 3-kinase, catalytic subunit alpha
p.o.	oral
PR	partial response
Rb	retinoblastoma protein
r_S	Spearmann correlation coefficient
RECIST	Response Evaluation Criteria in Solid Tumors
TNM	tumor-node-metastasis
T_P	total protein
TV	tumor volume
RTV	relative tumor volume
s.c.	subcutaneous
scid	severe combined immunodeficiency
SCLC	small cell lung cancer
SD	stable disease
SN-38	7-ethyl-10-hydroxy-camptothecin
SSA	sessile serrated adenomas
TK	tyrosine kinase
TKI	tyrosine kinase inhibitor
TS	thymidylate synthetase
TSA	traditional serrated adenomas
VEGF-A	vascular endothelial growth factor

List of publications and presentations

Poster

Rivera M, Becker M, Schlag PM, Schwan A, Merk J, Rosenthal A,·Hinzmann B, Hoffmann J,·Fichtner (2012) Characterization of 28 patient derived colorectal cancer xenografts and analysis for response markers to an antiangiogenic treatment. AACR 103rd Annual Meeting, Chicago

Rivera M, Wulf-Goldenberg A, Schwan A, Sers C, Hoffmann J, Fichtner I (2013) Diagnostics and targeted therapy in colorectal cancer: Establishment of a new cohort of patient-derived early xenograft models. 17th International AEK Cancer Congress, Heidelberg

Rivera M, Sers C, Schlag PM, Schwan A, Fichtner I, Hoffmann J (2013) Establishment of a new cohort of patient derived early xenograft models. First World Congress on Controversies in Gastroenterology, Berlin

Presentations

Rivera M, Sers C, Schlag PM, Kury A, Merk J, Hoffmann J, Walther W, Fichtner I (2015) Colorectal cancer patient-derived (PDX) models as platform for drug screening, molecular- and biomarker analysis. 36st Annual EORTC-PAMM Group Winter Meeting, Marseille

Rivera M, Sers C, Schlag PM, Kury A, Merk J, Hoffmann J, Walther W, Fichtner I (2015) Establishment of colorectal cancer patient-derived xenograft models as platform for drug screening, molecular and biomarker analysis. The 16th MDC/FMP PhD Retreat, Bad Saarow

Danksagung

Als erstes möchte ich mich herzlich bei Dr. Iduna Fichtner für die Aufnahme in ihre Arbeitsgruppe und die Überlassung des interessanten Themas, sowie die hilfreichen Ideen und Diskussionen bedanken. Dr. Jens Hoffmann danke ich dafür, mir die Gelegenheit gegeben zu haben, Teil der Firma EPO GmbH zu werden, was mir den Rahmen für die Anfertigung dieser Arbeit angeboten hat.

Dem Prof. Wolfgang Walther gitlt mein herzlichter Dank. Er war immer bereit mit mir sein breites Wissen zu teilen, weiterhin danke ich ihm für seine Unterstützung, Geduld und Motivation während der Anfertigung dieser Doktorarbeit.

Desweiteren möchte ich mich bei Prof. Roland Lauster bedanken, der diese Arbeit seitens der TU-Berlin betreut hat und nützliche Ratschläge dazu gab, Prof. Jens Kurreck, der die Begutachtung dieser Arbeit übernam, sowie Prof. Peter Neubauer, der sich bereit erklärte, den Vorsitz zu übernehmen.

Weiterhin möchte ich mich bei den Kollegen der AG Experimentelle Pharmakologie und EPO GmbH für das nette und freundliche Arbeitsklima, und die Unterstützung bei der Durchführung der praktischen Aufgaben bedanken. Mein besonderer und herzlicher Dank gilt an dieser Stelle Stephanie Tannert, die mich bei der Generierung der Resistenzlinien unterstützt hat und dabei viel Geduld, Freundlichkeit und Kompetenz entgegengebrachte; und Carsta Werner, die wertvolle Hilfe im Labor bei der Charakterisierung der Modelle leistete.

Nicht unerwähnt bleiben soll ein Dank an alle Kollenginnen, die in diesen Jahren mit mir das Büro geteilt haben: Maria, Maxi, Diana, Annika und Katharina haben mich durch diese Jahre begleitet, jede dieser Frauen hat mein Leben berührt und bereichert.Von ganzen Herzen möchte ich meiner Familie und vor allem meinen Eltern danken, die mir eine Ausbildung ermöglichten und an mich geglaubt haben.

Nicht zuletzt gilt mein Dank all diejenigen die mir Nahe stehen und mich während dieser Zeit persönlich unterstützt und motiviert haben, insbesondere meinem Lebenspartner Nadim El Sayed, dessen Liebe und Unterstützung mir in allen Lebenslagen Kraft gibt.

Eidesstattliche Erklärung

Hiermit versichere ich an Eides statt, dass ich die Dissertation selbständig verfasst und keine anderen als die angegebenen Hilfsmittel und Quellen verwendet habe. Wörtlich oder inhaltlich entnommene Stellen sowie Abbildungen aus benutzten Quellen wurden als solche gekennzeichnet. Weiterhin versichere ich, weder anderweitig die Promotionsabsicht erklärt noch ein Promotionseröffnungsverfahren eröffnet zu haben.

Maria Rivera